STUDIES OF RECENT ERUPTIVE PHENOMENA AT KĪLAUEA VOLCANO

A DISSERTATION SUBMITTED TO THE GRADUATE DIVISION OF THE UNIVERSITY OF HAWAIʻI AT MĀNOA IN PARTIAL FULFILLMENT FOR THE DEGREE REQUIREMENTS OF

DOCTOR OF PHILOSOPHY

IN

GEOLOGY AND GEOPHYSICS

DECEMBER 2015

By

Tim R. Orr

Dissertation Committee:

Bruce Houghton, Chairperson
Sarah Fagents
Scott Rowland
Don Swanson
Steve Businger

Acknowledgments

This work is the culmination of a plan, long set aside, that brought me to Hawai‘i more than a decade ago. I extend my sincere gratitude to my advisor, Bruce Houghton, for helping to finally bring this plan to fruition. Bruce’s support and advice have been invaluable, and I look forward to continued collaboration. In addition, Alison Houghton has been a gem, and I am grateful for her hospitality. I am also indebted to my dissertation committee—Sarah Fagents, Scott Rowland, Don Swanson, and Steve Businger—for their guidance and support.

This research would not have been possible without my colleagues at the Hawaiian Volcano Observatory (HVO), in particular Matt Patrick and Kelly Wooten, with whom I spend many long days in the trenches. I am appreciative to my supervisors, Jim Kauahikaua and Tina Neal, for permitting me to take time off to pursue my studies. HVO’s technical staff worked tirelessly to ensure continued operation of the webcam network from which many of the observations used in this dissertation are acquired. Thanks, too, to helicopter pilot David Okita, for always bringing me back from the field safely.

Finally, I am humbled by the unwavering love and support of my family, who were always there when I came home.

The data presented in this dissertation was collected in the normal course of my duties as a geologist at the Hawaiian Volcano Observatory, funded through the U.S. Geological Survey’s Volcano Hazards Program. Additional support was provided by Bruce Houghton under NSF grant EAR-1427357e.

Abstract

Kīlauea Volcano, on the island of Hawai‘i, hosts a broad range of basaltic eruptive styles that have traditionally been studied with relatively sparse observations and data. Recent advances in digital camera and webcam technology, however, as well as improvements in the sensitivity and acquisition rate of geophysical data, offer new opportunities to study these processes. Here, robust visual and continuous camera observations are integrated with high-rate geophysical data in four studies, to enhance our understanding of eruptive activity at Kīlauea: (1) A brief eruption on Kīlauea's East Rift Zone during 2007 led to a pause in the long-lived Pu‘u ‘Ō‘ō eruption. Activity resumed with the refilling of the Pu‘u ‘Ō‘ō crater, first by lava, and then by endogenous uplift. Filling culminated in the opening of a new eruptive fissure at Pu‘u ‘Ō‘ō, marking the start of a new period of eruptive activity. (2) During 2010, lava flows advanced toward the Kalapana Gardens subdivision on Hawai‘i's southeast coast, eventually destroying three homes. As the relatively low-discharge flow advanced into this area, it was laterally confined by low topography. Subsequent inflation was focused over the lava tube that developed in the flow, forming a long, sinuous tumulus that snaked across the gently sloping terrain. The unusual feature may be an analog for similar lava flow structures identified in New Mexico and on Mars. In addition, the sinuous tumulus was the source of frequent breakouts associated with cycles of deflation and inflation at Kīlauea's summit, providing a means of forecasting activity. (3) Kīlauea's ongoing summit eruption has been punctuated by small, impulsive explosive eruptions since it began in 2008. High-rate webcam imagery shows convincingly that these explosive events were triggered by rockfalls from the vent walls that directly impacted the top of the lava column, generating a rebound splash (Worthington jet). (4) The March 2011 Kamoamoa eruption, preceded by months of precursory changes, was exceptionally well documented with an array of geological, geophysical, and geochemical observations. This multiparametric monitoring suggests that the eruption was driven by an imbalance between the magma supplied to and erupted from the Pu‘u ‘Ō‘ō vent.

Table of Contents

List of Tables

List of Figures

Chapter 1

Introduction

1.1 Dissertation Overview

Volcanism at Kīlauea, on the island of Hawai‘i, spans a broad range of basaltic eruptive styles, including effusive lava flows, persistent lava lake activity, sustained fountaining, and impulsive explosive eruptions. This dissertation examines recent examples that encompass this range of styles, thus furthering our understanding of Hawai‘i’s volcanoes. To provide the volcanological context for these studies, which are presented in chronological order, I first review, in this chapter, Kīlauea’s eruptive history, with an emphasis on the ongoing Pu‘u ‘Ō‘ō eruption. This review extends Heliker and Mattox (2003) by updating the Pu‘u ‘Ō‘ō eruption chronology in a generalized fashion through August 2015. Eruptive activity is formalized as discrete episodes and sub-episodes based on eruption location and continuity, as shown in Table 1.1, by summarizing the episodes discussed in Heliker and Mattox (2003) and defining new episodes to highlight changes in the ongoing eruption.

Chapter 2 describes the activity between episodes 55 and 58 of the Pu‘u ‘Ō‘ō eruption during 2007—a brief period characterized by an eruption upslope from Pu‘u ‘Ō‘ō and subsidence of Pu‘u ‘Ō‘ō’s crater floor, followed by a short hiatus before activity resumed at Pu‘u ‘Ō‘ō. This general pattern of events is one which has been documented both before and since at Pu‘u ‘Ō‘ō, and it offers a way to forecast eruptive changes at Kīlauea.

Chapter 3 focuses on Pu‘u ‘Ō‘ō’s tube-fed pāhoehoe flow field in 2010 and describes the formation and evolution of a long sinuous, ridge-like tumulus over the active lava tube. Breakouts from the base of the tumulus coincided with geodetic changes at Kīlauea’s summit, and could be reasonably forecast on a time scale of about a day. The sinuous tumulus may also be an analog for similar features in New Mexico and on Mars.

Chapter 4 shifts attention to Kīlauea's ongoing (since 2008) summit eruption in Halemaʻumaʻu, describing the evolution of the active vent and, specifically, the triggering of small, impulsive explosive eruptions via wall rock collapses during 2011.

Chapter 5 presents a multidisciplinary overview of the 2011 Kamoamoa eruption (episode 59) and advances our understanding of the shallow portions of the magmatic system connecting Kīlauea's summit and Puʻu ʻŌʻō.

Chapter 6 weaves the dissertation's conclusions into the broader volcanological context and suggests possible avenues for further research.

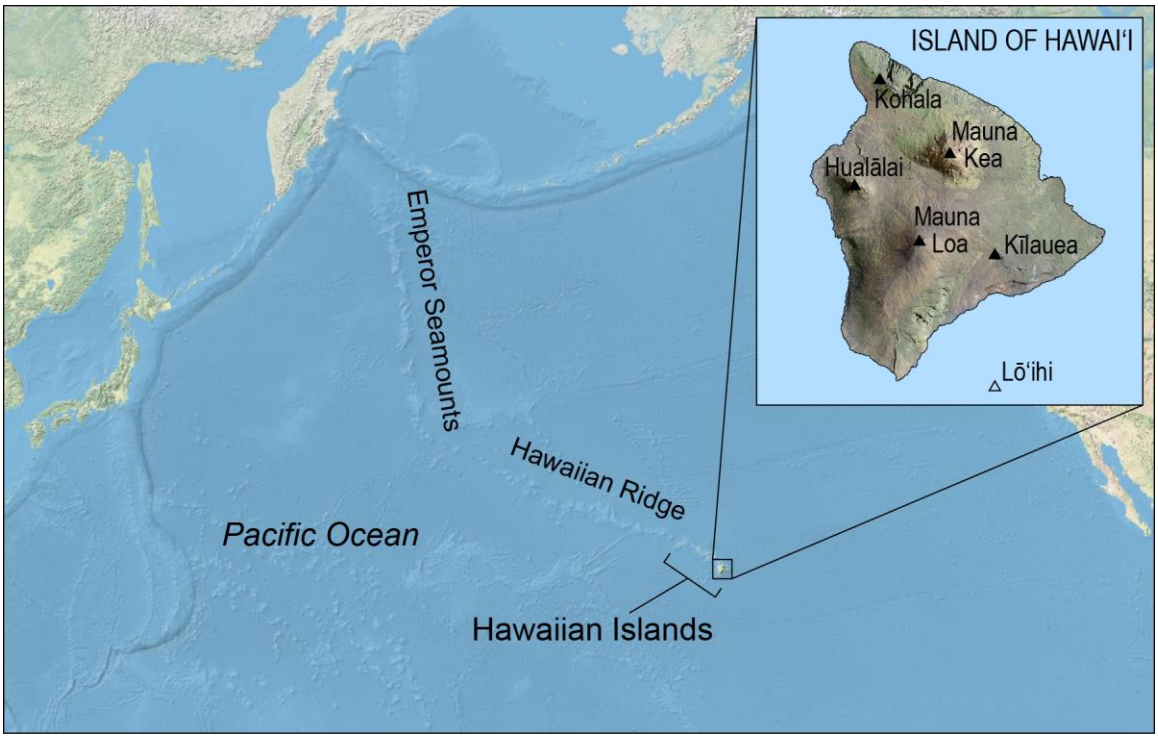

Figure 1.1 Map of northern Pacific Basin, showing Emperor Seamounts, Hawaiian Ridge, and Hawaiian Islands. Base map generated through ESRI World Physical Map service. (Inset) Map of island of Hawaiʻi showing summits of its volcanoes.

1.2 Kīlauea magmatic system and structure

Kīlauea Volcano is the youngest and southeastern-most of the five volcanoes that compose the island of Hawaiʻi. Hawaiʻi itself is at the southeast end of the Hawaiian-Emperor chain of seamounts and islands that extends across the Pacific Ocean (Fig. 1.1)

and records some 70 m.y. of volcanic activity (Clague and Dalrymple, 1987). Kīlauea is built on the southeastern flank of Mauna Loa (Fig. 1.2), and the two volcanoes interact in a complex and not yet well understood way that modulates their respective eruptive activity (Miklius and Cervelli, 2003; Trusdell, 2011). South of Kīlauea is Lō‘ihi Seamount, the youngest active volcano in the chain. Eruptive activity at Kīlauea is fed by basaltic magma thought to rise from a zone of partial melting at depths of 60 to 90 km in the upper mantle (e.g., Eaton and Murata, 1960; Wright, 1984; Wyllie, 1988; Sen and Jones, 1990; DePaolo and Stolper, 1996) and then collects within storage reservoirs ~1–5 km beneath Kīlauea’s summit (e.g., Fiske and Kinoshita, 1969; Ryan, 1987; Baker and Amelung, 2012; Poland et al., 2014; Wright and Klein, 2014). From there, magma can erupt within Kīlauea’s summit caldera or along either of its two sub-radial rift zones (the East and Southwest Rift Zones), or rarely in the Koa‘e fault system that connects the two rift zones (Fig. 1.2). In additional to these major structural features, the south flank of Kīlauea is also broken by large intersecting faults that form a series of steep, south-facing scarps in the Hilina fault system (Fig. 1.2).

1.3 Early eruptive history

Most of Kīlauea is surfaced by tube-fed pāhoehoe lava flows erupted since about 1000 CE (Holcomb, 1987). Recent studies show that this effusive period was preceded by an interval lasting about 1200 yr (ca. 200 BCE to 1000 CE) that was dominated by explosive activity, which produced the Uwēkahuna Tephra (Fiske et al., 2009). The effusive activity of the last millennium was interrupted by explosive eruptions between ca. 1500 and 1800 CE, probably following the formation of the present summit caldera, which formed the Keanakāko‘i Tephra (Swanson et al., 2012). This repeated alternation between effusive and explosive activity suggests a cyclicity to Kīlauea’s eruptive activity—one represented by shield-building and lava overflows during prolonged periods of relatively high magma supply, and a deep caldera and explosive activity during prolonged periods of relatively low supply (Swanson et al., 2014). Other layers of ash interbedded with lava flows exposed in fault scarps on Kīlauea’s south flank (Easton, 1987) could be interpreted to mean that this cyclicity, in some form, extends back at least 50 ka.

Kīlauea's written historical period begins in 1823 (Ellis, 1963), shortly after ca. three centuries of mostly explosive activity ceased at the summit and shortly after eruption of the Keaīwa Lava Flow of 1823 from Great Crack on Kīlauea's Southwest Rift Zone (Ellis, 1963, pg. 165; Stearns, 1926). The Keaīwa Lava Flow is the youngest of several relatively young lava flows that may have been erupted shortly after (and perhaps during) the ca. 1500–1800 CE explosive period (e.g., the Kamoʻoaliʻi Lava Flow; Stearns, 1926), though the timing of these flows is far from certain. Upon arrival at Kīlauea's summit in 1823, Ellis found that the caldera contained a ~120-m-deep central crater surrounded by a narrow ledge of fresh black lava and surmised that lava had recently filled the caldera to that level before emptying through fractures (along the SWRZ) and feeding the Keaīwa Lava Flow (Ellis, 1963, pg. 165). According to Ellis's Hawaiian guides, similar eruptions had happened ever since the end of the ca. 1500–1800 CE explosive period (Ellis, 1963, pg. 171).

These observations imply another form of cyclicity—one characterized by repeated episodes of slow caldera filling and pressurization followed by the abrupt diversion of magma into the rift zones, as first envisioned by Dana (1887). Taken to the extreme, this cyclicity could have occurred throughout the ca. 1500–1800 CE explosive period, with repeated emptying of the summit reservoir dropping the caldera floor below the level of the water table (now ~615 m below Kīlauea's summit; Keller et al., 1979; Mastin, 1997), leading to sequences of explosions, followed by lava partly filling the caldera again to restart the cycle. This interpretation is supported by the presence of juvenile tephra within most units of the Keanakākoʻi Tephra (e.g., McPhie et al., 1990; Swanson et al., 2012). Such a cycle may have occurred during 1790 CE, perhaps with lava erupting low on Kīlauea's East Rift Zone (Ellis, 1963) and accompanied by collapse of the summit caldera, which led to deadly explosions (e.g., Swanson et al., 2015).

From this interpretation, it may be that other relatively young lava flows exposed along Kīlauea's East and Southwest Rift Zones, though not definitively dated to this time period, could be the products of successive fillings and drainage of the summit caldera as suggested for the Keaīwa Lava Flow. Regardless, this cyclical process continued over the decades following Ellis's visit (summarized below from Macdonald (1955) and Wright and Klein (2014)). After 1823, the caldera slowly refilled again, reaching a level about 15

m above that seen by Ellis, before collapsing in concert with an eruption on Byron Ledge in 1832. The caldera quickly began to refill with lava, and by 1840, the resurrected caldera floor had overflowed the previous black ledge and defined a broad 30-m-high dome centered near the present Halemaʻumaʻu site.

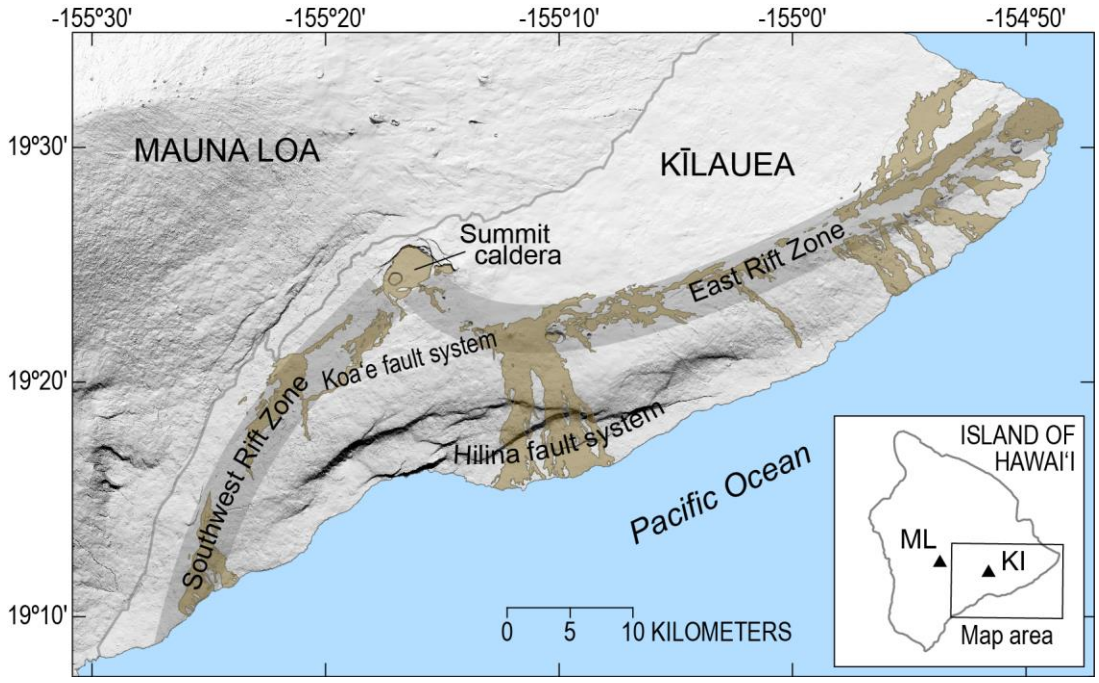

Figure 1.2 Shaded relief map of Kīlauea Volcano, showing major structural features and lava flows erupted 1790–1982 (brown). (Inset) Map of island of Hawaiʻi showing summits of Mauna Loa (ML) and Kīlauea (KI) volcanoes and map area.

This caldera floor subsequently dropped during eruption of the 1840 lava flow in the East Rift Zone. Afterward, caldera filling resumed and lava overtopped the previous high stand by 1846. Filling was accompanied by endogenous uplift, which built a 1-km-wide dome up to 90 m high, topped by an overflowing lava lake, on the caldera floor. Rubble that had accumulated around the base of the inner crater was pushed up by the uplift, creating a discontinuous 15- to 30-m-high collar of fragmented rock around the dome. The caldera floor dropped again in 1868, in association with simultaneous eruptions in Kīlauea Iki and the Southwest Rift Zone. Subsequent refilling was interrupted by major drainages in 1886, 1891, and 1894, all near Halemaʻumaʻu, but none

were association with an eruption. This marked the end to what was at least a century of cyclic behavior; the following interval from 1894 to 1907 marked a period of relative quiescence.

Nearly continuous eruptive activity focused at Halemaʻumaʻu returned in 1907, punctuated by filling and drainage at Halemaʻumaʻu in 1916 (no associated rift zone eruption), 1919 (coupled with Halemaʻumaʻu overflows and the Mauna Iki eruption in the Southwest Rift Zone), 1922 and 1923 (during middle East Rift Zone eruptions), and 1924 (coinciding with a lower East Rift Zone intrusion and summit collapse and explosions at Halemaʻumaʻu). Activity was again cyclic during this period, though focused at Halemaʻumaʻu, with relatively high summit lava levels culminating usually in rift zone eruptions. The period came to an end with drainage of Halemaʻumaʻu and attendant explosive eruptions in 1924, which caused major disruption to Kīlauea's magmatic system.

Seven brief eruptions occurred at the summit during the next decade, followed by a long quiescence that ended in 1952 when activity briefly returned to Halemaʻumaʻu. Rather than returning to the nearly continuous summit activity that characterized most of the 19th and early 20th centuries, the ensuing Kīlauea eruptions generally lasted only hours to weeks. The longest eruption of this period, until the onset of the Mauna Ulu eruption in 1969, was the 1967–1968 summit eruption in Halemaʻumaʻu, which lasted about 8 months.

The 1969–1974 Mauna Ulu flank eruption, which occurred in several stages, broken by a 3-month hiatus and briefly interrupted by eruptions at the summit and the upper parts of both rift zones, alerted scientists to the potential for long-lived rift zone eruptions. The Mauna Ulu eruption was followed by several more short-lived eruptions in the summit area and along the rift zones before the onset of the Puʻu ʻŌʻō eruption in 1983. The Puʻu ʻŌʻō eruption is ongoing as of August 2015.

1.4 The Pu‘u ‘Ō‘ō eruption

1.4.1 1983–1986: High fountaining at Pu‘u ‘Ō‘ō

The Pu‘u ‘Ō‘ō eruption (Fig. 1.3) began on January 3, 1983, following 24 hours of elevated East Rift Zone seismicity in the area of the eventual eruption site—an 8-km-long fissure system that first reached the surface about 15 km down-rift of the summit. After activity initially jumped from one fissure to another (episodes 1–3; Wolfe et al., 1988), it localized at a single vent, Pu‘u ‘Ō‘ō, in June 1983. Thereafter, a series of moderate to high lava fountains produced short-lived ‘a‘ā flows that buried much of the surrounding area (episodes 4–47; Fig. 1.4a; Table 1.1; Wolfe et al., 1988; Heliker et al., 2003). Tephra fallout and lava from this vent built the Pu‘u ‘Ō‘ō cone, which grew to a height of 255 m above the pre-eruption landscape by 1986 (Wolfe et al., 1988; Heliker et al., 2003).

1.4.2 1986–1992: Continuous effusion from Kupaianaha

In July 1986, the conduit beneath Pu‘u ‘Ō‘ō ruptured and fed fissures for about a day both up-rift and down-rift of Pu‘u ‘Ō‘ō (Table 1.2). The following day, a new fissure opened 3 km down-rift of Pu‘u ‘Ō‘ō. Sustained eruption from this fissure eventually formed the Kupaianaha lava shield (Fig. 1.4b). This shift in the eruption to a down-rift vent marked a change in eruptive style from episodic Hawaiian fountaining to nearly continuous effusion (episode 48; Table 1.1). A broad, tube-fed pāhoehoe flow field developed over the next 5.5 years, extending southeast from the vent into the ocean and eventually engulfing the community of Kalapana in 1990 (Heliker and Wright, 1991; Mattox et al., 1993; Hon et al., 1994). During effusion from Kupaianaha, the vent at Pu‘u ‘Ō‘ō widened progressively and formed a crater that often contained a small lava lake (Heliker et al., 1998, 2003).

Lava effusion from Kupaianaha began to decline in mid-1990 (Kauahikaua et al., 1996), and activity at Pu‘u ‘Ō‘ō waxed commensurately, presumably as the conduit between the two vent systems became progressively blocked (Mangan et al., 1995). The Pu‘u ‘Ō‘ō lava lake rose 65 m during this period and flooded the surrounding crater floor, and the summit of Kīlauea began to inflate (Kauahikaua et al., 1996). These changes were accompanied by several small intrusions into Kīlauea’s upper East Rift Zone (Table

1.2). In November 1991, the lava lake withdrew and the crater floor fell 75 m as a fissure opened between Puʻu ʻŌʻō and Kupaianaha and erupted for three weeks (episode 49; Fig. 1.4b; Table 1.2; Mangan et al., 1995; Heliker and Mattox, 2003). Lava reappeared in Puʻu ʻŌʻō a few days after the fissure eruption and refilled the crater to its previous level within weeks. The eruptive output from Kupaianaha, which dropped dramatically during episode 49, continued to fall thereafter and finally ceased altogether on February 7, 1992 (Kauahikaua et al., 1996).

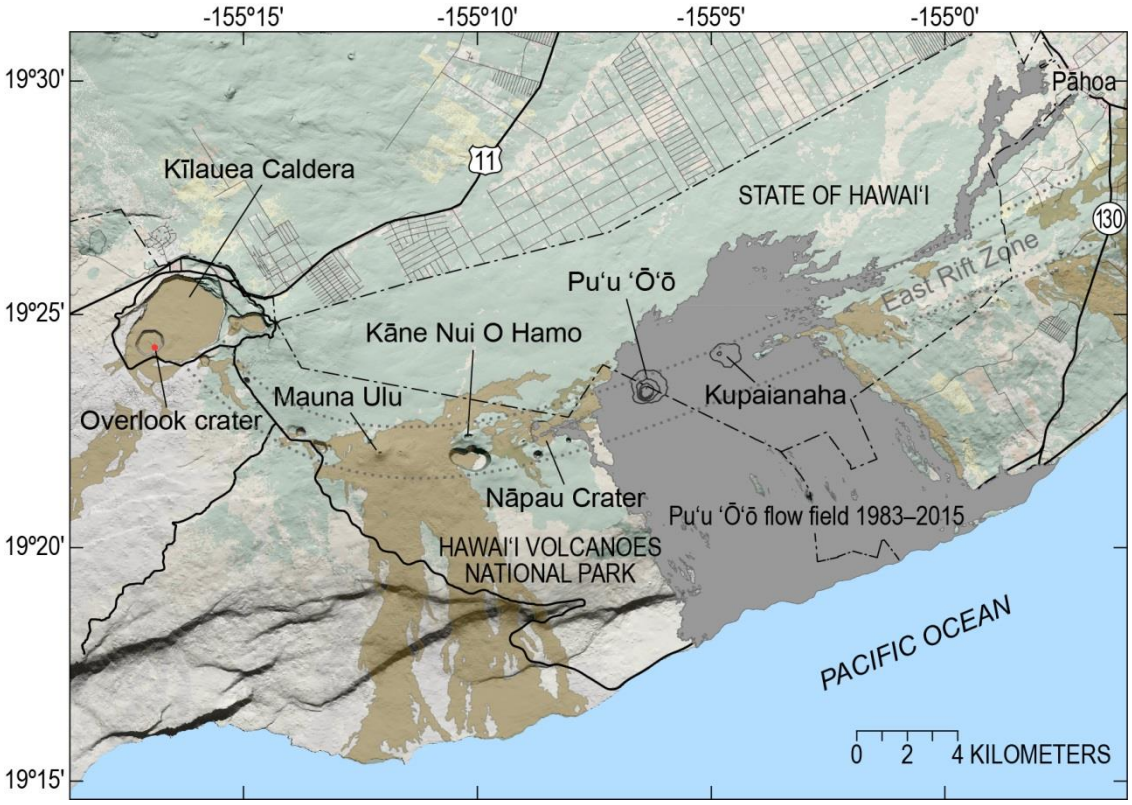

Figure 1.3 Map of Kīlauea's summit caldera and upper and middle East Rift Zone showing location of lava flows and road network. Gray, ongoing Puʻu ʻŌʻō eruption (as of August 2015); brown, older historical flows; red, active summit lava lake (ongoing since 2008). Lands managed by Hawaiʻi Volcanoes National Park and the State of Hawaiʻi are outlined. Base map is a partly transparent regional land cover map from National Oceanic and Atmospheric Administration draped over a 10-m digital elevation model.

Table 1.1 Eruption statistics for episodes 1–61 of Pu‘u ‘Ō‘ō eruption as of August 31, 2015

Episode	Repose period before episode (days)	Episode start Date (mm/dd/yy)	Episode start Time (HST)	Episode end Date (mm/dd/yy)	Episode end Time (HST)	Duration (days)	Subaerial lava coverage (km^2)	DRE volume ($\times 10^6$ m^3)
1–47		01/03/83	0031	06/26/86	1635	1,207.7	39.8	387
48–49		07/18/86	1205	02/07/92	(0000)	2,030	47.8	505
50–53		02/17/92	~1930	01/29/97	1852	1,808	32.7	618
54 (Nāpau eruption)		01/30/97	0240	01/31/97	0033	0.9	0.2	0.3
55	24.3	02/24/97	~0700	06/21/07	(0000)	3,768	62.1	1,660
Crater filling		02/24/97	~0700	03/28/97	~1430	32	—	—
Ep 55 flow		03/28/97	~1430	08/17/02	(0000)	1,967	38.3	—
Mother’s Day flow		05/12/02	~0835	09/23/04	(0000)	865	22.8	—
MLK flow		01/18/04	0554	01/24/04	(0000)	56	0.4	—
PKK flow		03/20/04	2112	06/21/07	(0000)	1,188	30.9	—
56 (Father’s Day eruption)		06/19/07	0015	06/19/07	0045	0.02	0.002	[0.001]
57–58	12.7	07/01/07	~1800	03/07/11	(0000)	1,344	40.6	630
Crater filling		07/01/07	~1800	07/20/07	2355	19	0.07	[1.05]
Perched channel flow (58a)		07/21/07	0006	02/10/08	(0000)	204	10.3	—
TEB flow (58b)		11/21/07	0604	03/07/11	(0000)	1,202	30.6	—
59 (Kamoamoa eruption)		03/05/11	1709	03/09/11	2230	4.2	1.4	[2.7]
60	16.5	03/26/11	1009	08/15/11	(1200)	142	2.3	40
Crater filling (60a)		03/26/11	1009	08/03/11	1418	130.2	0.03	—
August 3rd breakout (60b)		08/03/11	1418	8/15/11	(1200)	12	2.3	—

Table 1.1 (Continued) Eruption statistics for episodes 1–61 of Pu‘u ‘Ō‘ō eruption as of August 31, 2015

Episode	Repose period before episode (days)	Episode start Date (mm/dd/yy)	Episode start Time (HST)	Episode end Date (mm/dd/yy)	Episode end Time (HST)	Duration (days)	Subaerial lava coverage (km^2)	DRE volume ($\times 10^6$ m^3)
61	5.2	08/20/11	1715	ongoing	—	—	22.1	~250
Crater filling (61a)		08/20/11	1715	09/21/11	0220	31.4	0.05	—
Peace Day flow (61b)		09/21/11	0220	11/07/13	(0000)	778	16.1	—
Kahauale‘a 1 flow (61c)		01/19/13	1123	04/18/13	(1200)	89	2.6	—
Kahauale‘a 2 flow (61d)		05/06/13	1719	6/28/14	(0000)	417	10.2	—
June 27th flow (61e)		06/27/14	0700	ongoing	—	—	21.0	—
Total							141.9	~4,093

Notes: Episodes 1–54, shown in detail in Heliker and Mattox (2003), are grouped here into appropriate categories based on eruption style and (or) location. Episodes 55–61 are subdivided to highlight significant flows and eruptive periods. Imprecise episode end times are shown in parentheses to indicate activity stopped overnight (0000; at the start of the day listed) or during the day (1200). In these cases, duration is rounded to the nearest day. Determination of lava volumes for episodes 1–54 is as described in Heliker and Mattox (2003). Determination of lava volumes for subsequent episodes are derived from SO_2 emissions as described by Sutton et al. (2003) and Elias and Sutton (2012), except for volumes in brackets, which were calculated from mapped surface area and estimated thickness, assuming 25% vesicularity. Because flows overlap, total subaerial coverage is for entire composited flow field.]

1.4.3 1992–1997: Flank vents and shield building at Puʻu ʻŌʻō

New eruptive vents formed on the west flank of the Puʻu ʻŌʻō cone ten days after Kupaianaha stopped erupting. This new period in the eruption, comprising episodes 50–53 (Fig. 1.4c; Table 1.1), saw the progressive burial of the west and south flanks of Puʻu ʻŌʻō beneath a lava shield and the nearly continuous eruption of lava to widen the existing tube-fed pāhoehoe flow field south of the rift zone (Heliker et al., 1998; Heliker and Mattox, 2003). The lava level within Puʻu ʻŌʻō varied widely over this time period, with subsidence and drainage events accompanying intrusive activity along the upper East Rift Zone (Table 1.2; Clague and Heliker, 1993; Okubo et al., 1996; Heliker et al., 1998, 2003).

Episode 53 ended on January 29, 1997, with an intrusion up-rift of Puʻu ʻŌʻō in, and adjacent to, Nāpau Crater (Table 1.2; Owen et al., 2000; Thornber et al., 2003; Heliker and Mattox, 2003). In response, the floor of Puʻu ʻŌʻō crater, originally 60 m below the northeast rim, dropped 150 m, and part of the western wall of the Puʻu ʻŌʻō cone collapsed. The intrusion culminated in a brief eruption, episode 54 (Fig. 1.4c; Table 1.1), which lasted for less than a day and was followed by a 24-day hiatus in eruptive activity (Heliker and Mattox, 2003).

1.4.4 1997–2007: Resumption of flank vents and shield building

Lava reappeared within Puʻu ʻŌʻō crater in late February 1997, marking the onset of episode 55 (Fig. 1.4d; Table 1.1), and rose to within 50 m of the crater's northeast rim before new vents opened and began to erupt on the west and south flanks during March–July (Heliker et al., 2003). The lava level in Puʻu ʻŌʻō fluctuated dramatically during this period but by June had risen high enough to flow over the crater rim for the first time since high fountaining ended in 1986 (Heliker and Mattox, 2003). Intermittent overflows continued until early 1998, even though a single dominant vent on the south side of the Puʻu ʻŌʻō cone was sending tube-fed flows southeast to the ocean by July 1997. The episode 55 lava tube was active until September 12, 1999, when an intrusion into Kīlauea's upper East Rift Zone triggered subsidence and drainage at Puʻu ʻŌʻō (Table

1.2; Cervelli et al., 2002). The crater floor dropped 65 m, stabilizing 120 m below the crater's northeast rim.

Lava reappeared at the bottom of Puʻu ʻŌʻō a few days after the intrusion and began to fill the crater. When the lava had reached within 65 m of the crater's northeast rim, 11 days after the September 12 intrusion, it began to erupt from a vent outside the crater, and the upper few kilometers of the episode 55 lava tube system were reoccupied. A string of rootless shields formed above breakout points along this tube section during its reoccupation and continued to grow during the months that followed, eventually merging to form a broad, ~2-km-long ridge that marked the trace of the tube. The crater at Puʻu ʻŌʻō filled to within 40 m of the northeast rim over the same period, and a new tube system developed, extending downslope from the rootless shields to the coastline southeast of Puʻu ʻŌʻō. Another intrusion occurred in the upper East Rift Zone in February 2000, resulting in an hours-long pause in eruptive activity, but Puʻu ʻŌʻō was not obviously affected otherwise.

The lava tube system began to deteriorate in December 2001, and rootless shields started growing over a branch of the tube (which by then had captured all discharge) in the same general area as, but just east of, the rootless shields that formed in 1999. The new rootless shields grew through April 2002, coalescing to form a 2.7-km-long ridge above the tube. At the same time, lava flows in Puʻu ʻŌʻō filled the crater to within 12 m of its northeast rim between January and April 2002. On May 12, 2002, the southwest flank of Puʻu ʻŌʻō ruptured, and lava poured out to form the Mother's Day flow (Table 1.1). By August, the new flow had captured the entire eruptive output from Puʻu ʻŌʻō and was transporting lava southeast to the ocean. The episode 55 vent established in 1997, and waning for months, was finally abandoned in August 2002.

In late 2003, after more than a year of relative stability, the lower reaches of the Mother's Day tube system began to atrophy during an increase in magma supply to the volcano (Poland et al., 2012) and, as in late 2001–early 2002, rootless shields began to grow along the active part of the lava tube closer to Puʻu ʻŌʻō. Eruptive activity at Puʻu ʻŌʻō also began to increase, and the crater filled until lava overtopped both the east and west crater rims. On January 18, 2004, a new vent opened on Puʻu ʻŌʻō's south flank,

Table 1.2 Kīlauea East Rift Zone intrusions, July 1986–present.

Intrusion Date	Volume ($\times 10^6$ m^3)	Comment
[July 18–20, 1986]		Episode 48 fissure eruption; intrusion from dike beneath Puʻu ʻŌʻō; precursory summit inflation
December 4, 1990		Upper East Rift Zone intrusion; eruptive activity increase at Puʻu ʻŌʻō; precursory summit inflation and upper East Rift Zone seismicity
March 26, 1991		Upper East Rift Zone intrusion; precursory summit inflation and upper East Rift Zone seismicity
August 21, 1991		Upper East Rift Zone intrusion; precursory summit inflation and upper East Rift Zone seismicity
[November 8, 1991]		Episode 49 fissure eruption; intrusion from Puʻu ʻŌʻō
Puʻu ʻŌʻō crater subsidence	(3.1) [3]	storage; precursory summit inflation
[February 17, 1992]		Episode 50 fissure eruption; intrusion from Puʻu ʻŌʻō
Puʻu ʻŌʻō lava lake draining	(~0.2) [9]	storage; precursory summit inflation
March 3, 1992		Upper East Rift Zone intrusion; precursory summit
Puʻu ʻŌʻō lava lake draining	(~0.1) [9]	inflation; episode 50 terminated
February 7–8, 1993		Upper East Rift Zone intrusion; no obvious precursors;
Puʻu ʻŌʻō crater subsidence	(3.1) [3]	episode 51 terminated
January 29–30, 1997		Middle East Rift Zone intrusion; Nāpau fissure
Puʻu ʻŌʻō crater subsidence	(13) [3]	eruption (episode 54); no obvious precursors;
Halemaʻumaʻu reservoir loss	(1.5) [1]	passive rift opening [1]; episode 53 terminated
Makaopuhi reservoir loss	(0.12) [1]	
Episode 54 erupted volume	0.3 [4]	
Dike volume	23 [1]	
September 12, 1999		Upper East Rift Zone intrusion; no obvious precursors;
Puʻu ʻŌʻō crater subsidence	(<1) [3]	passive rift opening [2]
Dike volume	3.3 [2]	
February 23, 2000		Upper East Rift Zone intrusion; no obvious precursors
[May 12, 2002]		Intrusion from Puʻu ʻŌʻō storage; Mother's Day breakout; precursory summit inflation, upper East Rift Zone seismicity, and Puʻu ʻŌʻō filling
[January 18, 2004]		Intrusion from Puʻu ʻŌʻō storage; MLK breakout; precursory summit inflation, upper East Rift Zone seismicity, and Puʻu ʻŌʻō filling

Table 1.2 (Continued) Kīlauea East Rift Zone intrusions, July 1986–present.

Intrusion Date	Volume ($\times 10^6$ m^3)	Comment
June 17–19, 2007		Upper and middle East Rift Zone intrusion; Father's Day eruption (episode 56); precursory summit inflation and upper East Rift Zone seismicity; episode 55 terminated
Pu‘u ‘Ō‘ō crater subsidence	(4.2) [8]	
Halema‘uma‘u reservoir loss	(1.8) [6]	
Pu‘u ‘Ō‘ō reservoir loss	(0.02) [6]	
Episode 56 erupted volume	0.001 [5]	
Dike volume	16.6 [6]	
[July 21, 2007]		Intrusion from Pu‘u ‘Ō‘ō storage; episode 58 fissure eruption; precursory summit inflation, upper East Rift Zone seismicity, and Pu‘u ‘Ō‘ō filling
Pu‘u ‘Ō‘ō crater subsidence	(1.3) [9]	
March 2011		Middle East Rift Zone intrusion; Kamoamoa fissure; precursory summit inflation, upper East Rift Zone seismicity, and Pu‘u ‘Ō‘ō and Halema‘uma‘u filling
Pu‘u ‘Ō‘ō crater subsidence	(5.5) [10]	
Summit lava lake draining	(0.8) [10]	
Halema‘uma‘u reservoir loss	(1.7) [7]	
Episode 59 erupted volume	2.7 [10]	
Outgassed volume	7.6 [10]	
Dike volume	15.6 [7]	
[August 3, 2011]		Intrusion from Pu‘u ‘Ō‘ō storage; Pu‘u ‘Ō‘ō flank breakout; precursory summit inflation, upper East Rift Zone seismicity, and Pu‘u ‘Ō‘ō and Halema‘uma‘u filling
Pu‘u ‘Ō‘ō crater subsidence	(2.5) [10]	
[September 21, 2011]		Intrusion from Pu‘u ‘Ō‘ō storage; Peace Day fissure eruption; precursory summit inflation, upper East Rift Zone seismicity, and Pu‘u ‘Ō‘ō and Halema‘uma‘u filling
Pu‘u ‘Ō‘ō crater subsidence	(1.0) [10]	
October 2012		Upper East Rift Zone intrusion; precursory summit inflation and upper East Rift Zone seismicity
Summit lava lake draining	(0.2) [9]	

Notes: Intrusions identified by seismic swarms in combination with (in most cases) summit deformation. Intrusions in brackets fed from Pu‘u ‘Ō‘ō magma storage; intrusions not in brackets fed from summit or East Rift Zone storage up-rift from Pu‘u ‘Ō‘ō. Volume losses shown in parentheses; footnotes indicate sources.

Source: [1]Owen et al., 2000; [2]Cervelli et al., 2002; [3]Heliker et al., 2003; [4]Thornber et al., 2003; [5]Poland et al., 2008a; [6]Montgomery-Brown et al., 2010; [7]Lundgren et al., 2013; [8]Chapter 2; [9]Hawaiian Volcano Observatory data; [10]Chapter 5

marking the onset of the short-lived Martin Luther King (MLK) flow (Table 1.1). Eruptive activity in Puʻu ʻŌʻō crater stopped at the same time, and the crater floor sagged by about 5 m.

The cessation of activity within Puʻu ʻŌʻō did not last, however, and lava was again erupting on the crater floor by early February 2004. This was followed by a brief resurgence of activity from the MLK vent in mid-February. In March, the Prince Kūhiō Kalanianaʻole (PKK) flow (Table 1.1) broke out from the lower south flank of Puʻu ʻŌʻō, finally relieving the pressure beneath the cone and marking the end of rootless shield growth along the Mother's Day tube system, which remained active until September 2004, when the Mother's Day vent finally died. This activity was supplanted by the PKK flow, which increased in vigor as the Mother's Day flow waned. The PKK flow reached the ocean southeast of Puʻu ʻŌʻō in November 2004, setting up a tube system which remained relatively stable for the next 2.5 years—until June 2007.

1.4.5 2007–2011: Down-rift migration to the episode 58 vent

An intrusion into Kīlauea's East Rift Zone near Mauna Ulu during June 17–19, 2007 (Table 1.2), resulted in the subsidence of Puʻu ʻŌʻō's crater floor, which dropped about 80 m, and culminated in a brief eruption on the northeast flank of Kāne Nui o Hamo lava shield (Father's Day eruption—episode 56; Fig. 1.4d; Table 1.1; Poland et al., 2008a; Fee et al., 2011). A 12-day hiatus in activity followed, ending with the return of lava to Puʻu ʻŌʻō on July 1 (episode 57; Table 1.1; see Chapter 2). The subsequent refilling of Puʻu ʻŌʻō crater was accompanied by several meters of endogenous uplift of the crater floor—evidence of pressure building beneath the cone. This pressure was relieved with the opening of fissures between Puʻu ʻŌʻō and Kupaianaha on July 21, 2007 (episode 58; Fig. 1.4e; Tables 1.1 and 1.2; Poland et al., 2008a). Activity quickly localized at the eastern end of the fissure system—the main episode 58 vent—and built a lava shield and a ~2-km-long "perched" lava channel, up to ~50 m above the preexisting surface (Patrick et al., 2011a). The channel facilitated flow advancement toward the northeast, sparking lava-inundation concerns in populated areas downslope along the East Rift Zone (Kauahikaua, 2007).

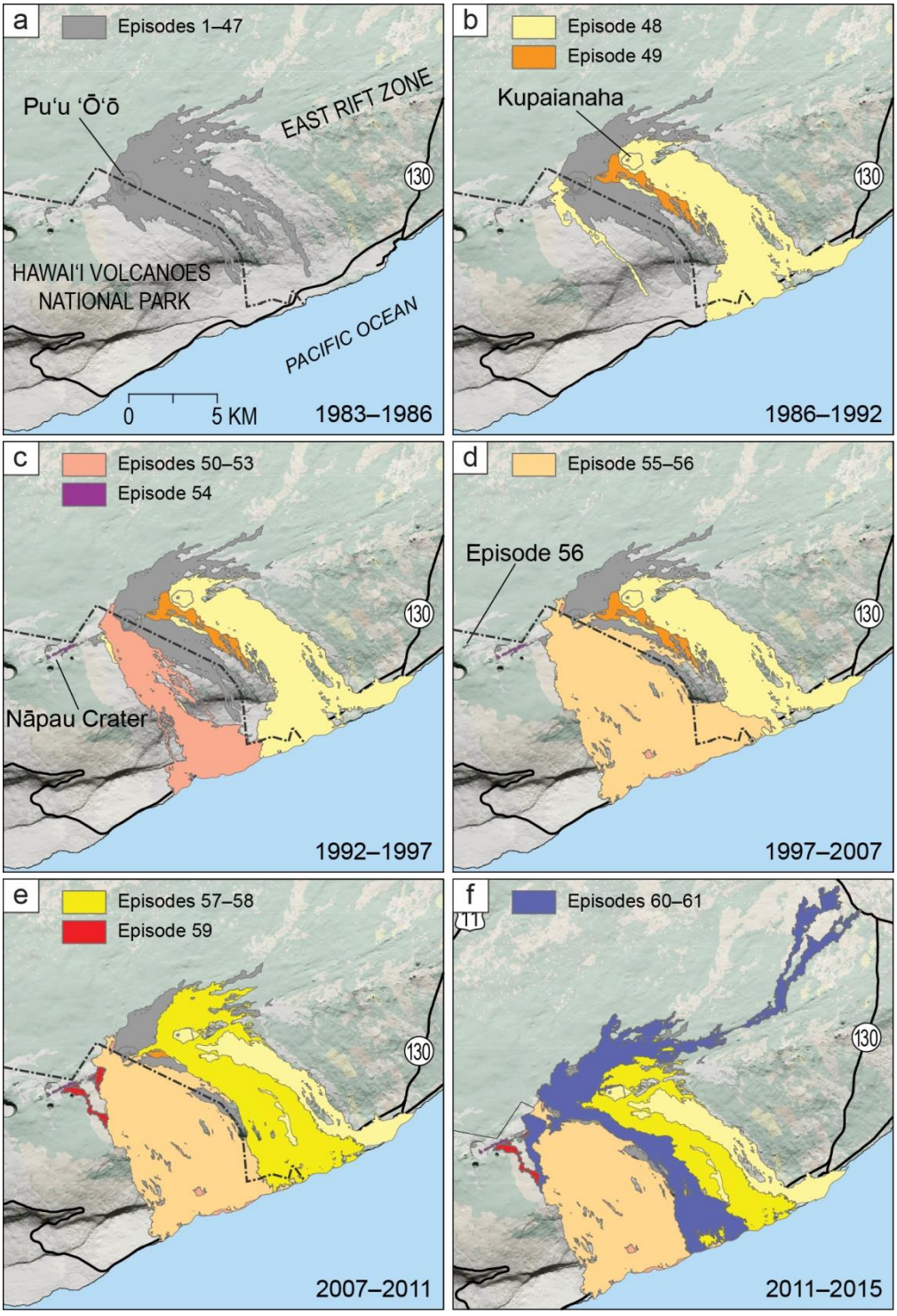

Figure 1.4 Maps of Kīlauea's middle East Rift Zone showing flows erupted 1983–2015 , subdivided by flows emplaced during (a) 1983–1986, (b) 1986–1992, (c) 1992–1997, (d) 1997–2007, (e) 2007–2011, and (f) 2011–2015, shifted to show full extent of episodes 60–61.

In November 2007, the southern flank of the shield ruptured over the episode 58 vent, and flows northeast of the vent stagnated as lava was diverted southeastward. At first, a series of rootless shields grew over the developing lava tube (Patrick and Orr, 2012), but this growth stopped after the flow reached the ocean near Kalapana in March 2008. Thereafter, the lava tube system transported lava to the ocean until early 2011 (see Chapter 3). It was during this period, in March 2008, that an eruptive vent (the Overlook vent) opened in Halemaʻumaʻu Crater, at Kīlauea's summit (Fig. 1.3; Wilson et al., 2008; Patrick et al., 2013; see Chapter 4). This marked the start of the first recorded instance of simultaneous, extended summit and rift eruptions at Kīlauea.

1.4.6 2011–2014 Shifting vents; flows transition to northeast

Puʻu ʻŌʻō's crater began filling with lava in mid-2010, mirrored by a rising summit lava lake at the Overlook vent, as well as by inflation and an increase in upper East Rift Zone seismicity. These increases culminated in a 4-day-long eruption between Puʻu ʻŌʻō and Nāpau Crater starting March 5, 2011 (Kamoamoa eruption—episode 59; Fig. 1.4e; Table 1.1; see Chapter 5). Puʻu ʻŌʻō's crater floor dropped 113 m and the lava lake in Halemaʻumaʻu dropped 143 m during the first day, and the eruption was followed by a 16-day hiatus in East Rift Zone eruptive activity.

Lava reappeared in Puʻu ʻŌʻō in late March 2011, and overflows from a slowly rising lava lake began to fill the crater. The summit lava lake likewise began to rise. Starting at the beginning of July 2011, the crater floor at Puʻu ʻŌʻō began lift endogenously, forming a dome topped by a circulating lava lake. Lava, erupting from the circumferential fault bounding the uplifting crater floor, flowed out of the crater and mantled the southwest flank of the cone. Uplift ended on August 3, 2011, when a fissure opened low on the west flank of Puʻu ʻŌʻō and erupted for the next 12 days (episode 60; Fig. 1.3f; Tables 1.1 and 1.2). Puʻu ʻŌʻō's crater floor dropped about 80 m, and the summit lava lake fell about 75 m.

After another short hiatus, lava began to fill Puʻu ʻŌʻō on August 20, 2011, marking the start of episode 61 (Fig. 1.4f), and it was overflowing the crater onto both the east and west flanks of Puʻu ʻŌʻō by mid-September. Overflows ended with the opening of a fissure high on the eastern flank of Puʻu ʻŌʻō on September 21, 2011 (Peace Day

flow—episode 61b; Tables 1.1 and 1.2). In response, the eastern part of the crater floor dropped about 20 m, and the summit lava lake fell slightly. The Peace Day flow advanced southeastward and reached the coast in December, where an ocean entry was sporadically active through the end of the year.

At the beginning of 2012, activity shifted upslope, and lava did not reach the ocean again until November, nearly a year later. At about the same time, lava began to erupt sporadically at Puʻu ʻŌʻō, filling the shallow crater formed in 2011. In mid-January 2013, lava overtopped the northeast rim of Puʻu ʻŌʻō and began to flow northeastward (Kahaualeʻa 1 flow—episode 61c; Table 1.1). The Kahaualeʻa 1 flow stopped in mid-April, but a second flow overtopped the northeast rim of Puʻu ʻŌʻō in early May and sent flows back into the same area (Kahaualeʻa 2 flow—episode 61d; Table 1.1). The Peace Day flow, also active throughout this period, entered the ocean until August 2013, when its activity shifted upslope once again, probably as its discharge waned. The Peace Day flow finally died in mid-November 2013. The Kahaualeʻa 2 flow was the only active lava flow for several months thereafter, slowly advancing about 9 km northeastward.

1.4.7 2014–2015 The Pāhoa lava flow crisis

Eruptive activity from vents at Puʻu ʻŌʻō began to increase in early 2014, feeding several short-lived flows onto the flanks of Puʻu ʻŌʻō. Then, on June 27, 2014, a series of fissures erupted lava on the northeast flank of Puʻu ʻŌʻō (June 27th flow—episode 61e; Table 1.1), ending the Kahaualeʻa 2 flow. After building a perched lava pond on the northeast flank of the Puʻu ʻŌʻō cone, the June 27th flow began to advance rapidly northeastward in early July. In mid-August, the flow intersected and entered a deep ground crack in the rift zone about 11 km from the vent. Lava, out of sight, continued to advance within the ground crack, pushing the crack open further as it was filled, and eventually emerged 1 km downslope several days later. The flow entered and exited three more cracks as it advanced to the northeast.

In early September, the flow veered northward, bypassing the Kaohe Homesteads subdivision, and then turned back northeastward and began to move directly toward the town of Pāhoa. The flow eventually reached the outskirts of the town, destroying one house and partly burying a cemetery and the community's rubbish transfer station in late

October and early November. The flow stalled just 155 m from the main street through Pāhoa.

A new branch of the flow, starting from the area of the ground cracks, began moving downslope in mid-November. This branch followed a slightly more northerly path and soon began to threaten the main shopping complex in Pāhoa and State Highway 130, the main transportation route serving the eastern tip of the island. Lava reached within about 500 m of the marketplace and highway before stalling in early March 2015. Lava flows remained active northeast of Puʻu ʻŌʻō thereafter, through late 2015, but were restricted to within about 9 km of the vent.

Chapter 2

The June–July 2007 subsidence and refilling of Pu‘u ‘Ō‘ō crater, Kīlauea Volcano, Hawai‘i

Published as:

Orr, T., 2014, The June-July 2007 collapse and refilling of Pu‘u ‘Ō‘ō Crater, Kīlauea Volcano, Hawai‘i. U.S. Geological Survey Scientific Investigations Report 2014–5124, 15 p.

2.1 Introduction

As outlined in Chapter 1, Kīlauea Volcano’s long-lived Pu‘u ‘Ō‘ō eruption changed dramatically in mid-2007. An up-rift intrusion and eruption on June 17–19, 2007 (episode 56; Fig. 2.1) disrupted 10 years of nearly continuous lava effusion from vents on the southwest flank of Pu‘u ‘Ō‘ō cone. In response, the floor of Pu‘u ‘Ō‘ō crater dropped dramatically over a period of 3 days, and the eruption paused for 12 days.

Eruptive activity returned to Pu‘u ‘Ō‘ō late on July 1 (episode 57), and lava, erupting from two vents on the crater floor, was sighted on July 2. A lava lake developed on the floor of Pu‘u ‘Ō‘ō crater over the next several days as the crater began to refill. By July 8, the crater floor had begun to lift in a somewhat piston-like fashion and, eventually, uplift superseded refilling. As uplift progressed and refilling waned, new vents opened along the circumferential fractures bounding Pu‘u ‘Ō‘ō crater. Lava from these vents began to fill the West Gap and Puka Nui pits—collapse pits on the west flank of Pu‘u ‘Ō‘ō cone positioned at a higher elevation than the crater floor. Just before midnight on July 20, vent activity at Pu‘u ‘Ō‘ō ceased, and the floor of the crater began to subside rapidly. Minutes later—shortly after midnight—a new fissure eruption began on the east flank of Pu‘u ‘Ō‘ō. This marked the onset of episode 58, a new phase in the Pu‘u ‘Ō‘ō eruption that continued until March 2011. Figure 2.2 shows a timeline that highlights the main eruptive events that occurred during the June to July 2007 interval.

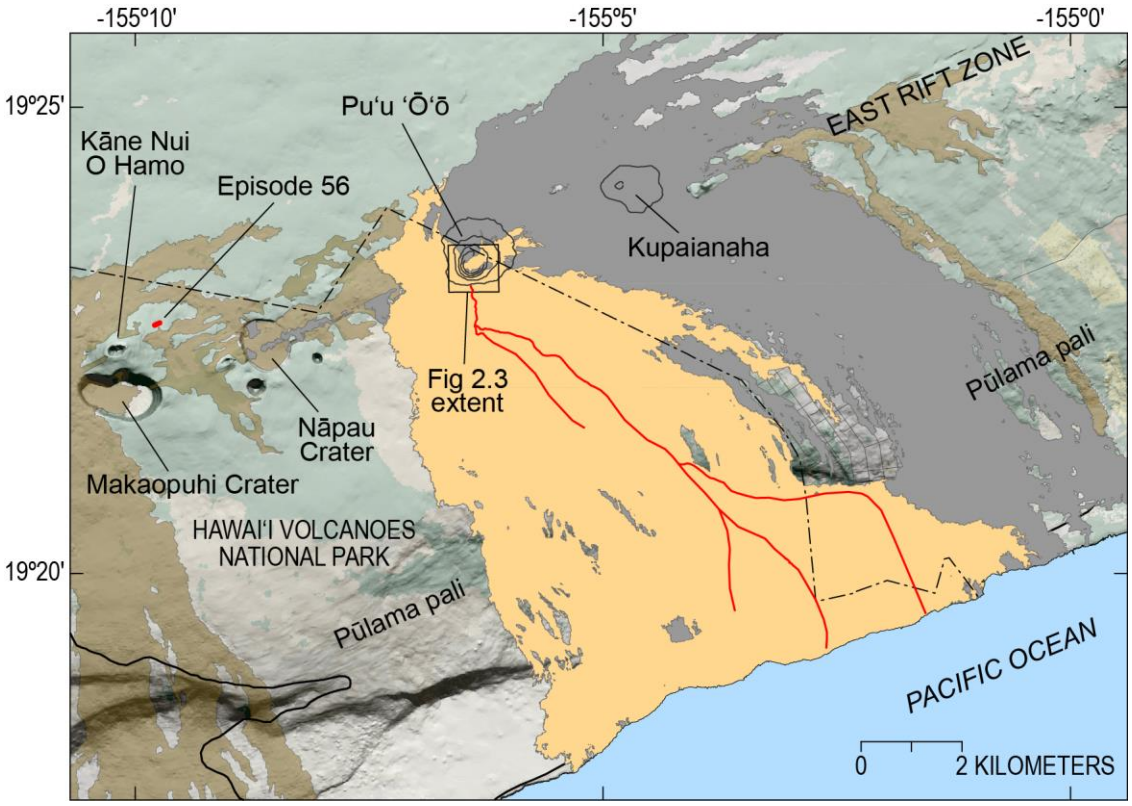

Figure 2.1 Map of Kīlauea's middle East Rift Zone showing main geographic features and Figure 2.3 map extent. Red, episode 56 eruption site; orange, episode 55 flow field); red lines, lava tube system active in 2007; gray, 1983–1997 Pu'u 'Ō'ō lava flow; brown, historical lava flows from 1790 through 1979.

We report here on the transitional interval between the June 17–19, 2007, up-rift intrusion and eruption (episode 56) and the July 21, 2007, onset of the episode 58 eruption. This brief but interesting period includes subsidence of the Pu'u 'Ō'ō crater floor following the June 17–19 event, the partial refilling of Pu'u 'Ō'ō crater as magma returned to and repressurized the shallow magma chamber beneath Pu'u 'Ō'ō (episode 57), and the second subsidence of the Pu'u 'Ō'ō crater floor, that accompanied the onset of episode 58. This sequence of events—up-rift intrusion, followed by crater subsidence and refilling, culminating in new breakouts from the flank of the cone—is a pattern that was seen in three instances at Pu'u 'Ō'ō prior to the June–July 2007 sequence discussed here, and in one instance since then. Recognition of this pattern provides important guidance for responding to future intrusions at Pu'u 'Ō'ō.

2.2 Data collection

Occasional ground observations and helicopter flights provided only brief and intermittent glimpses of the changes within Puʻu ʻŌʻō during episode 57. Gaps in field observations occurred July 8–11 and July 14–18. The entire interval was monitored by a telemetered, near real-time web-based camera (webcam) and strategically positioned digital time-lapse cameras. A continuous digital-image record, as corroborated by direct field observations, documents progressive and sudden changes in eruptive conditions within the crater that can be correlated with real-time shallow deformation near Puʻu ʻŌʻō.

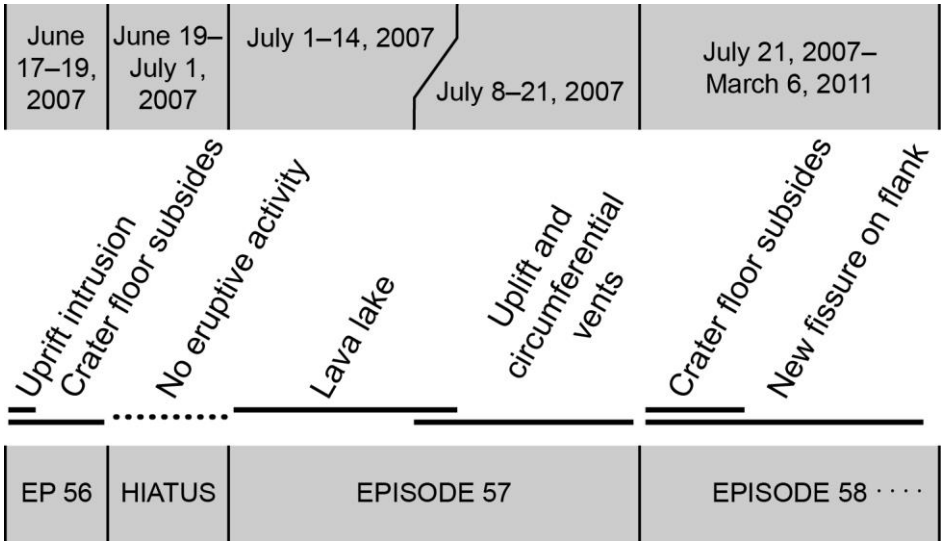

Figure 2.2 Timeline for episodes 56, 57, and 58, with emphasis on main eruptive events of June–July 2007.

The pan-tilt-zoom webcam, of the type described by Hoblitt et al. (2008), was positioned on the north rim of the Puʻu ʻŌʻō crater (Fig. 2.3) in a long-term deployment that spanned the study period. The Puʻu ʻŌʻō webcam acquired a series of three overlapping images spanning the length of the crater with a repeat interval of 1 minute. Image pixel resolution was 640 × 480. Custom time-lapse camera systems, of the type described by Orr and Hoblitt (2008), were deployed on the east and northwest rims of Puʻu ʻŌʻō (Fig. 2.3). These cameras required manual exchange of camera memory cards to retrieve data. The eastern camera photographed the eastern part of the crater, including

the East vent, with an acquisition interval of 1 minute. Operation of this camera was sporadic due to malfunctions, and image acquisition was limited to parts of June 18–19, June 21, June 25–27, July 5, and July 13. Image pixel resolution was set at 640 × 480. The northwestern camera captured images of the western part of the crater, including a partial view of the West vent, and was programmed with an acquisition interval of 1 minute and a pixel resolution of 640 × 480. This camera operated flawlessly, acquiring images for the period June 18–July 19, but subsequent images were lost when the part of the Puʻu ʻŌʻō cone on which the camera was positioned collapsed into the crater on July 21.

The webcam's angular field of view (AOV) in the vertical direction was calculated using the equation:

$$\alpha = 2 \cdot \tan^{-1}\left(\frac{d}{2 \cdot f}\right) \tag{2.1}$$

where

α represents the vertical AOV,

d represents the size of the camera's optical sensor in the vertical direction (2.4 mm for a camera with 1/4" optical sensor), and

f represents the focal length (4 mm; the focal length of the webcam at maximum wide-angle).

Solving for α, the camera's vertical AOV is found to be 33.4°. Each vertical image pixel, therefore, is equal to 0.07º (33.4º/480 pixels). The horizontal distance between the webcam and the steep southern wall of the crater, which comprised blocks of Puʻu ʻŌʻō cone, was ~245 m. At that distance, the approximate vertical size (h) of each pixel at the optical center of the webcam images was calculated at 0.3 m using the equation:

$$h = D \cdot \sin(\alpha) \tag{2.2}$$

where

D is the horizontal distance between the webcam and the southern crater wall, and

α is the vertical AOV of each pixel as solved above.

Changes in pixel size, because of the webcam view angle and crater wall slope, are small and, thus, ignored.

The y-pixel value for the intersection between new lava on the floor of the crater and the south crater wall was recorded from a webcam image captured as close in time to 1200 Hawaiian Standard Time (HST) as possible (visibility dependent) each day, starting July 4, when crater visibility first improved, through July 20, the last day before the onset of episode 58. These measurements were made along a vertical axis at an x-pixel of 320 ±5 on the middle image of the three webcam images that compose the crater panorama. Crater uplift was recorded in the same fashion, along the same centerline, using an obvious rock face above the level of infilling as a reference point.

A laser rangefinder survey on July 13 determined the vertical distance from the crater rim to feature surfaces within the crater. The east rim of the crater had a known elevation of 860 m, allowing elevations of these measured surfaces to be calculated. The dimensions of the crater, and of the lava surface accumulating within it, were estimated from existing crater maps. These data were used to calculate the volume of accumulated lava, as well as to constrain the rate of infilling and to track uplift of the crater floor by way of webcam images, as described above.

Deformation of the Puʻu ʻŌʻō edifice was recorded by an electronic borehole tiltmeter installed at a depth of ~3 m about 500 m north of the crater rim at an elevation of 700 m (Fig. 2.3). Data from this tiltmeter (designated POC) were used to infer inflation and deflation of the shallow magmatic source beneath Puʻu ʻŌʻō.

Five samples of episode 57 lava, the locations of which are shown in Figure 2.3b, were collected on July 19, 2007. Three samples were the glassy crust and drapery from the edge of lava flows (two were cold and erupted days earlier; one was warm and

probably erupted hours earlier). One sample was air-quenched spatter collected from the ground surface near an eruptive vent. One molten sample was collected by rock hammer and quenched in water. Whole-rock major analyses for all five samples were performed at the Washington State University GeoAnalytical Laboratory in Pullman, Washington (USA), using wave-length dispersive X-ray fluorescence techniques (Johnson et al., 1999). Microbeam quantitative analysis was performed on one sample by Carl Thornber at the U.S. Geological Survey Denver Microbeam Facility under the conditions described by Thornber et al. (2002).

2.3 Eruption chronology

2.3.1 Setting the stage (early 2007)

Relatively steady lava effusion from Puʻu ʻŌʻō's southwest flank vents, typical of prolonged episode 55 activity, prevailed throughout early 2007 and until the June 17 event. The floor of Puʻu ʻŌʻō crater was about 5 m below the crater's east rim, which stood at an elevation of 860 m. Several outgassing vents were present on the crater floor and within three large collapse pits (West Gap pit, Puka Nui pit, and Martin Luther King (MLK) pit) that intersected the west and southwest edges of the crater (Fig. 2.3a). Most vents were topped by spatter cones, but the easternmost (East Pond vent) was a small pit with a circulating lava lake about 20 m below the pit rim, or 25 m below the east rim of the crater at an elevation of 835 m (Figs. 2.3a and 2.4a). In addition, lava was erupting from a vent on Puʻu ʻŌʻō's southwest flank where it flowed through the Prince Kūhiō Kalanianaʻole (PKK) lava tube (Figs. 2.1 and 2.3a) to feed active surface flows and ocean entries. The vent and lava tube names discussed here are informal names used by the Hawaiian Volcano Observatory for identification purposes.

2.3.2 Crater floor subsidence at Puʻu ʻŌʻō

The subsidence of Puʻu ʻŌʻō's crater floor was preceded by an eruption (episode 56) near the Kāne Nui o Hamo lava shield on the upper East Rift Zone of Kīlauea Volcano (Fig. 2.1) on June 17–19, 2007 (Poland et al., 2008a). The subsidence disrupted 10 years of almost continuous East Rift Zone eruption (since the onset of episode 55 in

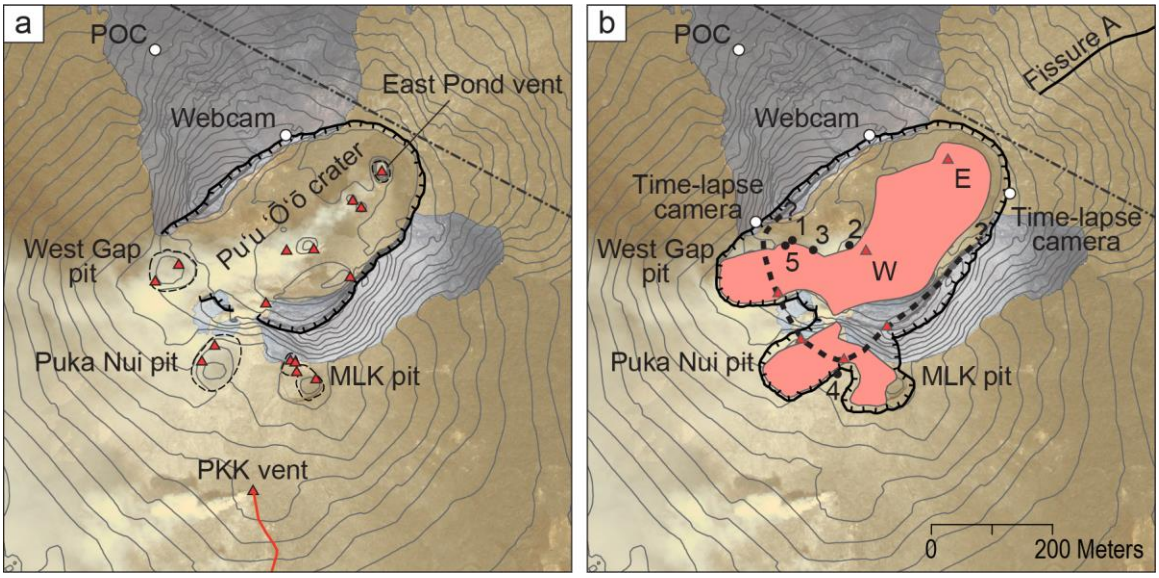

Figure 2.3 Maps of Pu‘u ‘O‘o before and after episode 57 showing crater, flank pits, active vents (red triangles), active lava tube (red line), and monitoring equipment (white circles). POC, tiltmeter; PKK, Prince Kuhio Kalaniana‘ole; MLK, Martin Luther King; hachured black line, crater rim; brown, flows erupted 1992–2007; gray, exposed Pu‘u ‘O‘o cone constructed 1983–1986. (a) Configuration of Pu‘u ‘O‘o in early 2007 before the June 17–19 intrusion. Rim buried on west and southwest side of cone by overflows from crater before 2007. (b) Configuration of Pu‘u ‘O‘o on July 21, 2007, after episode 57 ended. Pink, episode 57 flows; hachured black line, crater rim (connected to flank pits by subsidence of septa between pits and crater on June 17–19); dashed black line, approximate trace of fault accommodating uplift (question marks indicate uncertainty in continuation of fracture). Lava samples (black circles) include 1 = KE57-2647F; 2 = KE57-2649F; 3 = KE57-2650F; 4 = KE57-2651S; 5 = KE57-2652F. Also shown is southwest end of fissure A of episode 58 eruption.

1997). The intrusion started at 0216 HST with the onset of rapid deflation at Kīlauea’s summit. Deflation at Pu‘u ‘Ō‘ō began minutes later, signaling that the supply of magma to the middle East Rift Zone had been disrupted. Outwardly, however, no change was seen at Pu‘u ‘Ō‘ō for several hours, and the view was similar to that shown in Figure 2.4a. During a helicopter flight shortly after dawn (~0745 HST) on June 17, the lava surface within the East Pond vent was observed at its typical level. Also, lava continued to flow through the PKK lava tube and was feeding active surface flows and an ocean entry that appeared unchanged compared to observations from previous days.

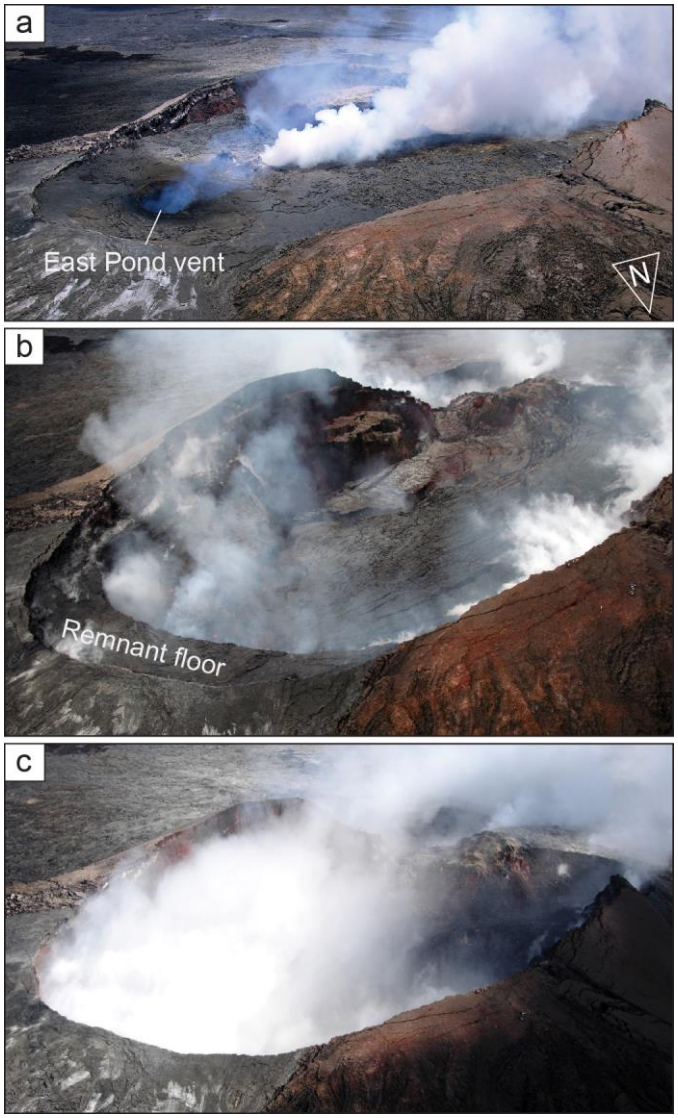

Figure 2.4 Time series of oblique aerial photographs of Pu‘u ‘Ō‘ō from nearly same vantage. (a) June 1, 2007. East Pond vent on east side of crater floor producing blue fume. (b) June 18, 2007, during subsidence of crater floor. (c) June 20, 2007, after subsidence of crater floor.

Starting at 0935 HST, though, the webcam perched on the north rim of the Pu‘u ‘Ō‘ō crater began to record small dust plumes caused by sporadic wall-rock collapses at pits and spatter cones on the crater floor. Visible subsidence of the crater floor began at about 1130 HST and continued throughout the day, along with more vent collapse. By the time of a second flight, at 1400 HST, the lava surface in the East Pond vent had dropped 3–5 m, and surface flows that were active downslope over the previous several days had noticeably diminished in vigor. Ground observations at Pu‘u ‘Ō‘ō shortly afterward were

enlivened by the frequent sound of rock slides from the south crater wall and wall-rock collapses in slowly enlarging pits on the crater floor. Many of the collapse events were energetic enough to be recorded by infrasound (Fee et al., 2011).

By the following morning (June 18), the crater floor of Pu‘u ‘Ō‘ō below the north rim of the crater had dropped ~30 m (Fig. 2.4b). A lava pond ~100 × 60 m across (long axis oriented north–south) filled a pit on the east crater floor, where the East Pond vent had been. Adjacent to this pond, to the west, another pit had formed and hosted a small lava pond ~15 m in diameter. The lava surface within both pits was estimated to be 40–45 m below the edge of a remnant slice of crater floor attached to the east rim of Pu‘u ‘Ō‘ō crater (Fig. 2.4b). This indicated that the lava level had dropped 20–25 m since the previous morning and was at an elevation of 815–810 m.

Elsewhere, subsidence of the south crater floor had caused slumping of the south wall of the Pu‘u ‘Ō‘ō cone. In addition, the West Gap and Puka Nui pits on the west flank of Pu‘u ‘Ō‘ō had approximately doubled in diameter and depth, while the MLK pit increased only in depth. Aerial views into a skylight on the eastern of the two branches of the PKK lava tube showed it had been abandoned. The ocean entry, fed by the western branch of the tube system, remained active, but the steam plume had diminished substantially.

By June 19, most of the crater floor was observed to have subsided. All three pits on the west flank of the cone had grown larger and deeper, consuming parts of the adjacent walls of the Pu‘u ‘Ō‘ō cone. At the coast, the ocean entry had dwindled to minor steaming with only sporadic drips of viscous-looking, residual lava draining into the ocean, indicating that the lava supply to the tube system had been severed. Though fume hampered views into Pu‘u ‘Ō‘ō on June 19 and 20, brief but slightly better views on June 21 (Fig. 2.4c)—after subsidence is thought to have stopped—suggested that the central part of the crater floor had subsided ~80 m and formed a concave depression, its floor composed of rubble at an elevation of ~775 m.

Fume prevented views into the crater in the days following the subsidence. Webcam images on July 4 showed a pit on the east side of the crater floor, with a depth probably similar to that of the central part of the crater, but separated from it by a septum 10–20 m higher. A part of the original crater floor, down-dropped by about 15 m,

remained attached to the east wall of the crater and formed a crescent-shaped shelf as wide as ~20 m. The lack of eruptive activity anywhere on Kīlauea after June 19 indicated that the volcano had entered an eruptive hiatus.

2.3.3 Refilling of Pu‘u ‘Ō‘ō

Following a repose period of ~12.5 days, infrasonic energy from Pu‘u ‘Ō‘ō resumed at ~1800 HST on July 1 (M. Garces, written communication, 2007), and weak flashes of red glow recorded by the webcam became apparent after dark at 1930 HST and continued overnight. A radiometer on the north rim of Pu‘u ‘Ō‘ō (Harris et al., 2005), pointed toward the center of the crater, began to record elevated temperatures at 0750 HST on July 2, suggesting that lava had begun to pond at the bottom of the crater. Lava erupting from two vents (referred to hereafter as the East vent and the West vent; Figs. 2.3b and 2.5) was sighted less than an hour later, verifying that episode 57 had begun. The two vents were positioned close to, but slightly north of, the positions of vents that had been active on the crater floor before June 17 (compare Figs. 2.3a and 2.3b). Within a few days, a growing lava lake spanned much of the length and width of the crater (Fig. 2.5).

Early on July 3, the POC tiltmeter began to record an unusual saw tooth-shaped signal that slowly grew in amplitude (Fig. 2.6a). The duration between peaks was ~1 hr, and the inflationary and deflationary limbs appeared to be relatively linear and symmetrical. This behavior was interspersed with, and eventually replaced by, a series of eight larger tilt excursions on July 3–6 (Fig. 2.6; Table 2.1) that were characterized by an abrupt and rapid inflation of 0.6–1.6 microradians and followed by an equally abrupt and rapid deflation. The inflationary and deflationary limbs were not linear and exhibited a decay pattern than created an obvious asymmetry to the shape of most events on the tilt graph. Event durations ranged from $1^h\ 46^m$ to $3^h\ 22^m$. Improved viewing conditions as the lava lake developed allowed the volcanic events that accompanied five of the eight large tilt excursions to be recorded, at least in part, by webcam and also, in a few cases, by the time-lapse camera deployed on the northwest rim of Pu‘u ‘Ō‘ō.

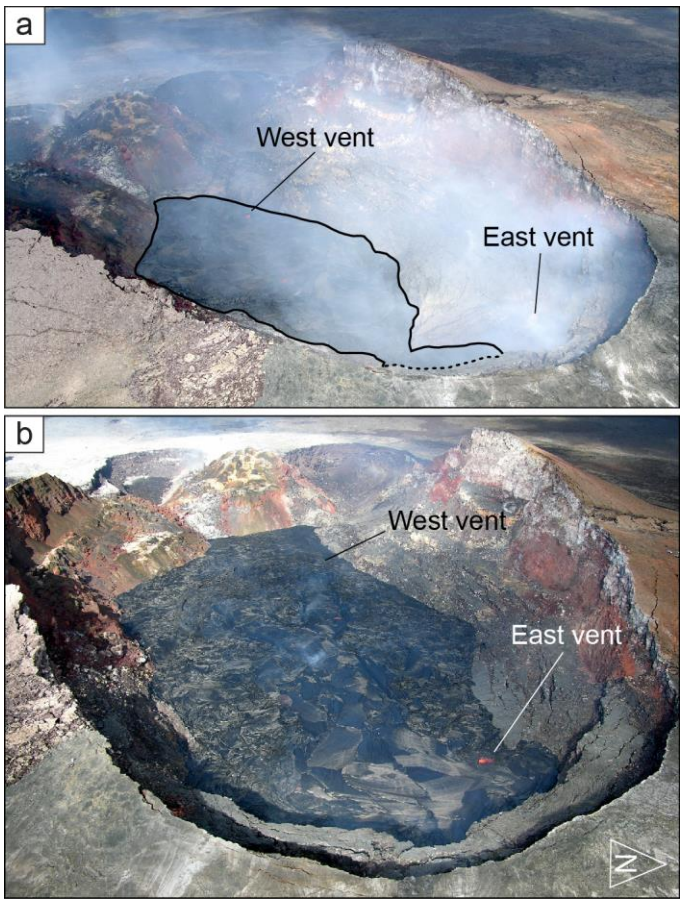

Figure 2.5 Oblique aerial photographs of Pu‘u ‘Ō‘ō during episode 57. (a) July 5, 2007. Lava lake outlined in black (dotted where hidden). West vent is main source of discharge with lava flowing northeast (toward lower right of photo) and spilling into pit on eastern side of crater. East vent producing little lava. (b) July 13, 2007, after discharge from both crater vents had waned and crater infilling had largely stopped.

During the four best-observed large tilt excursions (events 5–8 in Fig. 2.6a and Table 2.1; event 8 shown in movie 19 of Orr, 2011), the West vent stopped erupting just before the onset of rapid inflation, and the lava lake began to cool and crust over. Within minutes to a few tens of minutes, the lava lake began to drain back into the throat of the vent, leaving a funnel-shaped basin. The one observed exception was the fifth tilt excursion—the smallest of the large tilt excursions—during which the lava lake surface subsided, but lava did not obviously drain back into the vent. For all events, rapid inflation switched to rapid deflation, and, at the switch (or shortly after), lava began to erupt again from the vent and refilled the partly drained lava lake over the next several minutes. The rate of deflation decreased slowly over the next 1–2 hours, approaching, but

not quite reaching, the previous tilt level. Though the lava lake was not visible during every large tilt excursion, it is inferred that all tilt excursions exhibited similar eruptive behavior. The last large tilt excursion (event 8; Fig. 2.6) was followed by a small tilt excursion similar in shape and magnitude to the small saw tooth-shaped tilt events recorded at POC on July 3–4. Based on the webcam record, this tilt excursion was also accompanied by a drain-back event, but a commensurately smaller one that trailed the switch to deflation by several minutes. It is therefore possible that the small sawtooth-shaped tilt events described previously, and which preceded the 8 large tilt excursions, also correlated with brief eruptive slowdowns, that may or may not have been accompanied by drain-back behavior. (This inference is supported by observations made in 2010 and 2011 of a lava lake over a similarly located vent on Pu‘u ‘Ō‘ō’s crater floor. In this later case, a nearly identical small-amplitude saw tooth-shaped signal, as recorded by the POC tiltmeter, occurred repeatedly over periods of up to several days. The tilt signal corresponded to effusion slow-downs during inflation and pulses in effusion during deflation.)

Initially, the West vent was the dominant source of lava accumulation on the crater floor, and the East vent added very little to the lava output. By July 5, lava from the West vent had filled the central part of the crater floor to a depth estimated at 10–20 m and was spilling into, and filling, the east pit (Fig. 2.5a). Shortly after 1300 HST on July 6, coincident with the onset of prolonged inflation recorded by the POC tiltmeter, effusion from the East vent increased suddenly and that from the West vent stopped. Though the West vent began to erupt again by mid-morning on July 7, the East vent was the source of most of the erupting lava for the next several days (Fig. 2.5b). While both vents were erupting, East vent flows crossed the crater floor toward the west, often overwhelming the West vent (see movie 20 of Orr, 2011).

As lava pooled on the crater floor, it constructed low levees, impounding a perched lava lake that stood a few meters above the surrounding crater floor. Early in the afternoon of July 12, the West vent became inactive again, and flows from the East vent were the sole source of erupting lava (see movie 21 of Orr, 2011). By July 14, the output from the East vent had also waned, with flows rarely reaching halfway across the crater floor. The West vent reactivated the same day, however, and began to erupt sporadically,

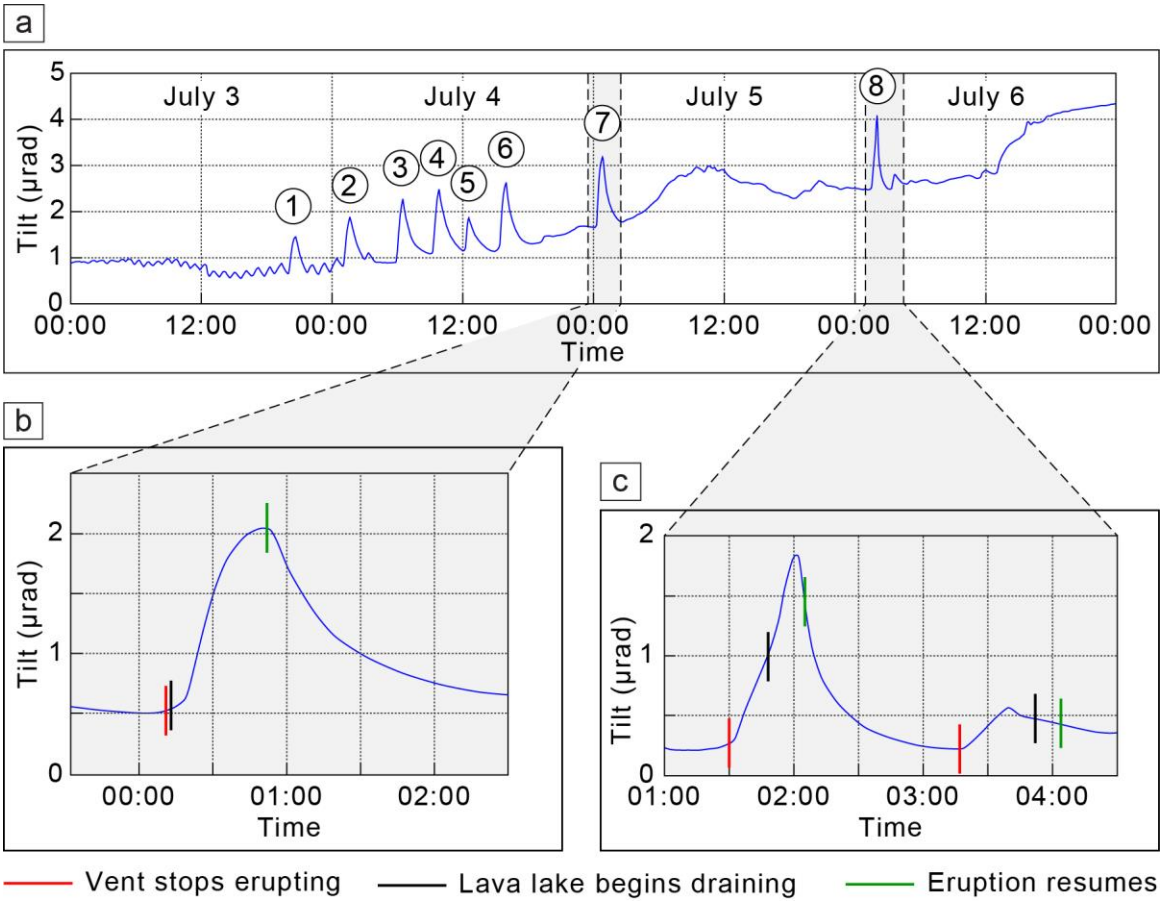

Figure 2.6 Line graphs showing saw tooth-shaped tilt signals at Pu‘u ‘Ō‘ō during (a) July 3–6. For the large tilt excursions, cessation of eruptive activity and lava lake drain-back corresponds to periods of inflation, and resumption of eruptive activity corresponds to subsequent deflation. Numbers correlate with event numbers in Table 2.1. (b) Detail of tilt event 7. (c) Detail of tilt event 8. Red lines in b and c correspond to cessation of eruptive activity, black lines correspond to onset of lava lake draining, and green lines correspond to resumption of extrusive activity.

feeding small flows that were confined to the west end of the crater. By July 16, cooling and subsidence of the lava lake and crater floor uplift left the levee walls standing several meters higher than the chilled surface of the lake (Fig. 2.7). Estimates from oblique aerial photographs compared to the known dimensions of the Pu‘u ‘Ō‘ō crater rim indicated that the crater floor, composed of new lava, had reached a maximum size of about 350 × 130 m, exclusive of the West Gap pit (Fig. 2.3b). The east part of the crater floor was ~30 m below the east rim of the crater, indicating that the lava had accumulated in the crater to a thickness of ~55 m.

2.3.4 Crater floor uplift

Superimposed on the infilling of the crater was the wholesale, piston-like uplift of the floor of the Puʻu ʻŌʻō crater. Starting July 8, and continuing through July 20, the Puʻu ʻŌʻō webcam recorded the slow upward movement of the crater floor, especially noticeable in slump blocks at the base of the south wall of the crater (see movie 18 of Orr, 2011). The slumped area had subsided during the broader subsidence of the crater floor on June 17–19, indicating that it was structurally within the bounds of the crater. The onset of uplift occurred at about the peak of eruptive activity. Qualitatively, eruptive activity from vents within the crater began to wane thereafter.

Table 2.1 Large saw tooth-shaped tilt events related to Puʻu ʻŌʻō lava lake draining and refilling.

Event Number	Date (2007)	Duration (hr:min)	Amplitude (μr)	Observed
1	July 3	1:46	0.6	No
2	July 4	2:01	1.1	Yes (in part)
3	July 4	3:22	1.4	No
4	July 4	2:54	1.4	No
5	July 4	2:47	0.7	Yes
6	July 4	3:08	1.5	Yes
7	July 5	2:28	1.5	Yes
8	July 6	1:46	1.6	Yes

The uplift was accommodated by a circumferential fault (or faults) within the Puʻu ʻŌʻō crater. The visible rim of the crater, and the rim on which the webcam viewing the uplift was located, did not move noticeably during the uplift. The webcam images suggest that the uplift was a doming of the crater floor, such that the amount of uplift was greatest over the west-central part of the crater (including the slump blocks at the base of the adjacent south wall), less on the west end of the crater, and the least at the east end of the crater. In fact, movement of the crater floor at the east end of the crater appeared to be just a slight tilting of the crater floor away from the center of uplift with no movement along a circumferential fault. No cameras had a view of the north side of the crater floor, so the presence or absence of uplift along a circumferential fault there is not known.

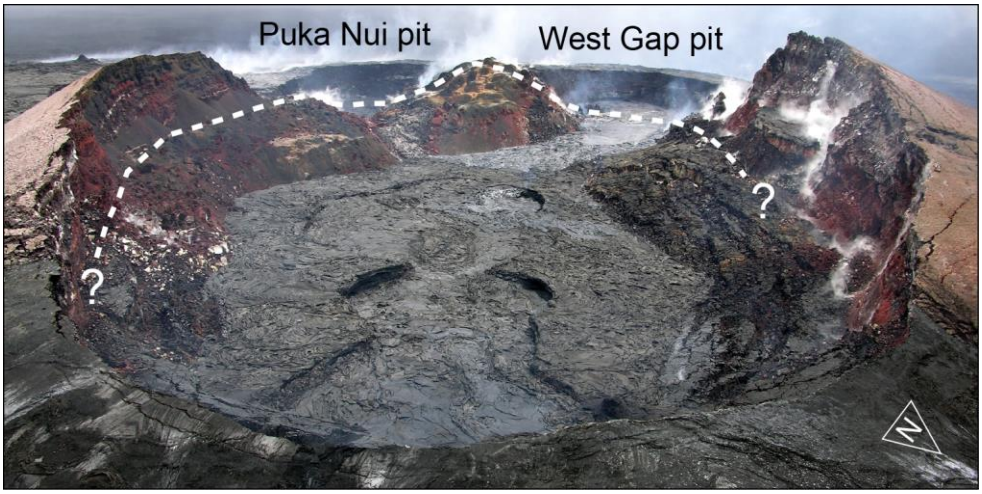

Figure 2.7 Oblique aerial photograph of Pu‘u ‘Ō‘ō crater on July 16, 2007, showing exposed lake levees following reduced discharge from crater vents, subsidence of lava lake surface, and uplift of crater floor. Note lava erupting from vent in West Gap pit in background and flowing back into the Pu‘u ‘Ō‘ō crater. Dashed white line, approximate location of circumferential fault accommodating uplift.

2.3.5 Opening of vents along crater-bounding fault

At 1500 HST on July 13, dense white fume began to emanate from rubble midway up the south wall of the West Gap pit, and lava broke the surface along a short fissure at that location at 1615 HST (Fig. 2.8a). The fissure was ~20 m higher than the level of the East vent erupting simultaneously on the crater floor. Lava began to cascade down into the West Gap pit, filling it slowly over the next few days before spilling eastward into the Pu‘u ‘Ō‘ō crater. A perched lava pond ~15 m deep formed within the West Gap pit (Figs. 2.7 and 2.8b).

White fume began to rise from the northwest edge of the Puka Nui pit (Fig. 2.3b) late in the day on July 15, and, by sunrise the following day, another fume source had opened on the southeast side of the Puka Nui pit. A small pad of lava, erupted from the northwestern fuming area some time on July 15 or 16, was observed already in place by early afternoon on July 16. The main activity within the Puka Nui pit, however, started at ~1630 HST on July 17 from the southeastern fuming area, and lava began to fill the pit slowly over the following days (Fig. 2.9). Shortly after dawn on July 18, another source of white fume appeared on the tephra slump blocks on the south side of the crater, east of the erupting vent in the Puka Nui pit, and weak spattering started a few hours later (Fig.

2.9). Though the vent on the tephra slump block fed no surface flows, the vents within the Puka Nui pit eventually filled the pit and, late on July 20, began to flow northeastward into Pu‘u ‘Ō‘ō crater, as well as southeastward into the adjacent MLK pit.

The vents that erupted in the West Gap and Puka Nui pits, and on the slump block on the south edge of Pu‘u ‘Ō‘ō crater, were all located along the circumferential fracture (crater-bounding fault) that was accommodating the piston-like uplift of the crater floor. All were located at a higher elevation than the East and West vents erupting on the crater floor, and all—except perhaps the vent on the northwestern side of the Puka Nui pit—remained active through July 20.

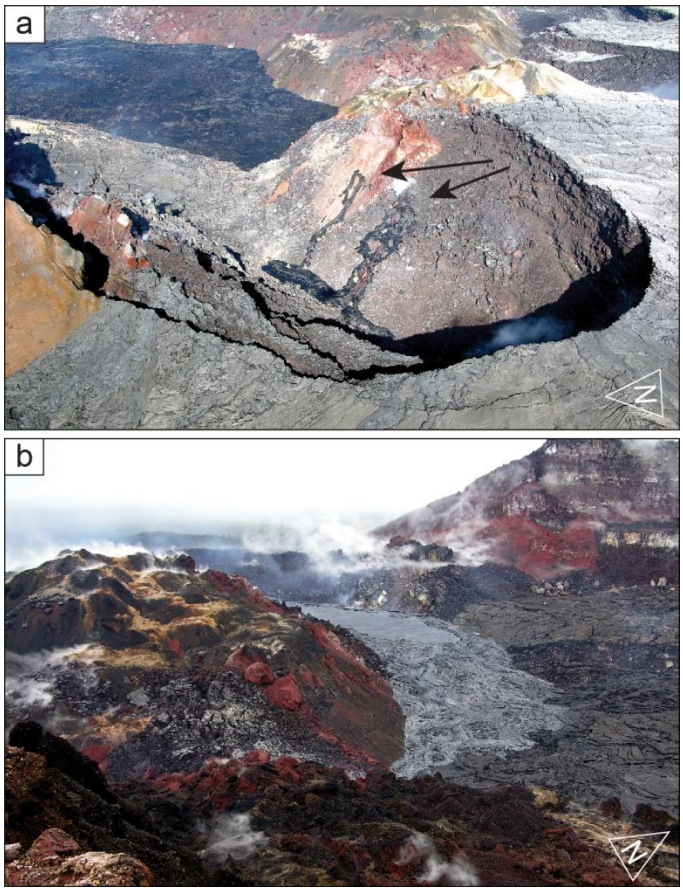

Figure 2.8 Photographs of West Gap pit at Pu‘u ‘Ō‘ō. (a) Lava erupting from short fissure on southern wall of West Gap pit on July 13, 2007. Eruption onset was less than two hours earlier. Lava beginning to pool at bottom of pit. Pu‘u ‘Ō‘ō’s crater at upper left of photo. Width of West Gap pit along axis extending from bottom left to top right is ~125 m. (b) Ground photograph showing lava from partly filled West Gap pit flowing back into the Pu‘u ‘Ō‘ō crater on July 16, 2007. Height of crater wall at upper right ~50 m.

2.3.6 Resumption of crater vent effusion

The East vent within Pu‘u ‘Ō‘ō erupted flows sporadically through July 20, but all were small and confined to the area immediately surrounding the vent. The West vent was also a source of small, sporadic flows during this period, but during mid-afternoon on July 18, lava began to erupt vigorously from the West vent. Though not matching the level of activity observed earlier in July, flows began to pond on the west side of the crater, largely confined by the levees from the earlier-formed lava lake. Activity increased over the following few days and, by late in the day on July 20, West vent flows had reached nearly to the east end of the crater, where they occasionally converged with small flows fed from the East vent.

2.3.7 Onset of episode 58

Eruptive activity within Pu‘u ‘Ō‘ō and from the vents along the crater-bounding, circumferential fault stopped at ~2250 HST on July 20, coincident with the abrupt onset of rapid deflationary tilt toward the southeast as recorded by the POC tiltmeter. Though their supply had been severed, lava flows continued to advance across the crater floor until ~2315 HST. At 2355 HST, the floor of Pu‘u ‘Ō‘ō crater began to subside rapidly. Minutes later—shortly after midnight on July 21—lava began to erupt from a new fissure high on the northeast flank of Pu‘u ‘Ō‘ō cone (Fig. 2.3b). The first acoustic signal from the direction of Pu‘u ‘Ō‘ō’s east flank was detected at 0006 HST and a higher amplitude signal appeared at 0013 HST (Fee et al., 2011), suggesting an eruptive onset at one of these two times. Definitive glow was first detected beyond the east rim of Pu‘u ‘Ō‘ō by webcam at 0039 HST. Over the next several hours, a series of four left- and right-stepping, en echelon fissure segments propagated ~1.5 km down-rift. This signaled the start of episode 58 of the long-lived Pu‘u ‘Ō‘ō eruption (Poland et al., 2008a).

Pu‘u ‘Ō‘ō underwent a prolonged, but rather dramatic, response to the episode 58 eruption. By the following day, the floor of the crater had sagged ~20 m, and a small pit had formed at the site of the West vent. Thick fume obscured views of the East vent and the east end of the crater. The center of the West Gap pit had dropped ~20 m, and a part of the northwest rim of Pu‘u ‘Ō‘ō, on the north side of the West Gap pit, had collapsed,

destroying the time-lapse camera located at that spot. Pre-existing cracks on the north rim of Pu‘u ‘Ō‘ō widened, and new cracks formed

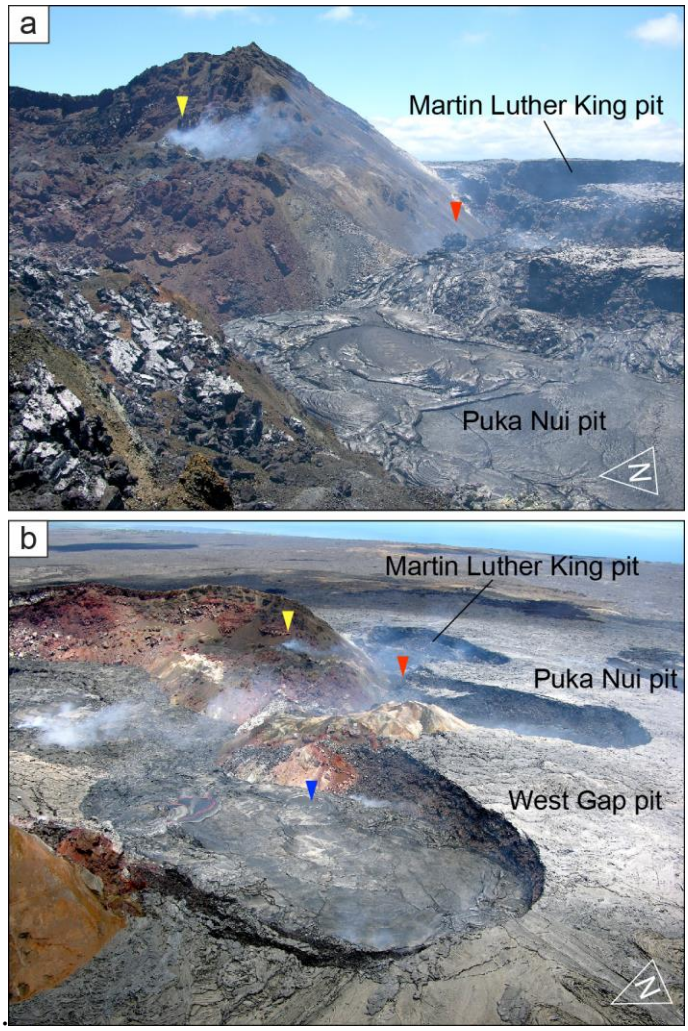

Figure 2.9 Photographs of Puka Nui pit and West Gap pit at Pu‘u ‘Ō‘ō. (a) Puka Nui pit, partly filled by new lava, on July 19, 2007. Source of lava denoted by orange arrowhead. Yellow arrowhead, location of spattering vent in tephra slump block on south side of Pu‘u ‘Ō‘ō’s crater. (b) Broader perspective of pits on southwest flank of Pu‘u ‘Ō‘ō on July 19, 2007. Orange arrowhead, vent in Puka Nui pit; yellow arrowhead, vent on tephra slump blocks; blue arrowhead, vent in West Gap pit.

Despite the presence of opaque fume that obscured most views into the crater, rare glimpses indicated that the crater floor continued to deepen over the following months, possibly in response to the slow draining of magma from beneath Pu‘u ‘Ō‘ō as the

episode 58 eruption evolved. Many collapses were recorded by nearby seismometers during this period, each accompanied by small, positive tilt offsets recorded on the POC tiltmeter. Some collapses deposited dust onto the window of the webcam enclosure on the north rim of the crater. The eventual result of crater subsidence was a bowl-shaped depression floored by rubble, its low point 95–100 m below the east rim of the crater.

2.4 Results and discussion

2.4.1 Crater floor subsidence

The shape of Pu‘u ‘Ō‘ō crater floor after the subsidence on June 17–19 was complex, but in simplest form can be approximated as a half-ellipsoid. A subsidence volume (V_c) can therefore be calculated from

$$V_c = \frac{\pi\, l\, w\, h}{6} \tag{2.3}$$

where

l	is the crater length,
w	is the crater width, and
h	is the amount of subsidence.

Using crater dimensions of 400 × 280 m (pre-subsidence dimensions), and a depth of 80 m, the derived volume of the crater subsidence is 4.2×10^6 m^3. This is similar to the volume-loss approximation of 3.65×10^6 m^3 of lava calculated by Montgomery-Brown et al. (2010) based on the length of time required for lava to reappear at Pu‘u ‘Ō‘ō. Experimental work on crater-collapse mechanisms by Roche et al. (2001) suggests that, following subsidence, Pu‘u ‘Ō‘ō’s crater was probably a column of brecciated material occupying a volume greater than that of the same material preceding the subsidence. Thus, the crater subsidence volume calculated here may represent a minimum value.

2.4.2 Crater infilling and uplift

Equation 2.3 above can also be used to calculate a bulk volume of filling within Pu‘u ‘Ō‘ō. Using the maximum lava lake dimensions of 350 × 130 m and a depth of 55 m, the bulk volume erupted in Pu‘u ‘Ō‘ō was ~1.3 × 10^6 m^3 by July 13, after which crater activity began to wane significantly. Likewise, assuming half-ellipsoids for the shape of the West Gap and Puka Nui pits, approximate bulk volumes can also be calculated for lava erupted from vents around the periphery of the crater. By July 20, lava had accumulated in the West Gap pit to a depth of ~15 m with a surface area of ~100 × 80 m and in the Puka Nui pit to a depth of ~15 m with a surface area of ~120 × 70 m. These dimensions yield volumes of ~0.06 × 10^6 m^3 and ~0.07 × 10^6 m^3, respectively.

The total bulk volume of lava accumulated within the Pu‘u ‘Ō‘ō crater, the West Gap pit, and the Puka Nui pit from July 1 to July 20, including both surficial lava flows and endogenous growth, was ~1.4 × 10^6 m^3 (the relatively small volume of lava erupted within Pu‘u ‘Ō‘ō from July 18 to July 20 is disregarded). The resulting bulk discharge rate, averaged over the 20 days, is 0.8 m^3 s^{-1}. Correcting for vesicle volume, using a modest void fraction of 25 percent (Wolfe et al., 1987), gives a dense rock equivalent discharge rate of 0.6 m^3 s^{-1}, which is about an order of magnitude less than the supply rate of magma to the volcano during the same period (Poland et al., 2012). This disparity suggests that most of the magma supplied to the volcano went into refilling and (or) repressurizing the magmatic system at the summit and along the East Rift Zone between the summit and Pu‘u ‘Ō‘ō.

Webcam images provided a way to track changes in both lava level and uplift within the Pu‘u ‘Ō‘ō crater, as shown in Figure 2.10. Because the measured crater floor level reflected the cumulative effect of both filling and uplift, actual filling can be isolated by subtracting the amount of uplift. The result (blue line; Fig. 2.10) shows—at least along the centerline of the images used to track changes—essentially no filling after July 9 and essentially no uplift before July 9. In other words, filling stopped once uplift began. The POC tilt record (Fig. 2.10) shows a slowly accelerating rate of inflation starting about July 3. On July 11, though, the tilt flattens, showing no net tilt gain or loss until about July 13, when slow inflation starts again. After July 13, however, shortly after the rate of uplift had increased, the tilt leveled out and showed no significant gain or loss

until late on July 20, just before the onset of the July 21 fissure eruption. The absence of inflation while the Pu‘u ‘Ō‘ō crater floor was uplifting suggests that this uplift was driven at a shallow level within the Pu‘u ‘Ō‘ō edifice, and (or) that pressurization of the shallow magma body beneath Pu‘u ‘Ō‘ō was almost completely accommodated by crater floor uplift.

The data show ~16 m of filling from July 4 to July 9. This brackets the minimum amount of crater filling and implies that 34 m (based on original estimate of maximum infilling of 50 m) of lava accumulated from July 2 (when filling probably started) to July 4. The filling curve for 34 m is shown as the dashed blue line in Figure 2.10. Based on the webcam images, the crater floor was lifted ~10 m between July 9 and July 20 (red line; Fig. 2.10).

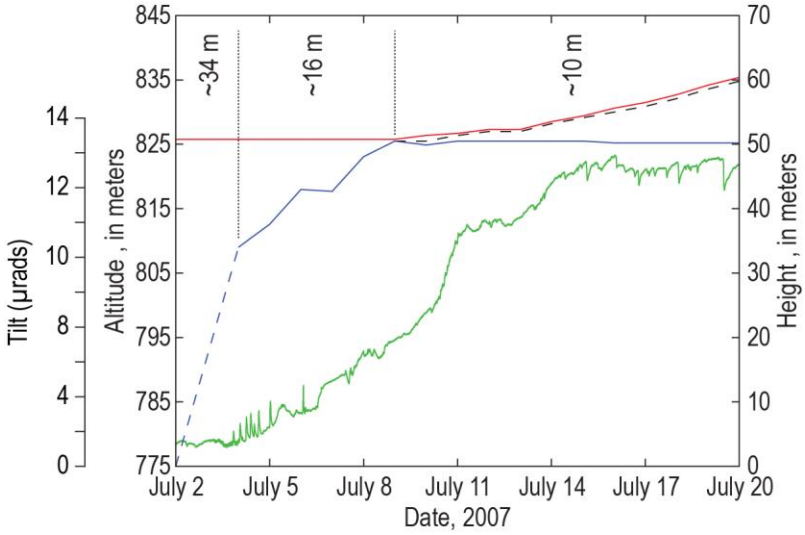

Figure 2.10 Graph showing elevation and height of Pu‘u ‘Ō‘ō’s crater floor from filling (blue) and uplift (red) in meters, for the period July 2–20, 2007. Dashed blue line, presumed July 2 to July 4 filling path; dashed black line, elevation of lava surface with uplift not subtracted out (i.e., the actual elevation of the crater floor); green, tilt at station POC in microradians.

2.4.3 Onset of episode 58

The western tip of the episode 58 eruptive fissure system was located ~110 m northeast of Pu‘u ‘Ō‘ō’s east rim (Fig. 2.3b). The tip of the fissure was 24 m lower than

the crater rim and ~6 m higher than the level of lava on the crater floor. Cracks that defined the westward extension of the fissure continued westward toward the crater rim, but did not intersect it. In addition, the tip of the fissure was bounded by a zone of circumferential fractures. Views of Pu‘u ‘Ō‘ō’s east crater wall in the months following the onset of episode 58, when the crater floor had reached a depth estimated at 95–100 m below the crater’s east rim, showed no evidence of a lateral connection between the crater and the episode 58 fissure.

These observations show that the episode 58 fissure was not fed from a lateral breach of the cone by lava that had accumulated within the Pu‘u ‘Ō‘ō crater. Instead, magma that fed the episode 58 fissures probably originated directly from the shallow conduit, bypassing the Pu‘u ‘Ō‘ō crater above. The subsequent depressurization (eruption) resulted in crater floor subsidence and perhaps some recycling of molten lava still present beneath the crusted surface of the lava lake on the crater floor.

2.4.4 Eruption petrology

Starting in April 2001, the olivine-phyric magma that had been erupting at Pu‘u ‘Ō‘ō changed to a mixture of olivine-only magma and a cooler magma containing clinopyroxene phenocrysts and glomerocrysts (± olivine ± plagioclase). This change is thought to be derived from the mixing of hotter and cooler components within the magmatic system (Thornber et al., 2015). Glass temperature and bulk MgO decreased slowly and finally stabilized at ~1,146º C and ~7.1 weight percent, and remained stable through the end of episode 55 in June 2007.

Episode 56, however, erupted a hotter (1,160º C) and more Mg-rich (8.7 weight percent MgO) olivine-only basalt, probably representing the primitive end-member for the mixed magma erupted since 2001 (Thornber et al., 2015). When the eruption resumed at Pu‘u ‘Ō‘ō with the start of episode 57, a cooler (1,143º C) low-MgO (~7.3 weight percent), olivine- and clinopyroxene-phyric lava (Table 2.2) erupted once again, and this hybrid magma continued to erupt during episode 58 (Thornber et al., 2015). This suggests that the magmatic system was not significantly disrupted by the episode 56 eruption, and that the presumed hybridization of hotter and cooler magmatic components likely occurs along the East Rift Zone en route to Pu‘u ‘Ō‘ō, possibly beneath Makaopuhi Crater (Fig.

2.1) where a zone of magma storage may exist (Fiske and Kinoshita, 1969; Swanson et al., 1976).

Table 2.2 Description and major element composition of episode 57 lava samples.

Sample no.:	KE57-2647F		KE57-2649F	KE57-2650F	KE57-2651S	KE57-2652F
Collection date/time:	7/19/07 11:00		7/19/07 11:15	7/19/07 11:20	7/19/07 11:55	7/19/07 12:25
Description:	Warm crust from hours-old lava flow		Cold crust of lava erupted since 7/2	Cold drapery at edge of lava flow 2–3 days old	Cold spatter erupted since ~1630 on 7/17	Molten core from 15-min-old stagnant toe; water quench
Analysis:	XRF	Microprobe	XRF	XRF	XRF	XRF
SiO2	51.16	51.31	51.15	51.16	51.20	51.26
Al2O3	13.71	13.39	13.67	13.73	13.68	13.82
FeOT	11.25	11.10	11.23	11.17	11.22	11.17
MgO	7.23	6.40	7.39	7.32	7.30	7.07
CaO	11.05	10.64	11.01	11.03	11.02	11.02
Na2O	2.34	2.32	2.31	2.33	2.33	2.36
K2O	0.41	0.429	0.41	0.41	0.41	0.42
TiO2	2.45	2.535	2.43	2.44	2.44	2.48
P2O5	0.23	0.25	0.23	0.23	0.23	0.24
MnO	0.17	0.16	0.17	0.17	0.17	0.17
Cr2O3	—	0.032	—	—	—	—
SO3	—	0.020	—	—	—	—
NiO	—	0.004	—	—	—	—
TOTAL (wt %)	100	98.56	100	100	100	100
MgO T (ºC)	—	1142.6	—	—	—	—

Notes: Glass temperature for sample KE57-2647F calculated by technique of Helz and Thornber (1987).

2.4.5 Trends in intrusive and eruptive activity

Most published overviews of the prolonged Pu‘u ‘Ō‘ō eruption, such as that in Chapter 1, tend to lump three decades of eruptive activity into a few paragraphs. In the interest of brevity, only the most profound changes are noted. This may give the false impression that the Pu‘u ‘Ō‘ō eruption is largely a “steady-state” eruption. In reality, the Pu‘u ‘Ō‘ō eruption represents a continuum of changes. Relatively steady conditions, though rife with small changes, may prevail for months to at most a few years, but the magmatic system inevitably breaks down. Such large changes commonly culminate in the transition to a new eruptive vent, or a major reorganization of the lava tube system

transporting lava away from the vent. With the benefit of time, trends have begun to emerge that forecast some of these profound changes.

One such trend—up-rift intrusion with or without eruption, accompanied by crater floor subsidence and eruptive hiatus—has repeated several times at Puʻu ʻŌʻō. Such sequences were initiated by the February 7, 1993, intrusion (Okubo et al., 1996; Heliker et al., 1998); the January 29, 1997, intrusion and eruption (Owen et al., 2000; Thornber et al., 2003); the September 12, 1999, intrusion (Cervelli et al., 2002); and the June 17, 2007, intrusion and eruption (Poland et al., 2008a; Montgomery-Brown et al., 2010). Activity resumed within Puʻu ʻŌʻō following each of these events, and crater refilling eventually culminated in the outbreak of lava from new vents on the flank of the Puʻu ʻŌʻō cone. The sequences in 1993 and 1999 involved the reoccupation of the previously active vent and a reorganization of the tube system, while the sequences in 1997 and 2007 (the focus of this report) led to the opening of new vents.

The pattern was repeated in 2011, when an intrusion and brief fissure eruption up-rift from Puʻu ʻŌʻō started on March 5 (Lundgren et al., 2013; see Chapter 5). The sequence of events that followed culminated on August 3, 2011, in a large, rapidly moving breakout on the west flank of the Puʻu ʻŌʻō cone (episode 60) and another subsidence of the crater floor of Puʻu ʻŌʻō. Recognizing that the pattern of intrusion, crater subsidence, and refilling could culminate in a major breakout on Puʻu ʻŌʻō allowed Hawaiian Volcano Observatory scientists to prepare a response well in advance of the August 3 event. As in July 2007, the crater floor prior to the August 2011 breakout began to lift bodily via endogenous accumulation, providing a tell-tale sign of the increased pressure within the Puʻu ʻŌʻō edifice. While not always present (there was no evidence of such endogenous uplift in 1993, 1997, or 1999), this uplift provides additional guidance for forecasting changes in activity in some instances.

2.5 Conclusions

In this chapter, I have presented a detailed chronology of the events associated with the June–July 2007 subsidence and refilling of the Puʻu ʻŌʻō crater on Kīlauea's East Rift Zone. Of special note was the transition from the surficial accumulation of lava to uplift of the crater floor via endogenous processes. The sequence of events in 2007 unfolded in

a somewhat predictable fashion, based on Pu‘u ‘Ō‘ō’s previous response to up-rift intrusions. Recognition of the pattern of East Rift Zone intrusion, followed by crater subsidence, refilling, and breakout at Pu‘u ‘Ō‘ō, provides guidance when preparing for future eruption crises that evolve similarly. In fact, the occurrence of another up-rift intrusion and eruption (episode 59) on March 5, 2011, followed a strikingly similar pattern, with crater floor subsidence, eventual refilling of the crater evolving into crater floor uplift, and culmination with the opening of a new vent (episode 60) on the west flank of Pu‘u ‘Ō‘ō. The lessons learned from episode 57 guided the Hawaiian Volcano Observatory in responding preemptively to the August 3, 2011, breakout.

Chapter 3

A sinuous tumulus over an active lava tube at Kīlauea Volcano: evolution, analogs, and hazard forecasts

Published as:

Orr, T.R., Bleacher, J.E., Patrick, M.R., and Wooten, K.M., 2015, A sinuous tumulus over an active lava tube at Kīlauea Volcano: Evolution, analogs, and hazard forecasts. Journal of Volcanology and Geothermal Research 291(0), 35–48.

3.1 Introduction

Pāhoehoe flow fields emplaced on low-slopes (<~2º) commonly thicken endogenously via flow inflation (Nichols, 1939; Wentworth and Macdonald, 1953; Walker, 1991; Chitwood, 1994; Peterson et al., 1994; Hon et al., 1994; Cashman and Kauahikaua, 1997; Kauahikaua et al., 1998; Self et al., 1998; Anderson et al., 1999; Anderson et al., 2005; Walker, 2009; Anderson et al., 2012; Hoblitt et al., 2012) and are usually broad because flow advancement is generally accompanied by considerable flow widening. As inflation progresses, the upper surface of the flow lifts, and the separation between individual flow lobes vanishes, forming a molten core of interconnected pathways within the flow (Hon et al., 1994; Kauahikaua et al., 1998; Self et al., 1998; Anderson et al., 1999; Schaefer and Kattenhorn, 2004; Anderson et al., 2005; Anderson et al., 2012; Hoblitt et al., 2012). Inflation broadly affects the entire flow because of this hydraulic connection. The result is a flat to hummocky flow surface bounded by steep, rifted margins.

Hummocky flow surfaces are characterized by the presence of tumuli—low, dome-like mounds, commonly 1–5 m high, but occasionally exceeding 10 m in height (e.g., Wentworth and Macdonald, 1953; Walker, 1991; Chitwood, 1994). Most tumuli are crudely circular to elliptical in map view with deep axial cracks (e.g., Walker, 1991) and form in response to magmatic overpressure within the flow as the flow's crust thickens

(Walker, 1991; Hon et al., 1994; Peterson et al., 1994; Anderson et al., 1999; Anderson et al., 2012). Those areas that inflate the most form tumuli, while the lows between tumuli experience significantly less, or even no, inflation. In practice, all low mounds that define the surface of hummocky flows, and which formed by inflation, are called tumuli.

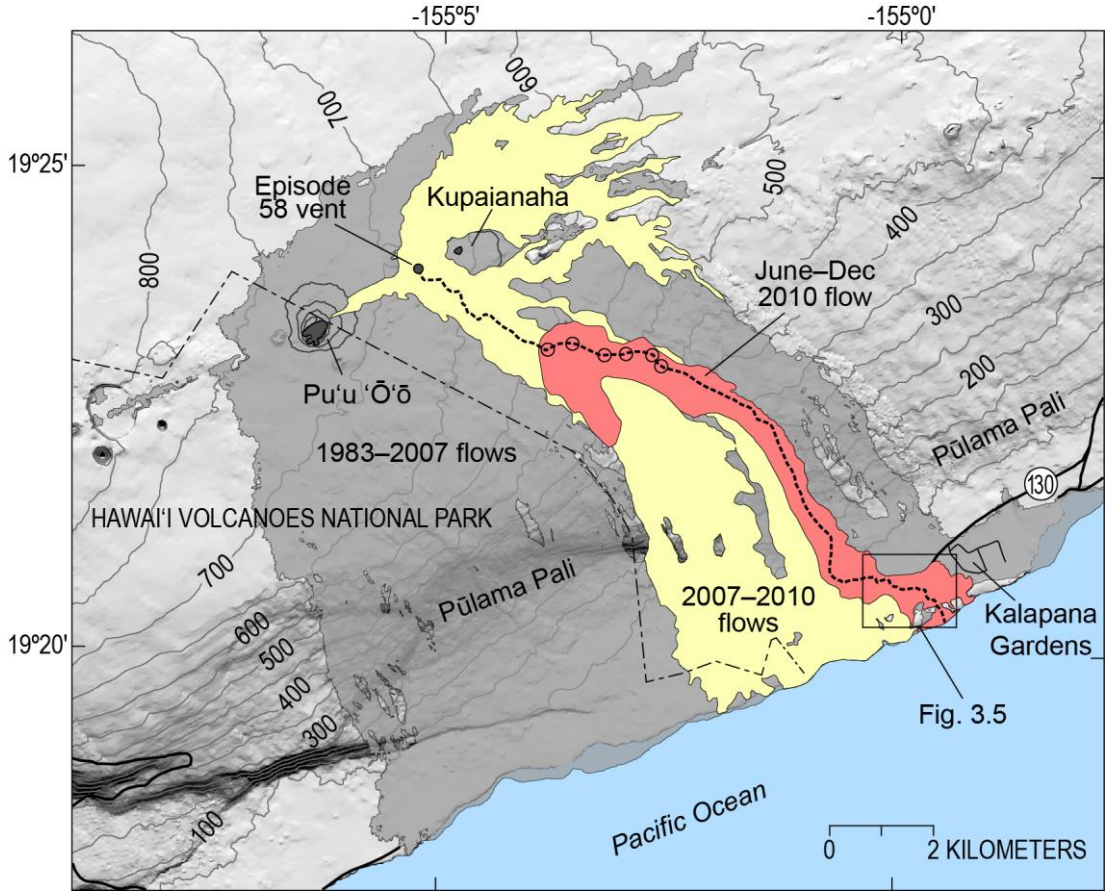

Figure 3.1 Map showing extent of Kīlauea's East Rift Zone lava flows 1983–2010 (one small flow erupted in 2007 falls outside area shown here). Gray, flows erupted from 1983 to 2007; yellow, episode 58 flow erupted 2007–2010; red, phase of episode 58 flow described here, erupted June–November 2010. Dashed black line, active lava tube; black open circles, rootless shields (not to scale) constructed over tube in June 2010. Contour interval, 50 m. Box shows map area for Figure 3.5.

In some instances, inflation is focused over preferred pathways, such as incipient tubes, within a flow to form a discontinuous series of elongate tumuli (Kauahikaua et al., 1998; Glaze et al., 2005). Such chains of tumuli can also form when pāhoehoe lava on a low-slope surface fails to spread out, for instance by lateral topographic confinement

(Glaze et al., 2005). In this case, the geometry of the flow alone focuses inflation within the flow's narrow width, so that tumuli appear to be aligned. While the formation of a series of tumuli over a well-established lava tube occurs relatively rarely (Walker, 1991; Anderson et al., 2012), such occurrences have been documented (Kauahikaua et al., 1998; Duncan et al., 2004). Where tumuli form over such lava tubes, they tend to be more elongate, sometimes with a sinuosity that matches that of the underlying lava tube (Keszthelyi and Pieri, 1993; Hon et al., 1994; Cashman and Kauahikaua, 1997; Self et al., 1998).

In July 2010, during Kīlauea Volcano's long-lived Puʻu ʻŌʻō eruption, a new lava flow reached the gently sloping southeast coast and encroached on homes within the Kalapana Gardens subdivision (Figs. 3.1 and 3.2), near the village of Kalapana. As the flow traveled across the coastal plain, it was confined by gentle topography that prevented significant spreading. A master lava tube developed quickly, and the roof of the tube evolved into a ~1-km-long, 10- to 20-m-wide sinuous tumulus (Figs. 3.3, 3.4 and 3.5). The tumulus grew gradually by flow inflation, but its development was punctuated by frequent breakouts from its flanks that slowly buried the tumulus and caused abrupt, irrecoverable uplift of its top. These breakouts occurred in response to recurring pressure fluctuations caused by cycles of deflation and inflation (DI events) at Kīlauea's summit (Fig. 3.6; Anderson et al., 2015), which were transmitted through the East Rift Zone to the eruption site and manifested as days-long fluctuations in vent discharge. Inflation in this latter context refers to deformation of the volcanic edifice and is different from superficial flow inflation.

I focus here on the development of the very long, sinuous tumulus described above and discuss the hazards posed by the breakouts that occurred in response to fluctuations in discharge. The lava tube breakouts, when they occurred, started about a day after the onset of edifice inflation during the DI events. This timing provided a means of forecasting breakouts that subsequently threatened Kalapana Gardens.

The appearance of the sinuous tumulus that formed along the tube at Kīlauea during July–November 2010, and the gradual inundation of the tumulus by its own breakouts, created unusual flow field morphology. This tumulus may be analogous to similar features preserved within topographically confined areas of the prehistoric

McCartys and Carrizozo flow fields (New Mexico, USA), as well as in the Tharsis volcanic province of Mars. Understanding how the inflated lava tube formed provides constraints on emplacement conditions in these other environments.

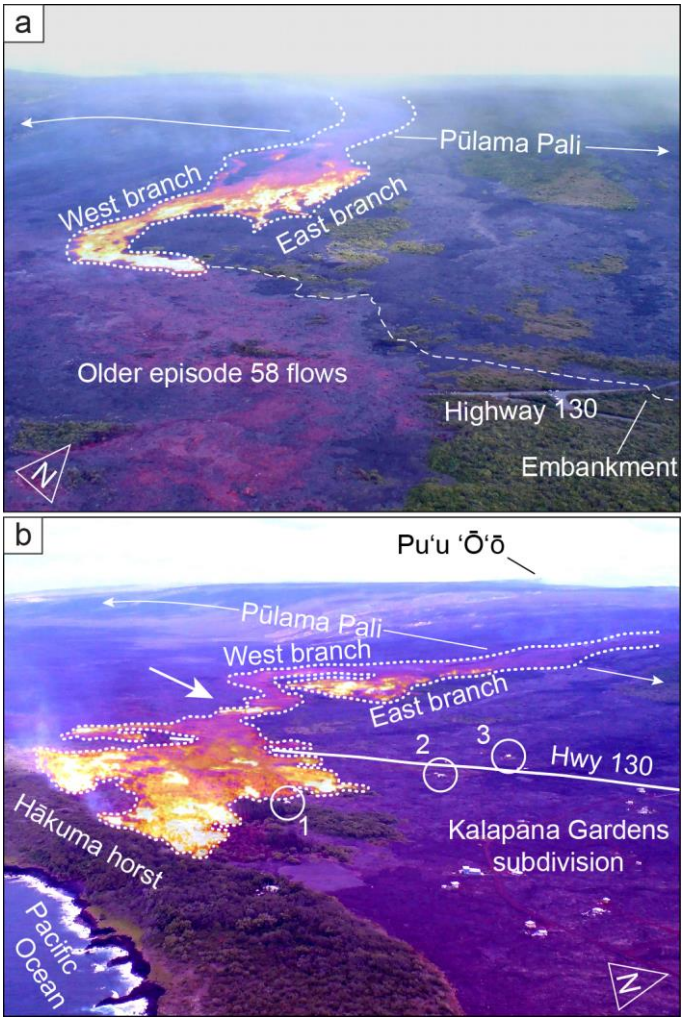

Figure 3.2 Aerial photographs with infrared overlays showing flow advancement across coastal plain. Warmer colors indicate higher temperatures; areas of bright yellow to white, active or very recently active flows. (a) Abrupt eastward turn in flow direction at base of Pūlama Pali on July 14, 2010. White dotted line, active flow margin. Flow surface at lower left with mottled violet coloration, previously emplaced episode 58 flows. Dashed white line, trace of lava tube formed later. (b) Flow butted against Hākuma horst and filling in adjacent graben on July 23, 2010. White dotted line, active flow margin. White arrow, study area at narrow part of flow. White circles, houses labeled in Fig. 3.7a. House 1 destroyed July 25.

3.2 Eruption monitoring methods

3.2.1 Flow field mapping

Lava flow hazard assessments were conducted on almost a daily basis during the study period because of the proximity of lava flows to Kalapana Gardens. The margins of the active flows were mapped simply by walking around each flow while recording a track log with a handheld Global Positioning System (GPS) device. While time-consuming, this gave us a simple way to measure flow progress and to gauge other flow properties such as vigor, flow inflation, and potential flow paths. The flow's advance rate was very slow and therefore of little immediate concern. The initial western edge of the flow as it advanced across the coastal plain was not mapped on the ground due to time constraints, nor was most of the perimeter of the August 2, 2010, breakout, which is described below. The flow edges in these cases were approximated from oblique aerial photographs taken during weekly helicopter observation flights. The mapping was compiled using ESRI® ArcGIS software. Updated flow maps, accompanied by a descriptive hazard assessment, were then transmitted via email to Hawai'i County Civil Defense (HCCD; the agency charged with disaster preparedness and response in Hawai'i) on a near-daily basis. More immediate hazards-related concerns, when present, were transmitted directly to the HCCD administrator via text message.

3.2.2 Webcams and time-lapse cameras

Webcams and time-lapse cameras have long played a role at Kīlauea and are now among the standard tools used by many groups, including the United States Geological Survey's Hawaiian Volcano Observatory (HVO), to monitor and study eruptive activity (e.g., Thornber, 1997; Poland et al., 2008b; Paskievitch et al., 2010; Orr, 2011). During the activity described here, two webcams provided images (1296 × 960 pixels) of the coastal flow field in real-time. Both were Stardot® Netcam SC webcams which transmitted images via the Verizon® cell phone network using an Airlink® Raven XE cellular modem. One camera was positioned on the second-floor patio of a house in Kalapana Gardens roughly 1.6 km from the sinuous tumulus. It operated almost continuously starting on September 18, 2010, and archived an image at HVO

automatically every 30 minutes. The other webcam was positioned on Pūlama Pali, the 300-m-high slope overlooking the coastal flow field near Kalapana Gardens (Pūlama Pali is the common-usage name for this prominent slope, for which an official name has not been designated by the United States Board on Geographic Names), roughly 1.1 km from the sinuous tumulus. It began operation on November 9, 2010, and an image was archived at HVO every 5 minutes. The webcams were programmed to automatically switch to a near-IR mode in low-light conditions. The images produced by the webcams were useful in determining the onset times of many of the breakouts, particularly those that occurred at night when the near-IR mode was functioning.

As many as six time-lapse cameras were deployed simultaneously along the crest of the sinuous tumulus, or adjacent to it, during the study period, specifically to document the evolution of the tumulus described in this paper. The cameras were of two types—low-cost Wingscapes® time-lapse cameras mounted on inexpensive tripods and more robust (and expensive) systems custom built at HVO (Orr and Hoblitt, 2008) and mounted on heavy surveying tripods. The built-in light sensor on the Wingscapes® cameras, meant to turn the cameras off at night, was removed to allow continuous photography. The time-lapse images from both system types provided start times for some breakouts and offered a unique look at tube-roof uplift in a few instances. Both systems recorded images only on-site, requiring frequent visits to exchange camera memory cards. The Wingscapes® cameras required regular exchange of internal batteries; the batteries for the HVO-constructed cameras were charged via a small solar panel. Image sizes varied from 1600 × 1200 to 3264 × 2448 pixels, depending on deployment.

3.3 Tumulus geometry measurements

3.3.1 Digital Elevation Models

Accurate topographic measurements of the sinuous tumulus, such as by using kinematic GPS, were not made during the tumulus's development due to insufficient field time. However, a Digital Elevation Model (DEM) of the distal part of the tumulus was created well after emplacement from oblique aerial photographs using the Agisoft® Photoscan Professional software package. The aerial photographs were captured from

helicopter in July 2014 with a Canon® EOS 60D digital SLR camera (18 megapixel image resolution). Photo registration is based on targets (white crosses) visible within the photographs and located by kinematic GPS (vertical and horizontal accuracy empirically determined to be ~5 cm). Target heights were transformed from ellipsoidal coordinates to orthometric coordinates using the National Geodetic Survey GEOID12a model. The horizontal and vertical accuracy of the resulting DEM is estimated at 10 cm.

The pre-eruption surface was taken from a June 2006 Federal Emergency Management Agency (FEMA) coastal LiDAR survey with a horizontal accuracy of 30 cm and a vertical accuracy of 14 cm. The LiDAR data were transformed into a DEM using ESRI® ArcGIS 10.1, which was also used to perform DEM calculations and differencing between pre- and post-emplacement surfaces.

3.3.2 Crack and tumulus measurements

The width and depth of the axial (or dominant) crack on or near the crest of the sinuous tumulus were measured using a metal carpenter's tape at 20 locations along the part of the tumulus still exposed in 2014. The crack width was measured between piercing points; the crack depth that was measured is a minimum because the metal tab at the end of the tape prevented full insertion into the crack, as did roughness and rubble at the base of the crack. ESRI® ArcGIS 10.1 was used to measure the width of the tumulus at each location from a rectified aerial image mosaic created using Agisoft® Photoscan Professional.

3.4 Description of eruptive activity

This study focuses on the eruptive activity that occurred from June to November 2010, while the episode 58 vent was active.

3.4.1 June–July 2010 eruptive activity

The lava tube transporting lava from the episode 58 vent to the Pacific Ocean ruptured at an elevation of ~600 m in early June 2010, and the new breakout captured the entire East Rift Zone eruptive output (Fig. 3.1). At first, the surface flow advanced slowly

across gently sloping (2–3º) terrain near the breakout point, sequentially constructing six low rootless shields over the developing lava tube.

The front of the lava flow reached the upper slope of Pūlama Pali in early July, at the eastern end of the Hilina fault system that cuts Kīlauea's southeastern flank. Following the eastern margin of older episode 58 lava flows, the active flow gained speed and began traveling southward down the ~6º slope of Pūlama Pali. As it neared the base of the slope, the flow split into two branches—a more rapid western branch and a slower, broader eastern branch (Fig. 3.2). The western branch reached the base of the slope at an elevation of ~40 m on July 14. Blocked by older, inflated episode 58 flows to the south, the active flow turned sharply to the east, seeking the easiest path across the gently sloping (<2º) coastal plain (Fig. 3.2).

Traveling 400–500 m day^{-1}, the western branch of the flow advanced in a sheet-like fashion following the margin of an inflated flow (generally less than 2 m high) emplaced a few months earlier (Fig. 3.2a). The northern side of the advancing flow abutted a gentle slope (≤1º) with mostly small-scale (<1 m-high) flow features. Confined by low topography on both sides, the flow remained narrow (Fig. 3.2), rarely exceeding a width of 80 m. In a few places the entire flow was less than 30 m across. The flow thickness after its initial emplacement was ~1 m but locally may have been as much as 2 m along its axis. Assuming an average thickness of 1 m and the area of the coastal flow as mapped each day, a bulk discharge of ~0.6 m^3 s^{-1} is derived for the advancing lobe. The average void space fraction for the upper meter of the flow was measured after emplacement at 40%, which yields a dense rock equivalent (DRE) discharge that rounds to 0.4 m^3 s^{-1}. This is an order of magnitude less than Kīlauea's long-term East Rift Zone DRE discharge of ~4 m^3 s^{-1} (converted from ~0.13 km^3 yr^{-1}; Sutton et al., 2003). Based on field observations, the discharge of the eastern branch appeared to be comparable to (or slightly less than) that of the western branch. Together, the eastern and western flow branches constituted the entire output from the episode 58 vent—the only active vent. This calculation implies that the East Rift Zone eruptive output at that time was ~1 m^3 s^{-1}, or roughly a quarter of the long-term rate.

On July 17, the flow reached a low (~6-m-high), south-facing embankment, on the southern side of State Highway 130 (Fig. 3.2), and spilled down into a shallow graben

bounded to the south by the Hākuma horst. The flow moved slowly eastward, filling the graben and destroying one home while threatening others in Kalapana Gardens. This same subdivision was inundated previously by lava in 1990 (Mattox et al., 1993), and about 30 houses had since been built—or rebuilt—upon the 1990 lava flows. On July 25, lava topped the Hākuma horst and flowed into the ocean. The flow's eastward advancement stopped within a few days, having reached within ~50 m of two other homes.

The volume of lava accumulated within the graben between July 17 and July 25 is derived by subtracting the underlying topography from the new flow surface, assumed to form a level plain with an elevation of 15 m (the elevation of the Hākuma horst at the point where it was topped). Flows emplaced outside the bounds of the graben during this period were assumed to have a thickness of 1 m, based on field observations, and a time span of 192 hours was used (mapping was completed on both days at about 1100 HST). Using these values yields a bulk discharge of ~0.7 $m^3 s^{-1}$ and a DRE discharge that rounds to 0.4 $m^3 s^{-1}$, consistent with our earlier calculation.

A relatively well-developed lava tube had formed as early as July 26, establishing a subsurface connection between the episode 58 vent and the Pacific Ocean (Fig. 3.1). Part of the tube's path, extending ~1.5 km from the buried trace of Highway 130 to the base of Pūlama Pali, was well expressed by a distinct line of fume easily followed on the ground. The lava tube approximately followed the centerline of the flow and crudely traced the shape of the older underlying episode 58 flow margin through much of this zone. Over the following ~10 days, lava from the eastern flow branch crossed and buried most of the lava tube within ~0.5 km of the base of the slope.

3.4.2 Sinuous tumulus formation and morphology

By late August 2010, the lava tube roof had begun to arch up in response to flow inflation. This formed a 1-km-long tumulus with a pronounced sinuosity (Fig. 3.3). The tumulus was a single continuous feature, not a series of adjacent or overlapping tumuli. Where the lava flow was very narrow, nearly its entire width was involved in the inflation, and in a few places one edge of the tumulus coincided with the edge of the flow. In one location, buried early in the study period, patches of the older flow ~20 m

apart bounded both sides of the tumulus, showing that the entire width of the flow at that location had evolved into the tumulus.

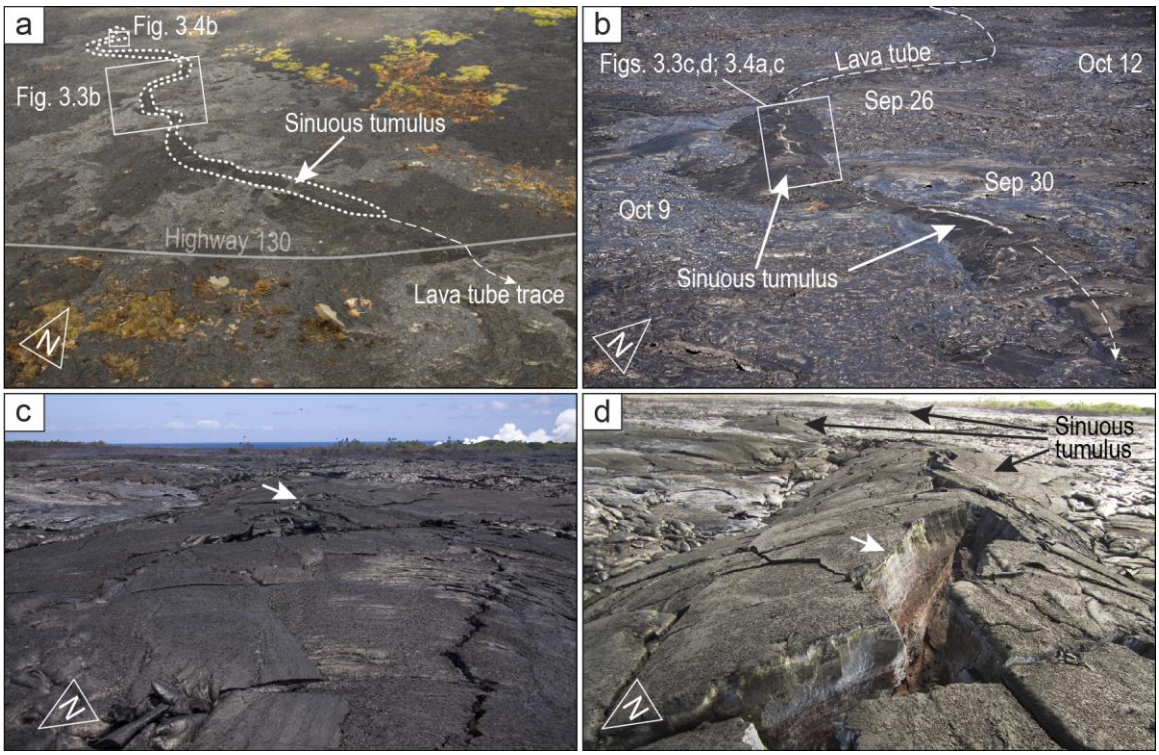

Figure 3.3 Photographs of sinuous tumulus in study area. (a) October 19, 2010, photograph showing distant perspective of sinuous tumulus. Dashed white line, lava tube trace; arrowhead denotes flow direction. Partly transparent white line, buried trace of Highway 130. White boxes, approximate area of coverage of 3.3b and 3.4b. Dark lava surface along and adjacent to tube trace is early-formed lava surface emplaced July 2010. Lighter-colored lava surfaces are younger tube breakouts. (b) October 14, 2010, photograph of sinuous tumulus. Dashed white line, approximate trace of lava tube beyond ends of pronounced tumulus. Four recent breakouts prior to October 14 labeled. White box, approximate coverage area of 3.3c and d,and 3.4a and c. (c) August 23, 2010, photograph and (d) November 16, 2010, photograph demonstrating inflation and tumulus uplift. White arrows mark matching point in (c) and (d).

The tumulus was covered by a network of cracks (the most pronounced sub-parallel to the trend of the tumulus) that appeared to have largely evolved from early-formed cooling joints (Figs. 3.3, 3.4 and 3.5; Peck and Minakami, 1968; Hon et al., 1994; Rossi and Gudmundsson, 1996; Schaefer and Kattenhorn, 2004). As a result, the axial crack was not simply a single linear feature, but instead jogged sharply along its trend,

especially where it adjusted to bends in the tumulus (Fig. 3.5a), and in some places was divided into sub-parallel en echelon segments. Where narrow, the tumulus was topped by a relatively well-developed axial crack (Figs. 3.3 and 3.5a) that exposed textures indicative of inflation (Hon et al., 1994; Anderson et al., 1999). The axial crack widened and deepened as inflation progressed and the tumulus evolved, and was up to ~0.7 m wide and ~2.9 m deep after activity ceased (Table 3.1). In places where the tumulus was broad, the axial crack was much narrower or even non-existent, with inflation of the tumulus apparently accommodated by a few sub-parallel cracks (Fig. 3.5b).

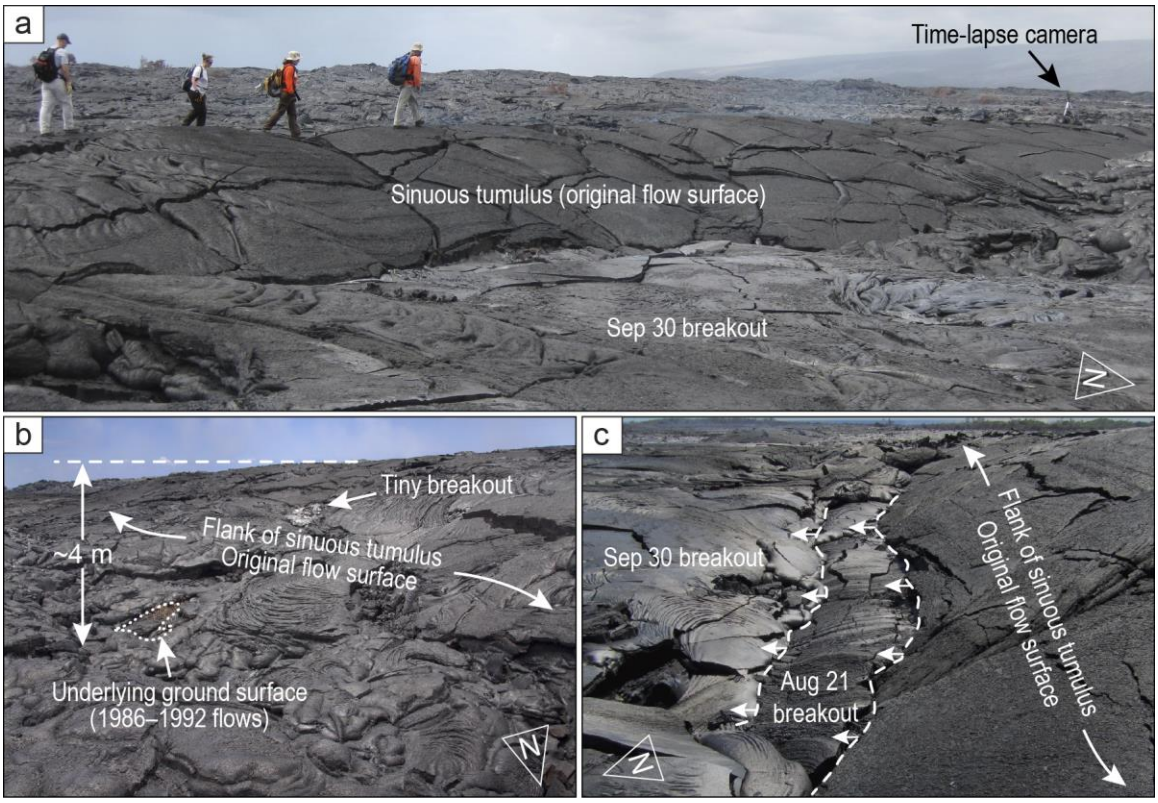

Figure 3.4 Photographs of sinuous tumulus in study area. (a) October 5, 2010, photograph showing northeast flank of sinuous tumulus. September 30 breakout in foreground. Photograph by WB Garry, NASA. (b) August 23, 2010, photograph showing ~4-m-high tumulus in contact with underlying 1986–1992 lava surface. Note tiny breakout which leaked through tumulus side ~3 m above base on August 18. (c) October 1, 2010, photograph showing breakouts from flank cracks (dashed white lines; arrows show breakout flow direction) parallel to tumulus trend. Exposed tumulus ~2.5 m high. Note August 21 breakout surface not buried by September 30 breakout.

The flanks of the tumulus expressed no significant inflation rifts as is seen on the sides of inflated sheet flows (Hon et al., 1994; Hoblitt et al., 2012). However, long cracks with minor vertical offset formed along the lower flanks of the tumulus in response to local breakouts. There was also no apparent vertical asymmetry in the growth history of the two flanks of the tumulus anywhere along its length (Anderson et al., 2012), nor did the axial crack contain lava squeeze-ups, as is often seen on other tumuli (Walker, 1991; Duraiswami et al., 2001; Anderson et al., 2012). The upslope end of the sinuous tumulus was buried early on by other flows, and the tumulus there emerged from beneath this younger cover, indicating that it extended farther upslope. Indeed, short sections of the tumulus farther upslope were visible through holes within this younger cover up to the base of Pūlama Pali. The terminus of the tumulus, roughly coincident with the buried trace of Highway 130, sloped down and merged with the surrounding flow surface in a fashion typical for tumuli (Walker, 1991; Rossi and Gudmundsson, 1996).

The tumulus stood up to ~4 m above the surrounding lava surface. This was, however, an apparent height because the flanks of the tumulus were partly inundated by breakouts from the tumulus itself (described below). Differencing of the pre- and post-emplacement surfaces show that the sinuous tumulus had a maximum height of nearly 8 m (Table 3.1).

3.4.3 DI events and breakouts: August–November 2010

During 2010, cycles of deflation and inflation (DI events) at Kīlauea's summit (Fig. 3.6; Cervelli and Miklius, 2003; Poland et al., 2011), recorded across the summit tiltmeter network, deformed the edifice and caused variations in discharge from the episode 58 vent. Generally, within a few hours of the onset of summit deflation, a tiltmeter on the north flank of Puʻu ʻŌʻō likewise recorded the onset of deflation. This was followed, over the next day, by a decline in the abundance and vigor of surface flows as well as a pronounced diminution in the steam plume created by lava entering the ocean. These decreases in flow field activity were observed repeatedly, and reductions in discharge are inferred to have accompanied all DI events.

Deflation at Kīlauea's summit switched invariably to rapid inflation, usually within a day or two (Fig. 3.6). After a few hours, Puʻu ʻŌʻō likewise began to inflate, and

discharge from the episode 58 vent increased soon after that. In most cases, recovery of the magmatic system resulted in a surge in output from the vent, which commonly resulted in short-lived breakouts from points along the lava tube between the top of the Pūlama Pali and the ocean, where the carrying capacity of the tube was exceeded. In some instances, the delay between the onset of the inflation phase of a DI event and its related breakout was such that, by the time the breakout started, the deflation phase of the next DI event had already begun.

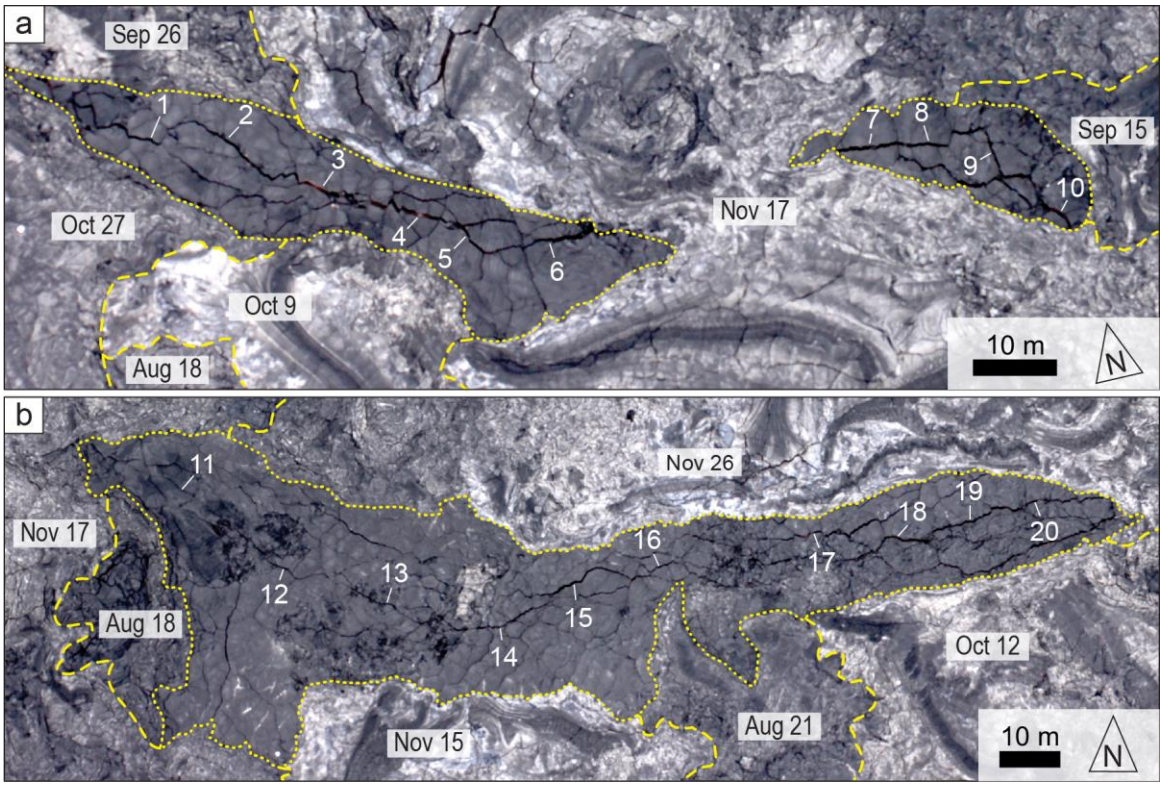

Figure 3.5 Rectified aerial image mosaics showing part of sinuous tumulus and related breakouts.Tumulus outlined with dotted yellow lines; contact between breakouts demarkated by dashed yellow lines (labeled with start date in 2010). Numbered locations correspond to measurements recorded in Table 3.1. Flow direction in tube from left to right and (a) is immediately upstream from (b).

Table 3.1 Sinuous tumulus and axial crack measurements.

Station	Crack width (m)	Crack depth (m)	Tumulus height (m)	Tumulus width (m)	Aspect ratio
1	0.32	1.5	5.6	9.7	0.58
2	0.30	2.9	5.5	13.5	0.41
3	0.72	1.6	5.6	9.4	0.60
4	0.55	1.9	4.8	11.2	0.43
5	0.33	1.6	4.6	13.5	0.34
6	0.41	1.9	5.1	12.1	0.42
7	0.59	1.7	5.0	7.0	0.71
8	0.40	1.9	5.6	10.7	0.52
9	0.31	2.2	5.6	10.6	0.53
10	0.55	1. 8	4.0	6.9	0.58
11	0.09	1.4	5.0	19.7	0.25
12	0.21	2.0	5.6	44.9	0.12
13	0.22	1.8	6.4	30.8	0.21
14	0.30	1.4	6.6	28.6	0.23
15	0.40	1.4	6.7	28.4	0.24
16	0.26	1.6	6.4	12.6	0.51
17	0.36	1.5	7.5	16.6	0.45
18	0.50	2.4	7.7	16.9	0.46
19	0.36	1.8	7.5	18.5	0.41
20	0.30	1.9	6.9	14.0	0.49

Notes: Table shows width and depth of dominant crack on or near crest of sinuous tumulus, width of exposed tumulus, tumulus height determined by differencing pre- and post-emplacement DEMs, and tumulus aspect (height/width) ratio at 20 locations spaced sub-equally along tumulus shown in Figure 3.5. Tumulus widths measured from rectified photo in direction approximately perpendicular to tube direction; crack width measured between piercing points; crack depth limited by depth to which metal carpenter's tape could be inserted.

Starting in August 2010, breakouts driven by DI events began to occur repeatedly from the sinuous tumulus that extended ~1 km inland from the buried trace of Highway 130 (Figs. 3.3 and 3.7). In all, 22 breakouts occurred from various locations along the tumulus in our study area from August through November (Table 3.2; Figs. 3.6 and 3.7). In addition, several other breakouts associated with DI events occurred outside the study area, both upslope and downslope. Thirteen of the breakouts from the tumulus can be related directly to DI events, and five others accompanied a general increase in tilt during the second half of November, after the repeated DI events ceased temporarily (Fig. 3.6). The correlation between the remaining four breakouts and DI events is not obvious. Specifically, a breakout on October 9 followed several days without a DI event, and may have been related to the inflated condition of the volcano at that time. A breakout on

October 12 began just a few hours after the start of the inflation phase of a DI event, but it may have been related to the earlier inflated condition of the volcano to which the October 9 breakout possibly responded. Two breakouts occurred several hours apart on October 15. Though both were probably related to the same DI event, the 17-hour delay between them makes the relation ambiguous. For this reason, only the earlier breakout is counted as being related to a DI event. Finally, a breakout on October 31 occurred just before the trough of a DI event. Because of the nearly 2-day delay between the onset of the previous inflation and the start of the breakout, the cause of the breakout is uncertain and it is not counted as being related to a DI event.

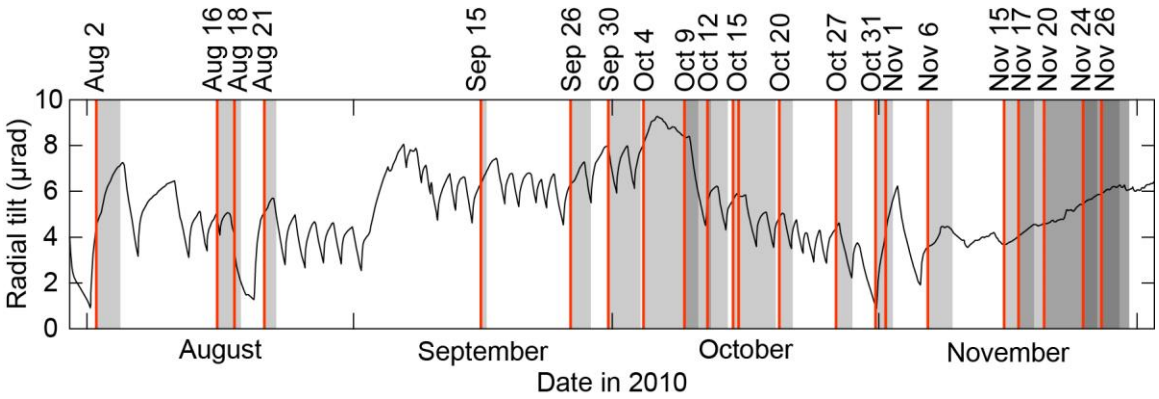

Figure 3.6 Graph showing onset times for sinuous tumulus breakouts compared to summit tilt. Red lines, breakout onset; black line, tilt recorded by UWE tiltmeter; gray boxes, approximate breakout durations (darker gray shows where boxes overlap, indicating multiple active breakouts).

Several of the breakouts were composed of multiple breakout points along the length of the sinuous tumulus and from both flanks (e.g., August 21 breakout; Fig. 3.7a). Many of these additional breakouts were small (hundreds of square meters or smaller), and all the individual breakouts associated with a particular event are grouped together. The areas of coverage shown in Table 3.2 reflect this. We suspected, but were not able to confirm directly that, during instances when there were multiple breakout points from the sinuous tumulus during a single event, the breakout point farthest upslope occurred first, suggesting a pulse of lava traveling through the tube and causing breakouts progressively downslope as the pulse advanced. This was certainly the case in a broader sense, with breakouts upslope, on Pūlama Pali, starting before breakouts on the coastal plain. That

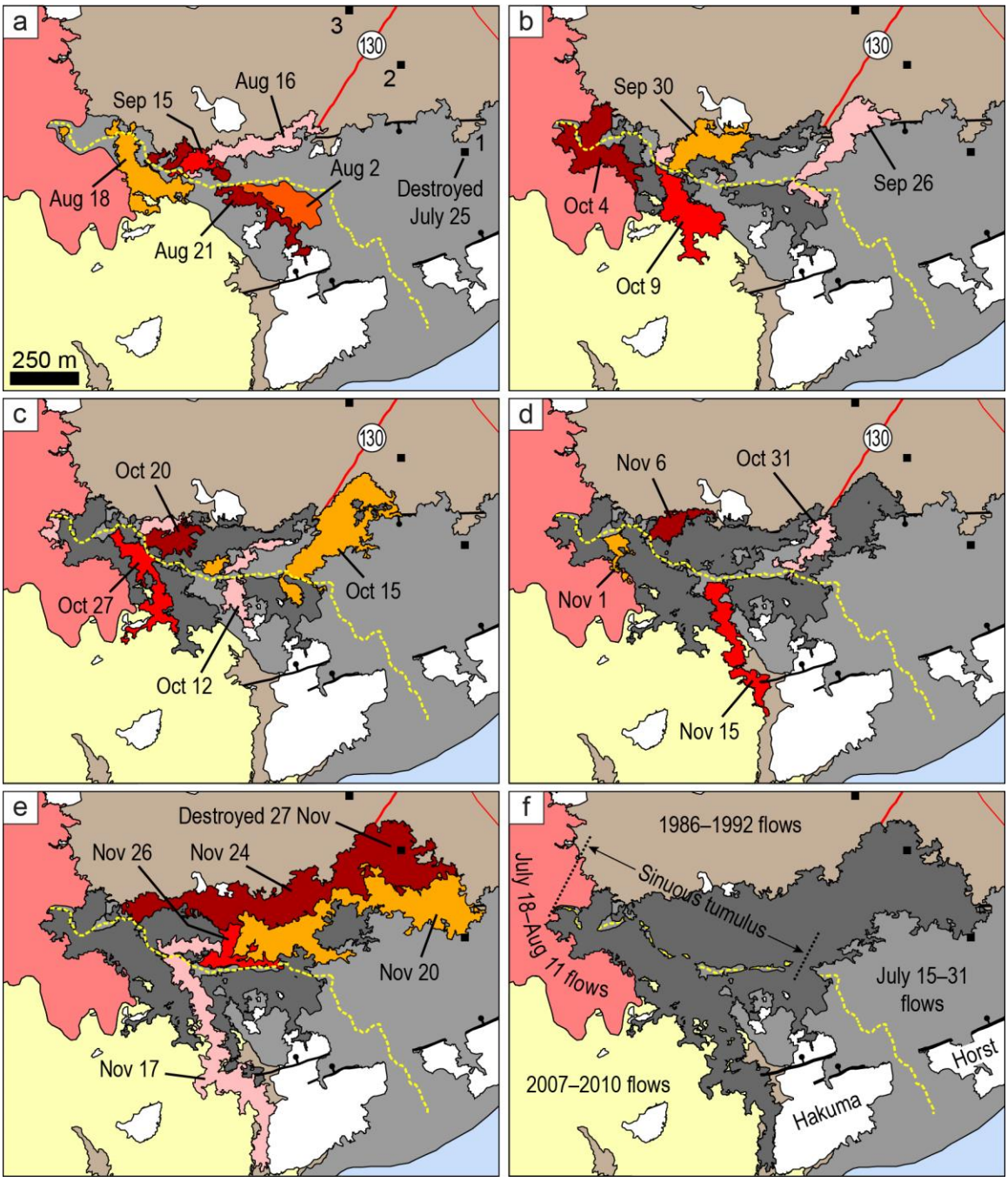

Figure 3.7 Maps showing sinuous tumulus breakouts. Pacific Ocean at lower right; Kalapana Gardens subdivision at upper right. Heavy red line, State Highway 130; thin red line, main entrance road into Kalapana Gardens; white, areas not covered by lava (forested); dotted yellow line, active lava tube; heavy black lines, normal faults of Hākuma horst and graben (ball–bar symbols on down-dropped side); black squares, houses shown in Fig. 3.2b. (a–e) Final extent of tube breakouts, labeled by start date. Dark gray area in each successive map (b–e) shows area covered by breakouts shown in previous panel. (f) Dark gray, composite of all tube breakouts erupted in study area August 1–November 30, 2010. Lava tube shown beneath breakout composite to highlight tumulus where lava surface not reburied after emplacement.

this also occurred on a smaller scale is supported by the fact that the breakout point farthest downslope (when there were multiple breakouts along the sinuous tumulus) was always the most voluminous and longest lived. Had it opened first, the other breakouts upslope would probably not have occurred. The volume of each breakout was indeterminable, but the area covered by each breakout might be an adequate proxy for comparing the relative sizes of the breakouts because all breakouts were erupted onto similar terrain. However, the area covered by each breakout from the tumulus within our study cannot be used to gauge the size of the pulse of lava traveling through the tube system because other breakouts from the tube corresponding with DI events often occurred outside the study area.

The larger breakouts had a vigorous start, with lava usually flooding from the tube as a sheet for tens of minutes to a few hours. These starts were easy to spot if they were in view of the webcams or time-lapse cameras, and they were often observed (and start time noted) by Kalapana Gardens residents and sightseers. Thus, the start times of most of the breakouts are relatively well constrained, often to a few minutes (Table 3.2).

The breakouts waned quickly (tens of minutes to a few hours), but weak activity—identified only because of our detailed daily mapping—sometimes continued for days. Because of this, the stagnation time of each breakout (Table 3.2) is poorly constrained, being bracketed by sequential field visits. Figure 3.6 shows the timing of the breakouts and their estimated duration compared to the tilt record from station UWE, one of Kīlauea's summit tiltmeters.

The breakouts were sourced from cracks flanking the lower sides of the tumulus and widened the flow dramatically, burying the lower ground on both sides of the sinuous tumulus and slowly inundating it (Figs. 3.3, 3.4 and 3.5). Flow inflation, at least early on, caused progressive growth of the tumulus so that much of it remained a topographic high and was not buried by these subsequent breakouts. The locations of these breakouts were not obviously related to the sinuosity of the tumulus (i.e., they did not preferentially occur either at bends or along straight sections of the underlying lava tube). At the onset of the breakouts, the tube roof was abruptly and irrecoverably pushed up. Inelastic uplift likewise helped the tube roof remain higher than the slowly thickening (by burial) flow field on both sides. Both mechanisms (inflation and inelastic uplift) permitted much of

Table 3.2 Timing and area of sinuous tumulus breakouts.

No.	Start Date/Time	End Date/Time (Bracketed)	Area (km^2)	DI Event Inflation Start	Delay (h)
1	Aug 2, 0200 (±4 hr)	Aug 4, ~1330 – Aug 5, ~1030	0.028	Aug 1, 1004	15.9
2	Aug 16, 0300 (±15 min)	Aug 17, ~2000 – Aug 18, ~1000	0.033	Aug 14, 2248	28.2
3	Aug 18, 0300 (±5 hr)	Aug 18, ~1000 – Aug 19, ~1000	0.037	Aug 16, 1112	39.8
4	Aug 21, 1500 (±3 hr)	Aug 22, 1000 – Aug 23, 1045	0.028	Aug 20, 1014	28.8
5	Sep 15, 1800 (±6 hr)	Sep 15, Night – Sep 16, Morning	0.009	Sep 14, 1814	23.8
6	Sep 26, 0445 (±5 min)	Sep 28, 1200 – Sep 28, 2000	0.043	Sep 25, 0844	20.0
7	Sep 30, 1430 (±1 hr)	Oct 4, 1200 – Oct 5, 1030	0.030	Sep 28, 1356	24.6
8	Oct 4, 1600 (±2.5 hr)	Oct 10, 1330 – Oct 11, 1100	0.039	Oct 3,1508	24.9
9	Oct 9, 1040 (±5 min)	Oct 11, 1400 – Oct 13, 1000	0.035	(no related DI event)	—
10	Oct 12, 0215 (±5 min)	Oct 13, 1200 – Oct 15, 1030	0.036	(uncertain relation)	—
11	Oct 15, 0045 (±5 min)	Oct 15, 1250 – Oct 16, 0830	0.004	Oct 14, 0553	18.9
12	Oct 15, 1740 (±30 min)	Oct 19, 1130 – Oct 20, 1300	0.066	(uncertain relation)	—
13	Oct 20, 1033 (±2 min)	Oct 21, 1530 – Oct 22, 1145	0.016	Oct 19, 1851	15.7
14	Oct 27, 0007 (±2 min)	Oct 28, 1100 – Oct 29, 1330	0.027	Oct 25, 2214	25.9
15	Oct 31, 1435 (±15 min)	Nov 1, 1400 – Nov 2, 1100	0.016	(uncertain relation)	—
16	Nov 1, 1839 (±2 min)	Nov 2, 1300 – Nov 2, 1800	0.007	Oct 31, 1810	24.5
17	Nov 6, 1646 (±5 min)	Nov 8, 0550 – Nov 8, 1800	0.013	Nov 5, 2053	19.9
18	Nov 15, 1314 (±2 min)	Nov 18, 1115 – Nov 19, 1030	0.028	(no related DI event)	—
19	Nov 17, 0555 (±1 min)	Nov 25, 1030 – Nov 27, 0930	0.076	(no related DI event)	—
20	Nov 20, 0458 (±1 min)	Nov 29, 1530 – Nov 30, 1000	0.162	(no related DI event)	—
21	Nov 24, 1642 (±2 min)	Nov 29, 1530 – Nov 30, 1000	0.143	(no related DI event)	—
22	Nov 26, 2018 (±1 min)	Nov 28, 1515 – Nov 29, 1000	0.017	(no related DI event)	—

Notes: Tables shows start date and time for each sinuous tumulus breakout (precision in parentheses), dates and times that bracketed end time of breakouts, and final area of breakouts. Date and time also shown for onset of summit inflation for DI events associated with breakouts, except where noted. Final column shows delay between onset of summit inflation and onset of breakouts, where applicable.

the early-formed emplacement surface to remain uncovered while the surrounding terrain was repeatedly buried by breakouts.

Because growth of the tumulus over the tube was more rapid in some areas than in others, the height of the tumulus varied along its length so that elongate, dark-colored whaleback structures were formed (Figs. 3.3, 3.4 and 3.5). The lower saddles between the whaleback structures were places that never hosted a breakout, and thus did not experience inelastic uplift. Some of the lows were eventually buried, subdividing what was originally a single long tumulus into an apparent chain of shorter tumuli (Fig. 3.5). The vertical evolution of the tumulus was not obviously related to its sinuosity, with higher parts of the tumulus just as likely to occur over straight sections as over bends in the tube.

Breakouts corresponding to the effusive surges caused by DI events occurred until mid-November. At that time, the DI events temporarily stopped happening, and the summit began a gradual inflationary trend. Along the studied section of the tube, this was manifested as a series of longer-lasting breakouts that covered correspondingly larger areas. Moreover, as many as three of these breakouts were active simultaneously, perhaps owing to an increase in discharge through the tube. Eventually, the tube upslope near the top of Pūlama Pali was unable to transmit the amount of lava it was carrying and, on November 29, it ruptured. The tube downslope from that point was abandoned thereafter, and the breakouts on the coastal plain subsequently stagnated. The November 29 breakout advanced downslope and eventually reached the coastal plain, where it buried most of the sinuous tumulus, leaving a few short segments partially exposed.

3.5 Discussion

3.5.1 Development of an inflated lava tube

Coastal flow emplacement during the Pu‘u ‘Ō‘ō eruption has generally followed a common pattern. The flows usually spread out upon reaching the gently sloped coastal plain, after traveling down the steeper slopes of Pūlama Pali, and advance by the progressive extension of pāhoehoe lobes (e.g., Peterson et al., 1994; Hon et al., 1994; Hoblitt et al., 2012). When fed at an eruption rate near or above the long-term average for

the Puʻu ʻŌʻō eruption, it usually takes one to three weeks for the leading tip of a flow to cross the coastal plain. Significant flow thickening via inflation and overplating occurs during this advance. On the other hand, when a flow is fed at an eruption rate well below the long-term average, or when a flow near or above the average rate is subdivided into smaller branches, the lava may stall on the hummocky surface of the coastal plain and make little forward progress. In such situations, it may take months before lava completely crosses the coastal plain, if it does so at all. In either case, once a flow tops the sea cliff, the inflating flow probably experiences a sudden drop in fluid pressure. Thereafter, the fluid core of the flow inland of the sea cliff chills quickly as lava is focused preferentially into the most energy efficient pathway between the base of Pūlama Pali and the ocean. Flow inflation and lateral spreading slow and stop, usually within a day or two, and a well-developed lava tube forms quickly.

The flow studied during July–November 2010 evolved in a slightly different fashion, in that it was easily confined by low topography because of its low discharge. As a result, the flow failed to spread out and crossed the coastal plain quickly despite its relatively low flux. Little inflation occurred before the flow poured over the low embankment on the south side of Highway 130. This embankment provided the same sort of topographic break that the sea cliff affords in other circumstances. Because of the inferred drop in fluid pressure, lava beneath the surface crust of the flow upslope from Highway 130 became concentrated along the thickest part of the flow. Thus, flow advance and lava tube formation occurred more rapidly than is typical for low discharge flows at Kīlauea and did not involve significant lateral spreading. Initial inflation across the entire width of the flow was minimal, and the flow failed to resurface itself as it usually does during flow emplacement through pāhoehoe lobe extension (Peterson et al., 1994). Morphologically, the flow had a relatively flat surface characteristic of sheet flows (Hon et al., 1994). The section of the lava tube between the base of Pūlama Pali and the Highway 130 embankment was, in a sense, isolated, and it evolved somewhat independently from other parts of the tube.

The inflation that occurred subsequently was focused along the axis of the incipient lava tube, which, when it began to form, was correspondingly thinner than the total thickness of the flow and probably had a wide, elliptical cross-section (Kauahikaua et al.,

1998). Conduction of heat through the roof, floor, and sides of the tube caused crustal growth and thickening. The subsequent corresponding pressure increase within the tube, due to decreasing cross-sectional area without a decrease in flow rate, forced the tube roof to arch up (Fig. 3.8; Hon et al., 1994; Kauahikaua et al., 1998). The result was a low, but well-defined, sinuous tumulus above the axis of the lava tube that meandered as a continuous feature across the coastal plain for a distance of ~1 km (Fig. 3.3). The height of the sinuous tumulus was further enhanced by irrecoverable uplift caused by the many breakouts from its flanks.

Peterson et al. (1994) describe another process by which an arched tube roof can form—accretion of lava onto levees during channelized flow. If the channel is sufficiently narrow these levees can grow together, forming an arched roof over the channel. While morphologically similar, the formation process is different from that described here, and the tube roof that forms in each case should be easily distinguishable in the field setting.

Inflation was possible only while the tube was completely full and lava was in contact with the tube roof. The depth of the axial crack on top of the tube gives an estimate of the time elapsed to develop a crust of that thickness. The empirical formula of Hon et al. (1994),

$$t = 164.8C^2 \tag{3.1}$$

where

t is time in hours, and
C is crustal thickness,

yields a total duration of ~57 days to form a 2.9-m-thick crust. The flow on the coastal plain at the measurement location, however, was active for a total of ~137 days, suggesting that the lava stream was in contact with the tube ceiling slightly less than half the time. Keszthelyi (2012) modified the formula of Hon et al. (1994) to better account

for emplacement and environmental conditions appropriate for Kīlauea's south coast. Using the Keszthelyi (2012) formula,

$$t = 323.5C^2 \tag{3.2}$$

yields a duration of ~113 days for formation of a 2.9-m-thick crust. This result indicates that the lava stream was in contact with the tube ceiling most of the time. Regardless, both results suggest periods during which head space separated the lava stream and tube ceiling.

The sinuous tumulus does not fit into any tumulus classification scheme defined previously, though it is most similar to the flow-lobe tumuli of Walker (1991) and Rossi and Gudmunsson (1996). Walker (1991) and Rossi and Gudmunsson (1996) classify flow-lobe tumuli by height/width and width/length aspect ratios. However, partial burial of the flanks of the sinuous tumulus by its own breakouts, combined with the extreme length and sinuosity of the tumulus, prevent a meaningful comparison with these parameters. For example, Rossi and Gudmunsson (1996) found that the flow-lobe tumuli that they measured had an average aspect ratio of 0.17 ± 0.06, while the aspect ratio of the sinuous tumulus varies from 0.12 to 0.71, depending on where along the tumulus's length the measurement is made (Table 3.1, Fig. 3.5).

No relation has been established between axial crack width and other geometrical tumulus parameters. In general, though, the width of the axial crack in the sinuous tumulus (Table 3.1) is much narrower than the axial cracks in similarly sized flow-lobe tumuli as described by Walker (1991) and Rossi and Gudmunsson (1996). This is consistent with our model that the sinuous tumulus was formed in part by inelastic uplift of the lava tube roof during breakouts, when the tube was overfilled by increased flux, and not entirely by inflation.

Anderson et al. (2012) found that some tumuli form over horizontal bends in the underlying flow pathways. Variations in height along the length of the sinuous tumulus showed no obvious correspondence to bends in the tube. In our case, height variations reflect the presence or absence of breakouts—the lowest areas along the tumulus were those that experienced no breakouts and, thus, little or no inelastic uplift. What controlled

the location of the breakouts along the tumulus, however, is not known, but may have been related to local variations in other factors, such as tube width, tube slope, or flow thickness.

3.5.2 Earth and Mars examples

Very long sinuous tumuli aligned with a lava tube, like that described here, have not been described before from Hawai‘i, though they have been observed both before and since. Very long tumuli, with no mention of sinuosity or tube relationship, are mentioned by Wentworth and Macdonald (1953), who call them “pressure ridges”. However, they lump together ridge-like features formed by inflation as well as those formed by lateral compression. Hon et al. (1994) mention “long sinuous ridges” that form over blockages in major lava tubes, but provide no additional description. Cashman and Kauahikaua (1997) also mention “sinuous tumuli” forming over lava tubes, but likewise provide no additional description. The large tumulus they studied (the Woodchip tumulus) did form over a lava tube, but it was a single elongate whaleback structure, about 230 m long and weakly sinuous, that formed in a large sheet flow. Kauahikaua et al. (1998) describe “a train of inflating, elongate tumuli” that developed over a Pu‘u ‘Ō‘ō lava tube on Kīlauea’s gently sloping coastal plain during 1996–1997. These tumuli were a source of breakouts during pulses of lava through the tube following eruptive pauses. The tumuli, however, were smaller and more equant than the sinuous tumulus describe here, though their positions followed the sinuous trace of the tube over which they developed (J. Kauahikaua, personal communication, 2013).

Glaze et al. (2005) describe a chain of very large tumuli on the 1843 flow from Mauna Loa (Hawai‘i). While those tumuli cluster along a linear trend, they are not shaped like the sinuous tumulus, and Glaze et al. (2005) found no evidence for a long-lived tube beneath the tumuli. Some elongate, crescent-shaped tumuli are present on the coastal plain portion of the 1859 Mauna Loa flow (F. Trusdell, personal communication, 2013), but they are no more than about 100 m in length. Their relation to a tube system is not known, and they are not mentioned by Walker (2009) who conducted a detailed study of tumuli and lava rises in the same area. Chitwood (1994) describes inflated lava fields in central and southeast Oregon, USA, and indicates that long narrow tumuli can form

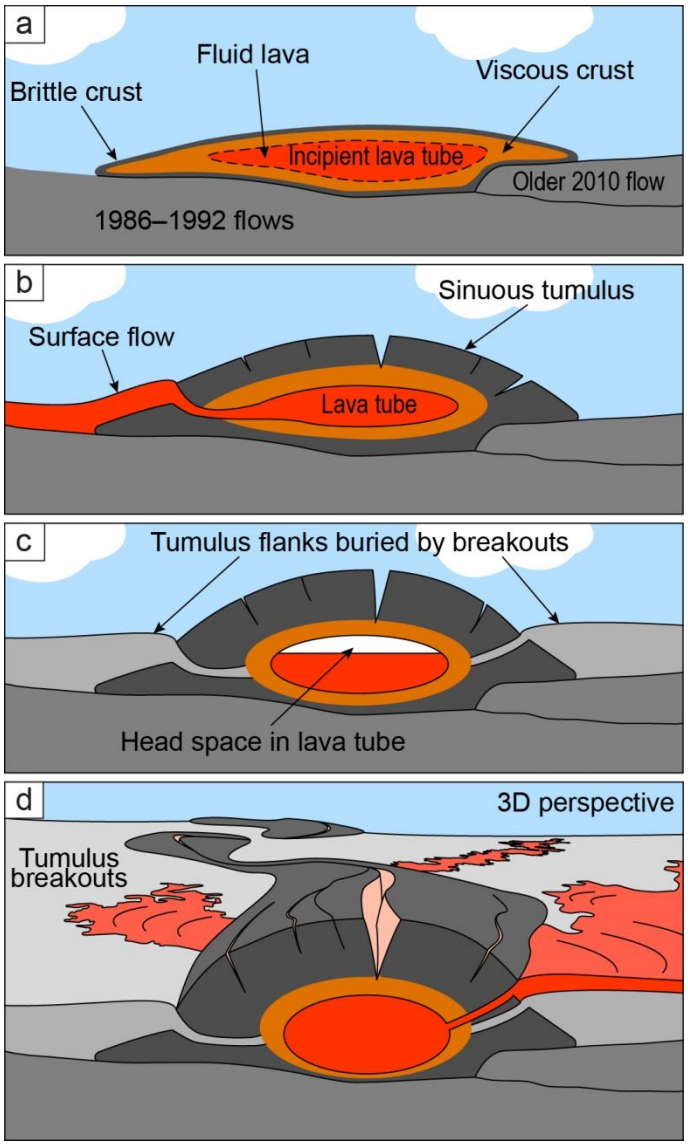

Figure 3.8 Cartoon showing idealized cross-section through lava flow and sinuous tumulus at different development stages. (a) Time step 1: Shortly after emplacment; well-developed tube not yet formed and inflation is minimal. (b) Time step 2: Tube has developed and tumulus has begun to form; pressurization of tube has resulted in breakout from tumulus flank. (c) Time step 3: Tumulus has undergone additional growth; breakouts, no longer active, have emerged from both flanks of tumulus, partly inundating it; head space has formed between lava stream and tube ceiling. (d) Time step 4: 3D perspective of tumulus showing active breakouts from several places along tumulus flanks in response to re-pressurization of lava tube.

over lava tubes but provides no discussion of tumuli dimensions and points to no specific examples. Finally, the Undara lava field in north Queensland, Australia, contains a 40-km-long sinuous inflation ridge ("The Wall"; Atkinson et al., 1975; Stephenson et al.,

1998) which has been suggested as an analog for lunar rilles (Atkinson and Atkinson, 1995). This 200-m-wide, flat-topped feature has been demonstrated to be a narrow, inflated sheet flow (J. Kauahikaua, personal communication, 2013), much like similar inflation ridges on the much younger Toomba basalt flow of north Queensland, Australia (Whitehead and Stephenson, 1998).

Only a few sinuous tumuli like the one observed forming in Hawai‘i during 2010 have been described world-wide. While many examples probably exist, the two we are aware of are found on the prehistoric Carrizozo and McCartys flows, New Mexico, USA. These are among the youngest and best preserved basaltic flow fields in the continental United States (Zimbelman and Johnston, 2002). The proximal and distal regions of both flows display evidence for flow inflation and were presumably linked by lava tubes (Keszthelyi and Pieri, 1993; Zimbelman and Johnston, 2001; 2002; Crumpler et al., 2007). The medial section of each flow is comparatively narrow due to confining topography and contains an elongate ridge that is, in some places, more than 10 m high. If the model presented here explains the formation of these ridges, then they are capped by lava emplaced early in each flow's history, and pāhoehoe flows that flank and partly inundate the ridges were sourced from the ridges themselves. Testing these expected relationships should help to determine if these sinuous ridges formed as described above, and will help constrain the emplacement conditions.

Sinuous ridges similar in size to those identified in Hawai‘i and New Mexico are observed within the plains flows of the Tharsis volcanic province of Mars (Fig. 3.9). Here, low shields and fissure vents erupted flows that coalesced to form a gently sloping plain. The sinuous ridges within the flows are up to 10 m in height and are the sources for small, local surface flows. Similar ridges found elsewhere across the surface of Mars have been interpreted as inverted fluvial channels (e.g., Burr et al., 2009; Williams et al., 2009; Burr et al., 2010; Zimbelman and Griffin, 2010; Lefort et al., 2012), eskers (Baker, 2001; Head and Pratt, 2001; Bleacher et al., 2003; Ghatan and Head, 2004; Banks et al., 2009), or eroded remnants of subsurface dikes (Head et al., 2006). The development of inverted fluvial channels and eskers involves flowing water, and all three of these proposed processes require significant erosion and regional deflation.

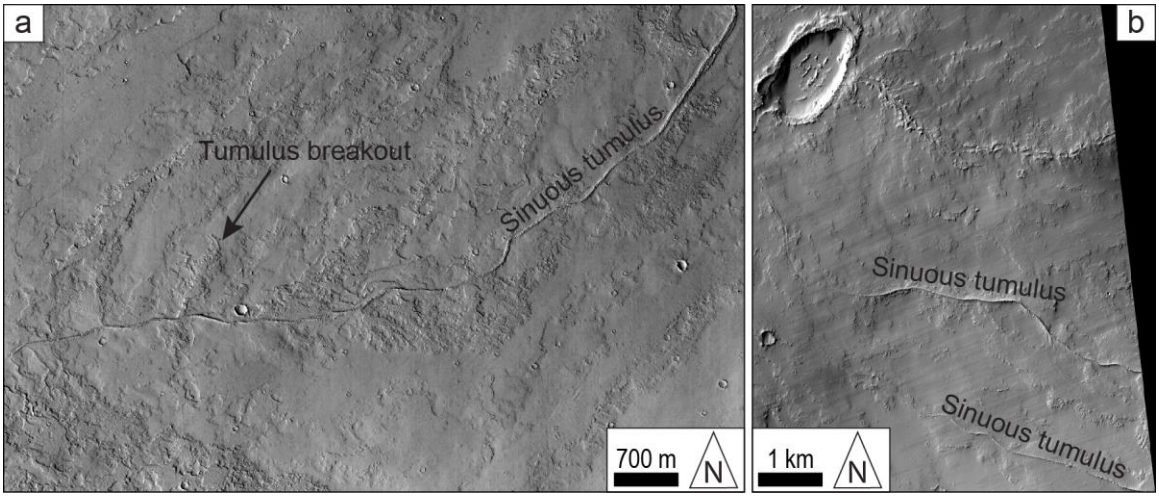

Figure 3.9 Images of sinuous ridges within Tharsis volcanic province of Mars. (a) Mars Reconnaissance Orbiter (MRO) Context (CTX) Camera image P07_003673_1774 (NASA/JPL-Caltech/MSSS) showing ≤10-m-high ridge (Solar Incidence Angle 53°; Sun ~ 37° above horizon). Arrow points to one example of small breakout sourced from ridge, but many are visible. (b) MRO High Resolution Imaging Science Experiment (HiRISE) Camera image ESP_027289_1790 (NASA/JPL/University of Arizona) showing low shield volcano in Tharsis plains (caldera at upper left; Solar Incidence Angle 54°; Sun ~36° above horizon) with two sinuous ridges that appear to be source of small surface flows. In both cases, ridge morphology appears where slopes decrease to <0.5º on lower flank of volcano.

Although the plains units of the Tharsis region do not display obvious confining topography to drive localized tube-related inflation, lava flow thicknesses across Mars are suggested to be on the order of tens of meters (Keszthelyi et al., 2008; Mouginis-Mark and Rowland, 2008; Hamilton et al., 2010; Hamilton et al., 2011), comparable to the confining topography described above and sufficient to enable this process on Mars. The interpretation of sinuous ridges on Mars as elongate tumuli over lava tubes provides new insight into such ridges. While alternative (e.g., regional deflation or fluvial) hypotheses are viable for some Martian sinuous ridges, the hypothesis that these features are inflated lava tubes is the most likely in volcanic terrains that do not show evidence of regional erosion. The tube formation processes described by Greeley (1987) and Peterson et al. (1994) may apply to flow fields on the flanks of much larger (hundreds of km in diameter) Martian shield volcanoes (Bleacher et al., 2007a,b) where slopes are several degrees or higher and distinct ridges, as shown in Figure 3.9, are not observed.

3.5.3 Forecasting lava tube breakouts

Forecasting volcanic activity is a driving motivation for volcano research and monitoring. Generally, forecasts for impending eruptive activity, especially the larger changes, improve as the time of the eruption approaches. During ongoing eruptive activity, though, there are myriad small changes that occur with little or no warning. During August–November 2010, however, activity at Kīlauea behaved in such a way that the occurrence, and to some extent the location and timing, of lava tube breakouts that threatened houses in the nearby Kalapana Gardens subdivision could be forecast. This information was disseminated in daily volcanic activity updates on the HVO webpage and was transmitted directly to HCCD to improve their preparedness in the event that homes were threatened.

The correlation between the inflationary phase of DI events at Kīlauea's summit and the subsequent increase in eruptive activity along Kīlauea's East Rift Zone has been seen in hundreds of instances over more than a decade of observation, and the period discussed here was no exception. The occurrence of breakouts from the active tube system hours after the onset of summit inflation became apparent shortly after the flow was emplaced. It was not a perfect correlation with regard to our study area—33 DI events occurred from the beginning of August to mid-November, but only thirteen were associated with breakouts from the sinuous tumulus (Table 2). However, the DI events also often resulted in breakouts from other parts of the tube system, both upslope and downslope from the sinuous tumulus. Thus, those DI events that were not followed by breakouts from the sinuous tumulus were typically associated with breakouts elsewhere along the tube system. It was also noticed that, on a few occasions (in particular September 30 and October 15), a coastal plain breakout spanned two DI events. In the September 30 case, the breakout waned quickly and was nearly inactive by October 2, but its activity had increased again by October 3, following another DI event. The same is inferred for the October 15 case, though a gap in observation prevented confirmation. Finally, the effusive surge following some DI events, in particular those of the smallest magnitude, may have been completely accommodated by the tube system without a breakout.

Despite these shortcomings, hazard assessments were predicated on the assumption that every DI event was capable of producing a breakout on the coastal flow field near Kalapana Gardens. The delay between the onset of the inflationary phase of the DI events and the start of the related breakouts ranged from 15.7 hours to 39.8 hours (Table 3.2), with an average delay of 23.9 hours. The goal when communicating with Hawai‘i County Civil Defense authorities was to provide an assessment of potential activity for the following 24 hours. The delay between the inflation onset and subsequent breakouts fits well within this scheme.

Each breakout from the sinuous tumulus partly inundated the adjacent flank of the tumulus while leaving other sections unburied. Not surprisingly, it was found that later breakouts were more likely to occur in areas that had not previously hosted a breakout, where the flank of the tumulus was not partly buried. With this in mind, a few attempts were made, with marginal success, to forecast the most likely points along the sinuous tumulus for the next breakout. Based on a visual inspection of the neighboring landscape, it was possible to make a rough estimate of the presumed flow direction for each of these potential breakout locations. However, there were simply too many spots along the tumulus from which breakouts could potentially occur for each DI event, and the breakouts did not always emerge from parts of the tumulus that were not covered, so this part of the hazard assessment was abandoned. Moreover, because the distance from the tumulus to the nearest house was too great for breakouts to pose an immediate hazard, there was ample time once a breakout began to assess its probable flow path.

Destruction of Kalapana Gardens and neighboring communities in 1990 was controlled, in part, by eruptive pauses and subsequent restarts (Mattox et al., 1993). These pauses caused the flow that was active on the coastal plain to stall, and resumption of activity through the tube system resulted in new breakouts that followed the inflated margins of the existing flow (Mattox et al., 1993). Repeated breakouts led to flow field widening and further destruction. While modern tiltmeters like those monitoring Kīlauea in 2010 were not in use at that time, other deformation tools showed a pattern of deflation and inflation similar to the DI events that caused variations in discharge in 2010. The 1990 events, however, were probably more akin to the “DID events” that occurred during 2000–2004 (Cervelli and Miklius, 2003; Poland et al., 2011), which were larger in

magnitude, more infrequent, and associated with a much larger surge in discharge. Regardless, the unsteady supply of lava through Kīlauea's East Rift Zone conduit, both in 1990 and in 2010, directly controlled the occurrence of lava tube breakouts near Kalapana, and these breakouts could be reliably forecast hours in advance using deformation data recorded at Kīlauea's summit.

3.6 Summary

Lateral confinement of a non-channelized basaltic lava flow by topography provides an important control on the flow's subsequent evolution. Rather than developing into a broad, inflated flow field, flow inflation may be focused directly over the tube, to form a long tumulus axial to the tube. The sinuous tumulus described here is one of a few examples known worldwide, and is the only one to have been observed throughout its formation. Its morphology and mechanism of formation were different than typical tumuli and, as such, it does not fit into any of the previously published tumuli classification schemes (Walker, 1991; Rossi and Gudmundsson, 1996). Its presence also shows conclusively that tumuli can form over major lava tube systems, a process questioned in the past (e.g., Walker, 1991).

Temporary increases in discharge pressurized the lava tube and caused inelastic uplift of the sinuous tumulus and breakouts from its flanks. The abrupt, forced uplift of the tube roof was in addition to flow inflation that occurred while the lava stream was in contact with the tube roof. The result was a sinuous tumulus composed of an early-formed lava surface surrounded by younger flows that emerged from the sides of the tumulus itself and buried the surrounding landscape. Eventually, low parts of the tumulus were buried by breakouts from adjacent areas of the tumulus itself. This subdivided the tumulus into a chain of shorter, elongate tumuli. It would not have been known that these were all part of a single, very long sinuous tumulus if its entire evolution had not been observed.

The ability of topography to confine a flow must be closely tied to the discharge. While all flows will be confined by sufficiently high topography, flows fed by lower discharges can be confined by correspondingly lower topography, even down to the centimetric-scale (Hon et al., 1994; Rossi and Gudmundsson, 1996; Hamilton et al.,

2013). We contend that the failure of the flow emplaced on Kīlauea's south flank during July–November 2010 to spread, thus causing its evolution into a sinuous, elongate tumulus, was controlled in part by its low discharge in this instance. A higher discharge, matching the long-term average at Kīlauea, would have likely resulted in a wider flow, more distributed inflation, and no tumulus above the axis of the tube that would have eventually formed. Sinuous tumuli found within narrow, topographically confined sections of the prehistoric McCartys and Carrizozo flows (New Mexico, USA) probably formed in an equivalent fashion, and we propose that these examples on Earth may be analogs for at least some sinuous ridges found within the Tharsis volcanic province and elsewhere on Mars.

Cycles of edifice deflation and inflation (DI events) at Kīlauea's summit cause decreases and increases in East Rift Zone output respectively. During the July–November 2010 study period, the decreases were manifested on the active flow field as diminutions in eruptive activity, while the increases led to breakouts from the active lava tube. As described above, many of these breakouts came from the section of the lava tube topped by a ~1-km-long sinuous tumulus. Though imperfect, the correlation between DI events and lava tube breakouts was used to forecast the possibility of new, potentially hazardous flows, which was communicated to Hawai‘i County Civil Defense.

Chapter 4

Explosive eruptions triggered by rockfalls at Kīlauea Volcano, Hawai‘i

Published as:

Orr, T.R., Thelen, W.A., Patrick, M.R., Swanson, D.A., and Wilson, D.C., 2013, Explosive eruptions triggered by rockfalls at Kīlauea volcano, Hawai‘i. Geology 41(2), 207–210.

4.1 Introduction

Ongoing eruptive activity at Kīlauea Volcano's summit (Wilson et al., 2008; Houghton et al., 2011) has been dominated by outgassing from a lava lake in a pit within Halema‘uma‘u Crater (Figs. 4.1 and 4.2). Since the onset of the eruption, the generally steady outgassing from the vent has been punctuated sporadically by dozens of small explosive eruptions, and hundreds of even smaller outgassing bursts (Patrick et al., 2011b). Associated with these bursts are "composite" seismic events, defined here as being characterized by an emergent high-frequency (HF) onset that transitions into long-period (LP) seismicity superimposed on a distinctive very-long-period (VLP) oscillation (Figs. 4.3 and 4.4). The VLP oscillation is often large enough to be seen in the raw velocity waveforms without the aid of filtering.

Continuously recording webcams have documented the eruption since its onset in 2008, and the video observations of lava lake dynamics and explosive activity are unparalleled. The video record, enhanced by near-daily field observations, shows that the explosive eruptions and outgassing bursts—which have occurred sporadically since the vent opened—were triggered by rockfalls from the vent walls onto the top of the lava column. Here we examine in detail rockfalls that occurred during January–March 2011, which was a period of slowly rising lava level within the vent. These were among the

best observed rockfalls, and they provide direct evidence that rockfalls can trigger explosive outgassing of low intensity at Kīlauea.

4.2 Eruption Overview

After a 25 yr hiatus in eruptive activity at the summit of Kīlauea, a new eruptive vent opened on March 19, 2008, forming a 35-m-wide opening on the southeastern wall of the 1-km-wide Halemaʻumaʻu Crater (Fig. 4.1; Wilson et al., 2008). By March 2011, the vent had evolved into a 150-m-diameter collapse crater that extended across the relatively flat floor of Halemaʻumaʻu (Figs. 4.1 and 4.2a). This widening was the result of the piecemeal collapse of the vent walls and overhanging portions of the vent rim into an underlying cavity holding an actively circulating lava lake (Figs. 4.1b and 4.2).

The lava lake first became visible in September 2008. Since then, its level has varied considerably, from high enough to overflow the vent to a low of at least 210 m below the rim, rising and falling within a roughly cylindrical vertical conduit (Fig. 4.1b). On a few occasions, the lava surface has dropped out of sight below 210 m, revealing a floor with a complex and changing arrangement of one to three smaller openings. Based on these observations, the minimum volume for the entire collapse crater indenting the floor of Halemaʻumaʻu was ~4×10^6 m^3, as of March 2011. The amount of lithic material of all size classes erupted from the vent to that time, however, totaled a mere 1.1×10^3 m^3, accounting for less than 0.1% of the collapse crater volume. Vent enlargement, thus, has occurred as a result of the collapse of wall rock into the vent and the transport of this material into the deeper magma system (Swanson et al., 2009).

Such collapses have been common throughout the eruption, and thousands of rockfalls have been observed, ranging in size from tiny fragments to massive slices of the vent rim with volumes exceeding 1×10^5 m^3. The largest several hundred of these rockfalls were followed by short-lived ash emissions from the vent (Fig. 4.2b). Dozens of times, these rockfalls triggered small explosive eruptions that deposited ash- to bomb-sized juvenile scoria and ash- to block-sized lithic clasts up to several hundred meters from the vent. The scoria pyroclasts are coated in lithic dust, and lithic fragments are distributed throughout their juvenile matrix (Fig. 4.2d; Wooten et al., 2009), showing a thorough mixing of lithic and juvenile components during eruption.

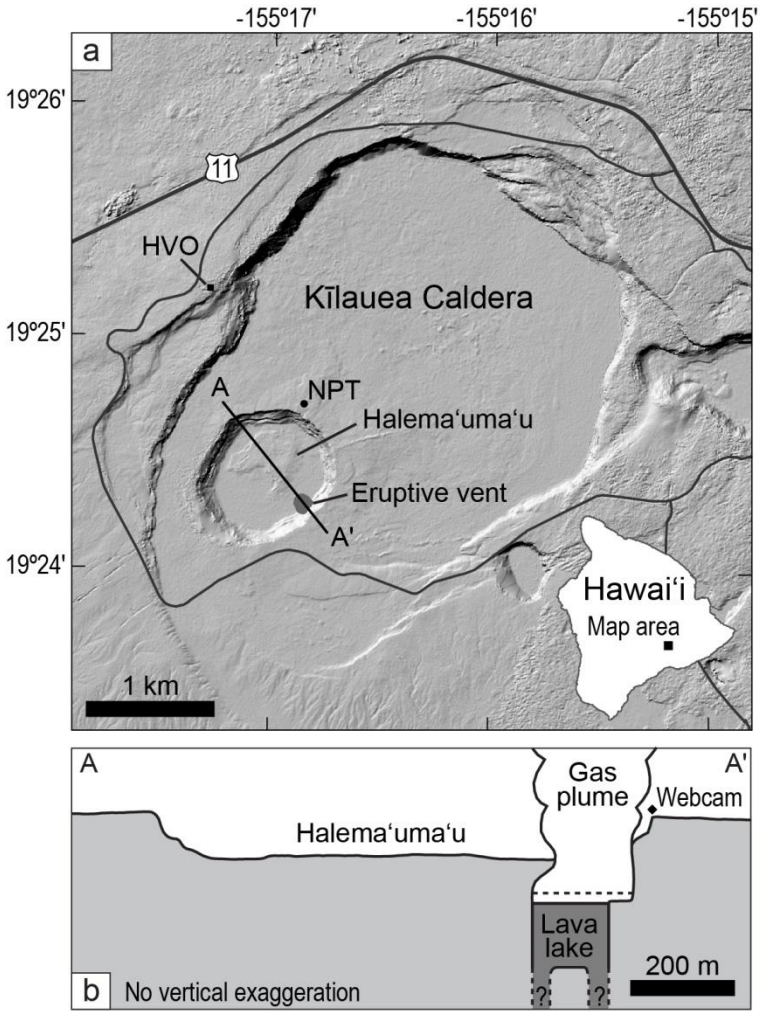

Figure 4.1 Map of Kīlauea Caldera and cross section through Halemaʻumaʻu. (a) Map shows location of eruptive vent on southeast edge of Halemaʻumaʻu. HVO, Hawaiian Volcano Observatory; NPT, North Pit seismometer. A–A′ denotes (b) cross section through Halemaʻumaʻu and eruptive vent, drawn to scale. Black diamond, webcam; dotted line, high lava lake level achieved in March 2011. Deeper conduits based on locations of upwelling lava following March 5–6, 2011, lava lake draining.

In mid-November 2010, the lava lake began to rise slowly as Kīlauea's magmatic system pressurized. By January 2011, the lava lake surface had reached to within ~100 m of the rim of the vent. Over the following 2 months, the lava level rose an additional 35 m, bringing it to within 62 m of the vent rim by early March (Figs. 4.1b and 4.2a). Then, on March 5–6, 2011, the lava lake dropped ~145 m over a period of about a day as summit magma intruded Kīlauea's East Rift Zone, where it fed a new eruption (episode

59; see Chapter 5). We focus here on the period from January to March 5, 2011, when the lava lake was at a high level.

4.3 Data Collection

The foundation of this study is the wealth of observational data collected during the summit eruption. In particular, we analyze video of the lava lake collected at ~4 frames per second using a Stardot® Netcam SC webcam operating in a near-infrared mode. This camera was positioned on the edge of Halemaʻumaʻu Crater, 85 m above the erupting vent (Fig. 4.2a). Video from this camera was used to time rockfalls and their associated explosive events and to elucidate eruption mechanisms. The video was telemetered to the Hawaiian Volcano Observatory, where it was time-stamped to Hawaii-Aleutian Standard Time (UTC –10 h) by the acquisition software (Milestone® XProtect Professional) based on the clock of the acquisition computer, which itself was synched to a network time-server. The image timestamp is precise to 0.01 s, but was found to be ~0.4 s slow. The image timestamps shown in Figure 4.3 have not been adjusted for this delay.

We compare the video data to seismicity from the vertical channel of station NPT, where the seismic signal is time stamped. NPT, one of Kīlauea's 10 summit seismic stations, is a broadband station (60 s–50 Hz sensitivity) located in an underground vault ~800 m north of the active vent (Fig. 4.1). The composite seismic events share the same frequency content across all of Kīlauea's summit stations, and thus the frequencies are an effect of the source, not the path the waves travel through or the site on which the seismometer sits. The seismic travel time between NPT and the vent is ~0.4 s (assuming shear wave velocity = 2.3 km s^{-1}; Chouet et al., 2010). Thus, the timing of the video data matches the timing of the seismicity, and no correction is required to directly compare the two. A 0.5 Hz low-pass minimum phase shift filter was applied to the seismic data to effectively reduce the noise and allow us to focus on the frequencies of interest.

4.4 Key Observations

Video and field observations during early 2011 showed, at times, an almost constant rain of lithic material from the vent walls into the lava lake. This disintegration process was accelerated by vent wall heating due to a slowly rising lava lake level. The

collapse of larger vent wall sections often took place as a sequence of failures that occurred progressively higher up the wall in a process similar in style to that of roof stoping above an underground cavity (e.g., Waltham et al., 2005, p. 57). These sequences of larger rockfalls, which typically spanned a period of several hours, were interspersed with many smaller rockfalls and usually culminated in catastrophic collapses of the vent rim. Examples of such rockfall sequences in 2011 occurred on January 17–18, February 14, February 15, March 2, and March 3 (Fig. 4.4). In every case, substantial rockfalls were associated with HF seismicity, and the largest of these with LP and VLP seismicity. This is apparent in the video record, which shows a one-to-one correlation between rockfalls and seismic events during periods when visibility was adequate, which includes most composite seismic events in early 2011.

In all of the larger rockfalls, the wall rock disaggregated into loose debris, enveloped by a cloud of dust, during descent (Fig. 4.2c). The impact of the rockfalls with the lava lake surface then resulted in the release of billowing ash clouds (Fig. 4.2b) and, in the case of the largest collapses, the visible ejection of juvenile tephra (e.g., Fig. 4.2d). The ash cloud and eruption of juvenile tephra always originated from the point of impact. There was also a general correspondence between the size of the rockfall and the resulting emission of pyroclastic material. Only the largest rockfalls triggered explosive eruptions that dispersed juvenile lapilli and bombs beyond the rim of the vent. The preexisting condition of the lava lake (i.e., whether capped by a crust or energetically spattering) seemed to have little bearing on the eruptive response following rockfalls. This is apparent during rockfall sequences where later rockfalls were just as likely to trigger an explosive eruption as earlier rockfalls, despite the lava surface being completely disrupted by the earlier rockfalls.

The start of the rockfalls for all visible events coincided closely with the onset of the emergent HF seismic energy. In many instances, steaming cracks, marking the line of eventual failure, opened on the floor of Halemaʻumaʻu up to several minutes in advance of the rockfall. A sudden increase in HF seismicity was coincident with the main body of the rockfall striking the lava lake surface (Fig. 4.3). Ash emission and outgassing followed this impact and corresponded to the onset of LP and VLP energy. The lava lake,

when not completely obscured by the ash cloud, sloshed visibly with a 7–12 s period that was intermediate to the dominant periods of the LP (1–2 s) and VLP (20–40 s) energy.

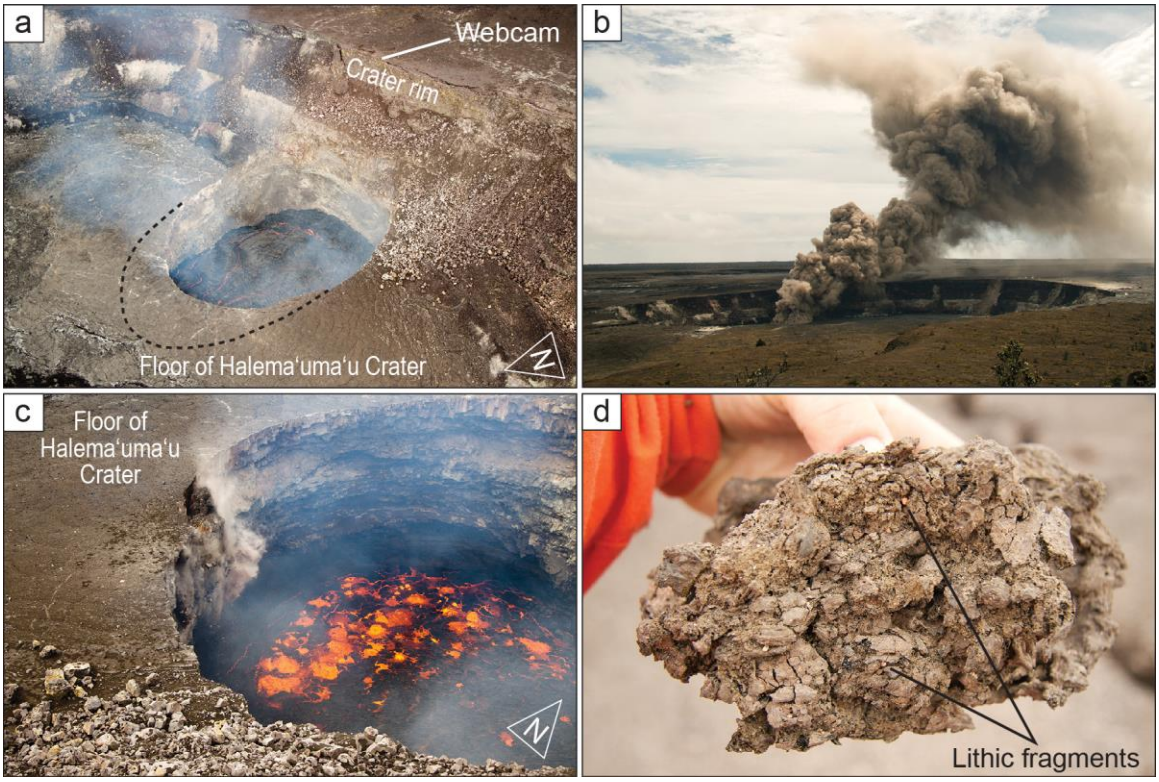

Figure 4.2 Photographs of lava lake in Halemaʻumaʻu, ash plume, and erupted tephra. (a) March 3, 2011, photograph looking east at lava lake in pit on floor of Halemaʻumaʻu Crater. Vent opening ~150 m across; lava surface ~65 m below vent rim. Dotted line, extent of vent overhang. (b) February 4, 2009, photograph showing ashy plume emanating from vent following rockfall. (c) March 3, 2011, photograph showing small collapse of vent rim and wall at 14:31. (d) Photograph showing scoria erupted during rockfalls on January 17–18, 2011. Note dusty brown coating and embedded lithic fragments (two identified).

4.5 Gas Slugs or Rockfalls?

The configuration of the vent in Halemaʻumaʻu in early 2011 (and throughout much of the eruption), with vertical to overhanging walls poised above a circulating lava lake, meant that rockfalls from the vent walls nearly always impacted the lava surface. When large enough, these collapses were accompanied by a composite seismic event. The webcam record shows a striking one-to-one correlation between composite seismic

events and rockfalls, where each discrete composite seismic event is linked to a visible rockfall, and each rockfall resulted in the emission of a short-lived ash plume. Such plumes have been a common feature of Kīlauea's ongoing summit eruption. Moreover, VLP duration and amplitude scales, in a qualitative sense, with the size of the rockfall.

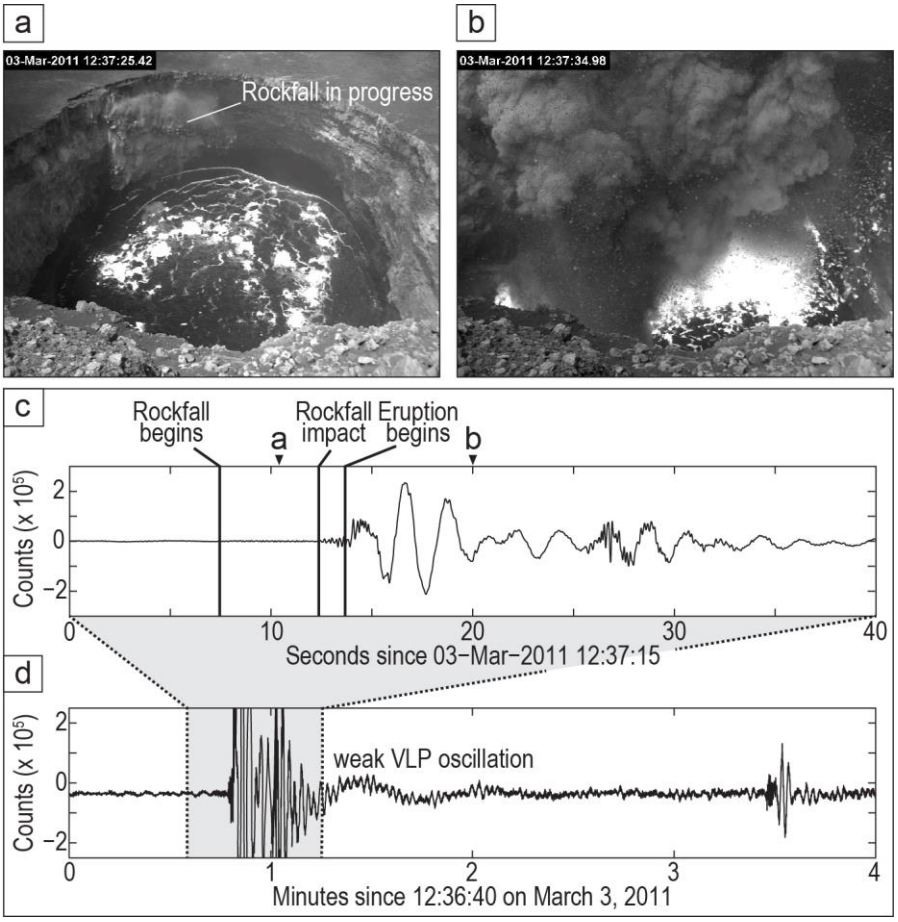

Figure 4.3 Comparison between video and seismicity for rockfall and explosive eruption at Kīlauea at 12:37 on March 3, 2011. (a) Webcam image showing rockfall in progress. (b) Webcam image showing weak explosive eruption in progress. (c) Line graph correlating station NPT seismicity with rockfall and subsequent eruption over interval of 40 s. Labeled vertical black lines, times for stages of collapse and eruption; lettered triangles, webcam images shown in (a) and (b). (d) Line graph showing 4 min of NPT seismicity spanning rockfall and explosive eruption to show associated very-long-period oscillation.

Chouet et al. (2010) proposed an alternate model for the composite seismic events. In their model, the emergent HF signal is related to the near-surface expansion and bursting of a gas slug, which then stimulates the LP and VLP response. Applying a two-

pole, zero-phase Butterworth filter to a selection of composite seismic events that occurred during the first year of the eruption, each of which are also associated with rockfalls, Chouet et al. (2010) report that the VLP onset precedes the HF seismicity by ~20 seconds. They cite this as evidence of an ascending gas slug. This method of filtering, however, is known to introduce acausal signal artifacts that produce erroneous onset times (Scherbaum and Bouin, 1997; Haney et al., 2012). By using a minimum phase shift filter, which is causal and preserves onset times (Haney et al., 2012), it is found that the rockfalls start at or before the onset of HF seismicity, and that HF seismicity increases abruptly upon rockfall impact, indicating that the rockfall is the source of the seismicity (Fig. 4.3). The transfer of a rockfall's momentum to the lava column during impact likely induces a pressure transient that is transmitted through the conduit (Patrick et al., 2011b). It is believed the pressure transient generates the decaying VLP oscillation, while the LP energy is related to the explosive outgassing process.

Gas slugs would be expected to burst at the point of lava upwelling, which has dominantly been at the northern edge of the lava lake. Indeed, the two relatively large (~10-m-diameter) gas slugs identified in the video record during 2008–2011 did just that. Only one of those gas slugs was associated with VLP energy, and neither was associated with appreciable HF seismicity or an explosive eruption. Instead, the outgassing and explosive bursts associated with the composite seismic events originate from the rockfall impact point, regardless of which point on the lava lake surface the impact occurs. This further excludes gas slugs as the cause of the outgassing that accompanies rockfall impact.

4.6 Eruption Mechanism

Although the observational data show unequivocally that rockfalls trigger outgassing, and in some cases weak explosive eruptions, the mechanism responsible for this response remains obscure. Several possibilities exist. For example, an active hydrothermal system is visible on some portions of the vent wall. Other evidence of this hydrothermal system is found in the eruption of hexahydrite ($MgSO_4 \cdot 6H_2O$) spherules from the vent following periods of rainfall (Hon and Orr, 2011), and in the ejection of sparse gelatinous lapilli of pure $MgSO_4$ during one explosive eruption. It is possible,

therefore, that water within the body of the rockfall may play a role in initiating an explosive response.

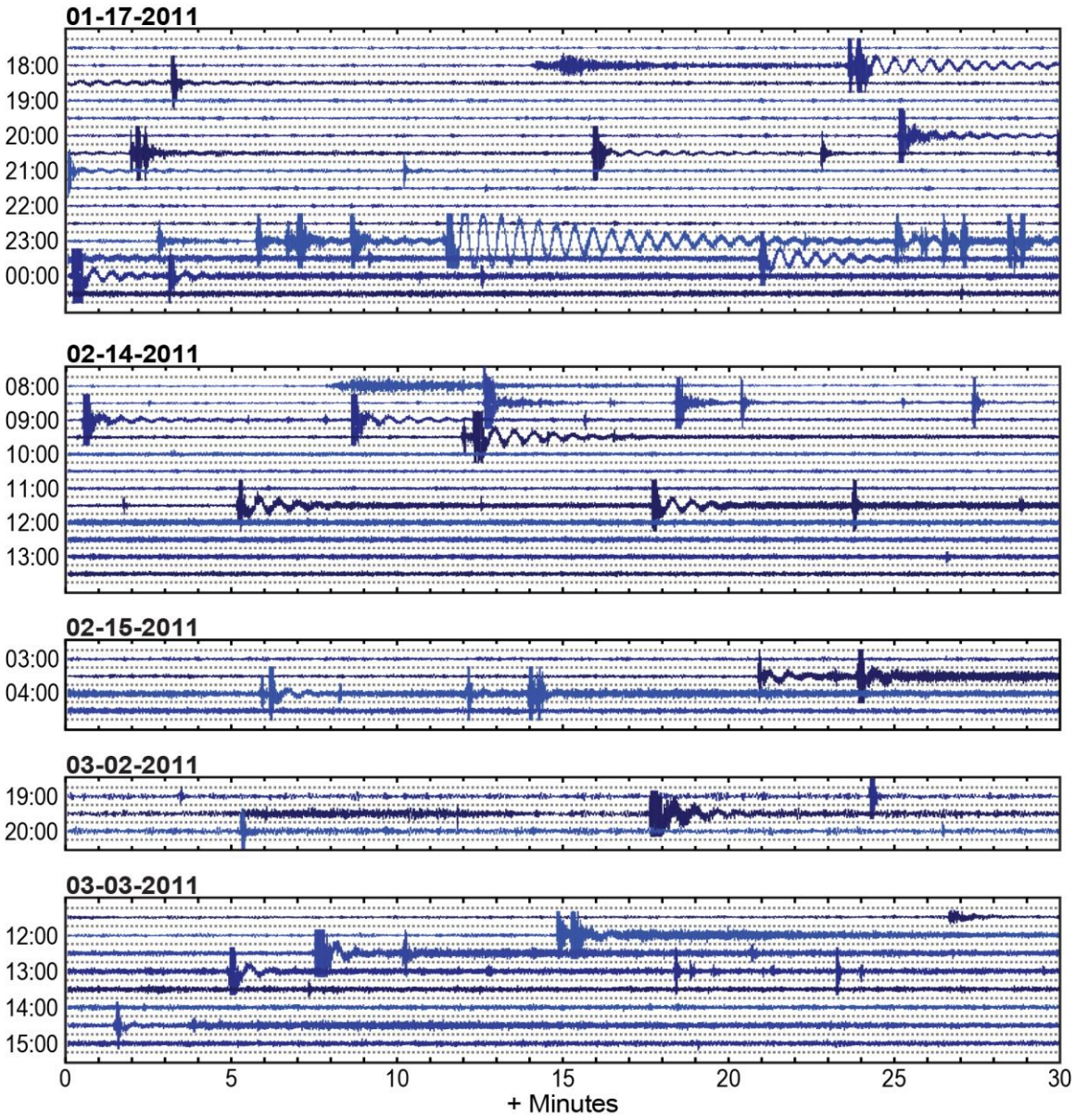

Figure 4.4 Seismic traces for periods encompassing rockfall sequences during January–March 2011. Nearly all impulsive seismic events shown here are related to rockfalls

Most lapilli and bombs erupted from the vent during explosive events are scoria with vesicularities up to 89%, and pyroclasts lofted from the vent at other times have vesicularities up to 95% (R. Carey, 2012, personal communication). These products

indicate a significant amount of dissolved and/or exsolved gas stored at a shallow level in the lava lake. A massive disruption to the top of the lava lake could abruptly release this gas, and may even trigger a run-away decompressive vesiculation that helps drive the explosive response. This may be further enhanced by the addition of a multitude of vesiculation surfaces provided by the rockfall (vesicles within the erupted tephra commonly contain lithic ash particles, suggesting that these were a catalyst for vesiculation). On the other hand, the observation that the explosive response is largely unaffected by the preexisting condition of the lava lake argues against the release of gas trapped beneath a capping crust as the driving mechanism behind rockfall-triggered bursts.

Another possibility is that the explosive eruptions are a manifestation of a rebound splash caused by the collapse of a rockfall's impact cavity. Such splashes, called Worthington jets, can occur in both liquids and granular materials (e.g., Worthington, 1908; Lohse et al., 2004; Gekle and Gordillo, 2010, and references therein) and are seen in everyday settings as simple as raindrops impacting a puddle, or a rock being tossed into a pool of water. Studies have shown that Worthington jets can achieve velocities 20–30 times higher than the velocity of the impacting object (Thoroddsen et al., 2004; Gekle and Gordillo, 2010), and that jet height in some instances can exceed the initial drop height (Worthington, 1908; Lohse et al., 2004). Furthermore, higher impact velocities result in higher jets (Harlow and Shannon 1967; Bergmann et al., 2006). Small jets, formed by tiny rockfalls impacting the lava lake surface, are seen often at Kīlauea. As the size of the rockfall scales up, however, the formation of a larger Worthington jet is not always directly observable because of the introduction of other factors such as occlusion by ash, fragmentation of the jet, and saturation of the webcam video from the incandescence of the freshly exposed lava. In general, though, the largest rockfalls triggered the most energetic eruption response, perhaps by creating a larger impact crater and a correspondingly larger Worthington jet. The coherence of the rockfall probably also plays a role in determining the height of the jet, with rockfalls that form a consolidated mass producing higher jets than rockfalls composed of loose debris. The collapse of the impact cavity could also temporarily trap air beneath the surface of the lava lake, similar to what has been observed in some Worthington jet studies (Lohse et

al., 2004; Gekle and Gordillo, 2010). This air, especially when heated, could then act as a supplementary driving mechanism.

In the volcanological scenario presented here, a rockfall plunging into the surface of the lava lake creates a deep impact crater in its wake, compressing the lava column beneath the impact site while decompressing that surrounding the impact site. The size of this crater should depend on the ratio between the rockfall's inertial force and the surface tension of the lava lake (i.e., the Weber number). The crater then collapses and, if the Weber number is high enough (Hsiao et al., 1988), forms a Worthington jet which, when it is composed mostly of lava from beneath the lake surface, undergoes immediate decompression and fragmentation. Some smaller lithic clasts are also swept back up in the jet, as is seen in jets formed during water impacts (Worthington, 1908; Harlow and Shannon, 1967). The rising fragments that compose the jet then travel through the lithic ash plume, incorporating additional rockfall material. Evidence of these interactions between the jet and the lithic rockfall is preserved in the tephra, which shows a thorough mixing of lithic and juvenile components and a coating of lithic ash to fine lapilli (Wooten et al., 2009). The formation of the Worthington jet is almost certainly coupled with several mechanisms that together drive the transient explosive eruptions triggered by rockfalls. These include decompressive and shock vesiculation (Carey et al., 2012), the release of trapped magmatic gas, the trapping of air, the release of volatiles within the lithic material of the rockfalls, and the introduction of vesiculation surfaces. The formation of a rebound splash, however, probably plays a primary role in this complex process.

4.7 Conclusions

Geologic observations have been crucial in developing our understanding of vent evolution and shallow degassing and outgassing processes at Kīlauea. These observations show that rockfalls within the vent, when they impact the top of the lava column, are capable of triggering transient outgassing bursts and weak explosive eruptions, possibly by generating a Worthington jet that may be closely coupled with other processes. This type of triggering mechanism has not been recognized before, and it seems likely that other small, enigmatic explosive events reported at Kīlauea over the past century, and

possibly at other open-system basaltic volcanoes as well, could have been triggered in a similar fashion.

Network-enabled webcams have become an important monitoring tool at volcano observatories around the globe in recent years and provide another way to study volcanic activity and its associated hazards (e.g., Paskievitch et al., 2010). The study here highlights the importance of using observational data, when available, to constrain eruption mechanisms based on geophysical interpretations.

Chapter 5

Kīlauea's 5–9 March 2011 Kamoamoa fissure eruption and its relation to 30+ years of activity from Pu‘u ‘Ō‘ō

Published as:

Orr, T.R., Poland, M.P., Patrick, M.R., Thelen, W.A., Sutton, A.J., Elias, T., Thornber, C.R., Parcheta, C., and Wooten, K.M., 2015, Kīlauea's 5–9 March 2011 Kamoamoa fissure eruption and its relation to 30+ years of activity from Pu‘u ‘Ō ‘ō. in: Carey, R., Cayol, V., Poland, M., Weis, D., (eds.), Hawaiian Volcanoes, from Source to Surface. American Geophysical Union Monograph 208, 393–420.

5.1 Introduction

The East Rift Zone of Kīlauea (Fig. 5.1) has hosted most of the volcano's eruptions since 1955, including the ongoing Pu‘u ‘Ō‘ō eruption, which began in 1983. The 30+ years of eruptive activity that ensued have provided an outstanding opportunity to study the evolution of a prolonged eruption—the first multi-decadal flank eruption at Kīlauea in over 500 years—with an ever-improving set of geological, geophysical, and geochemical monitoring tools. The 2008–ongoing eruption in the Overlook crater at Kīlauea's summit (Fig. 5.1) marks the first recorded instance of simultaneous rift zone and summit eruption at Kīlauea lasting more than a year and provides new insights into the connection between Kīlauea's summit and rift zone magmatic systems.

Over the course of more than 30 years, eruptive episodes included episodic high lava fountaining from Pu‘u ‘Ō‘ō (1983–1986); lava effusion from the Kupaianaha vent, 3 km east of Pu‘u ‘Ō‘ō (1986–1992); lava effusion from Pu‘u ‘Ō‘ō with occasional up-rift intrusions (1992–2007); and lava effusion from a vent 2 km east of Pu‘u ‘Ō‘ō (2007–2011). Repeated intrusions and fissure eruptions have resulted in eruptive pauses, reorganizations of lava flow and tube systems, and even the formation of new eruptive vents. The early 1990s, in particular, included several intrusions in the upper East Rift

Zone that caused hours- to days-long eruptive pauses and some minor subsidences at Pu‘u ‘Ō‘ō. More significant intrusions and eruptions occurred in 1997 (Owen et al., 2000; Thornber et al., 2003), 1999 (Cervelli et al., 2002), and 2007 (Poland et al., 2008a; Montgomery-Brown et al., 2010), the latter of which was accompanied by a shift in the locus of eruption away from Pu‘u ‘Ō‘ō to a new vent 2 km farther east (episode 58 vent). Figure 5.2, a cross section of Kīlauea’s summit and part of its East Rift Zone, conceptualizes the basic geometry of Kīlauea’s shallow magmatic system during episode 58.

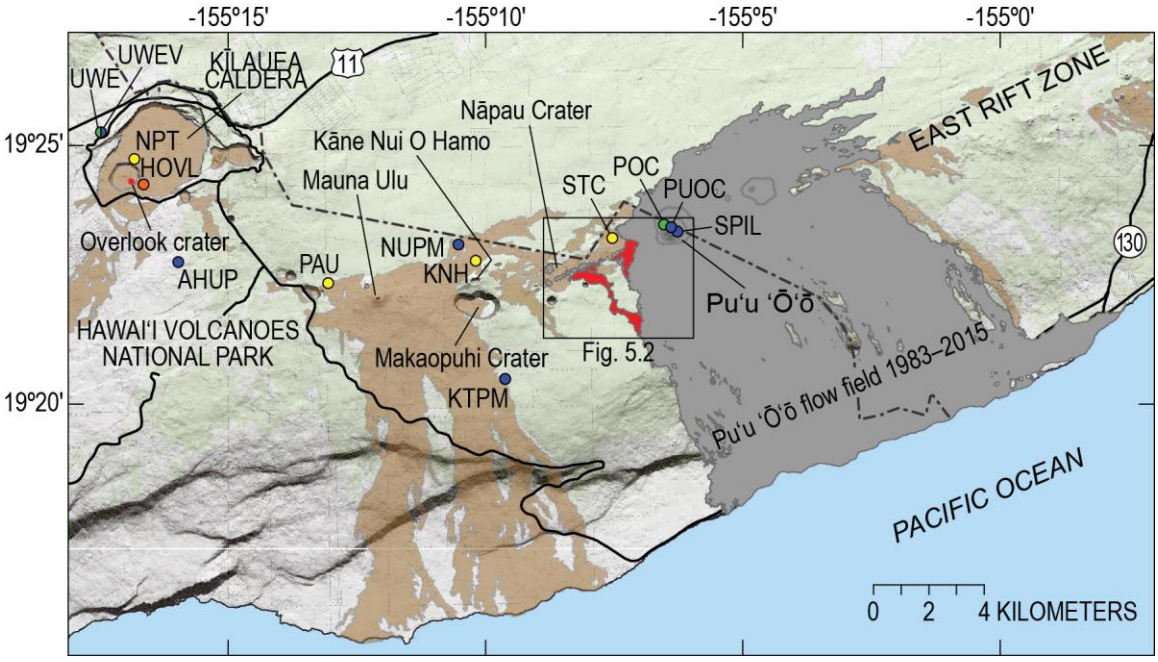

Figure 5.1 Map of Kīlauea’s summit and East Rift Zone during 2011 showing extent of flows erupted during March 5–9, 2011, Kamoamoa eruption (red) in relation to 1983–2011 Pu‘u ‘Ō‘ō flow field (pre-Kamoamoa; gray) and historical flows (brown). Area depicted in Figure 5.2 outlined. Blue circles, continuously recording GPS stations spanning summit (UWEV–AHUP), East Rift Zone near Makaopuhi Crater (NUPM–KTPM), and Pu‘u ‘Ō‘ō crater (PUOC–SPIL); orange circle, gravimeter (HOVL) near Overlook crater; yellow circles, seismic stations (NPT, PAU, KNH, STC); green circles, tiltmeters (UWE, POC).

During March 5–9, 2011, the Kamoamoa fissure eruption (Figs. 5.1 and 5.3), a few kilometers west (up-rift) of Pu‘u ‘Ō‘ō, marked the end of the eruptive vent established

east (down-rift) of Puʻu ʻŌʻō in 2007 and presaged a return of activity to Puʻu ʻŌʻō that continues as of August 2015. The Kamoamoa eruption was exceptionally well monitored by an array of geophysical and geological observations, supplemented by gas measurements and lava sampling. These data are used to examine the dynamics of the eruption at a level of fine spatial and temporal detail, which provides insight into how such episodes occur and their effect on the long-lived Puʻu ʻŌʻō eruption.

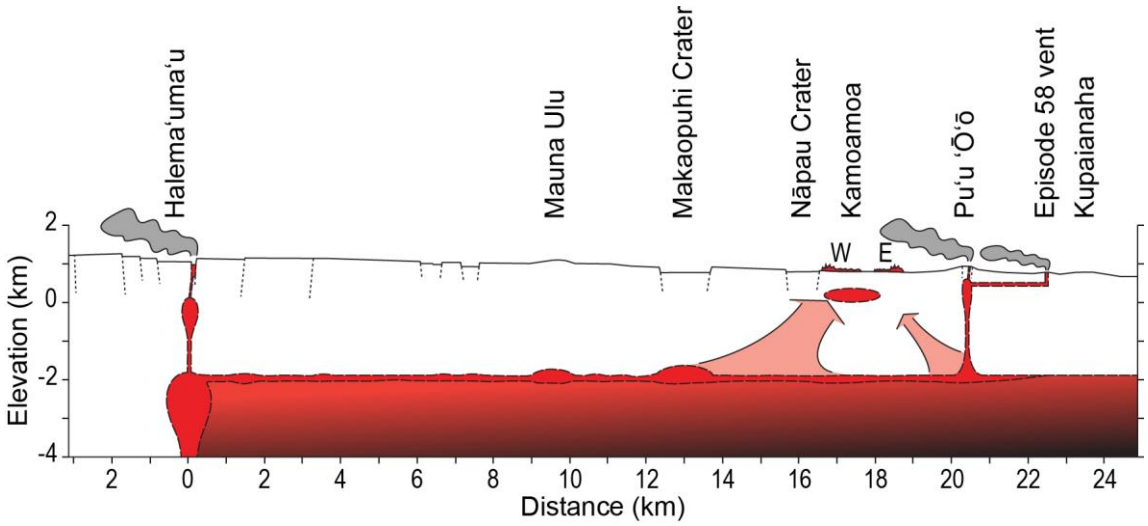

Figure 5.2 Conceptual model of Kīlauea's shallow summit and East Rift Zone magmatic system at time of Kamoamoa eruption. Elevation is relative to sea level; horizontal distance is flow path distance relative to summit magma chamber. Idealized pink arrows show sources and ascent of magma feeding Kamoamoa eruption (based on Lundgren et al., 2013). Main part of Kamoamoa dike shown connected to magma storage zone beneath Makaopuhi Crater and intersecting shallow magma body en route to surface; other part of dike shown coming from beneath Puʻu ʻŌʻō. Connection between ascending dike and Kamoamoa eruption site, although not shown, is implied. W and E refer to western and eastern Kamoamoa fissures, respectively.

5.2 The Puʻu ʻŌʻō eruption

In late May and early June 2010, after nearly 3 years with negligible eruptive activity within Puʻu ʻŌʻō, lava erupted in and partly filled Puʻu ʻŌʻō's crater, and another effusive surge occurred there in October 2010. This followed months of low discharge from the episode 58 vent (see Chapter 3) and repeated cycles of deflation and inflation

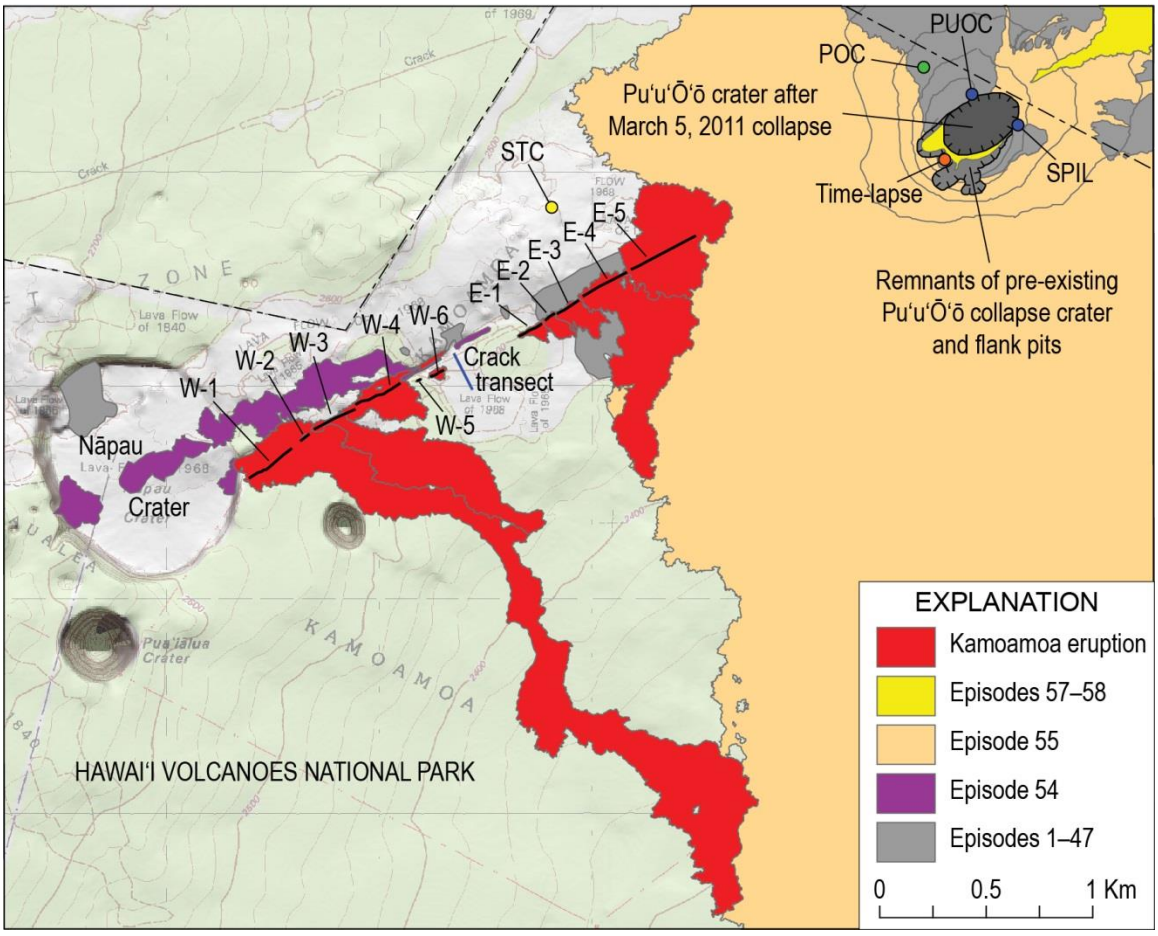

Figure 5.3 Map showing Kamoamoa lava flows and eruptive fissures (heavy black lines) in relation to Pu‘u ‘Ō‘ō, Nāpau Crater, and older Pu‘u ‘Ō‘ō flows erupted 1983–2011. Eastern fissure system comprises fissures E-1 to E-5; western fissure system comprises fissures W-1 to W-6. Yellow circle, seismometer (STC); orange circle, time-lapse camera; green circle, tiltmeter (POC); blue circles, continuous GPS stations (PUOC, SPIL); blue line, crack measurement transect.

(DI events) at Kīlauea’s summit (Anderson et al., 2015) that resulted in pronounced oscillations in the summit lava lake level (Fig. 5.4). The DI events were associated with decreases and increases in effusion through the episode 58 tube system—evidence that the cyclic deformation was associated with varying flux between the summit and Pu‘u ‘Ō‘ō. Starting on November 7, 2010, the DI events stopped occurring and relatively steady inflation ensued until mid-January 2011. This period was accompanied by an increase in the abundance of active surface flows fed by breakouts from the lava tube, as well as by crater filling at Pu‘u ‘Ō‘ō and a rise in lava lake level in the Overlook crater at

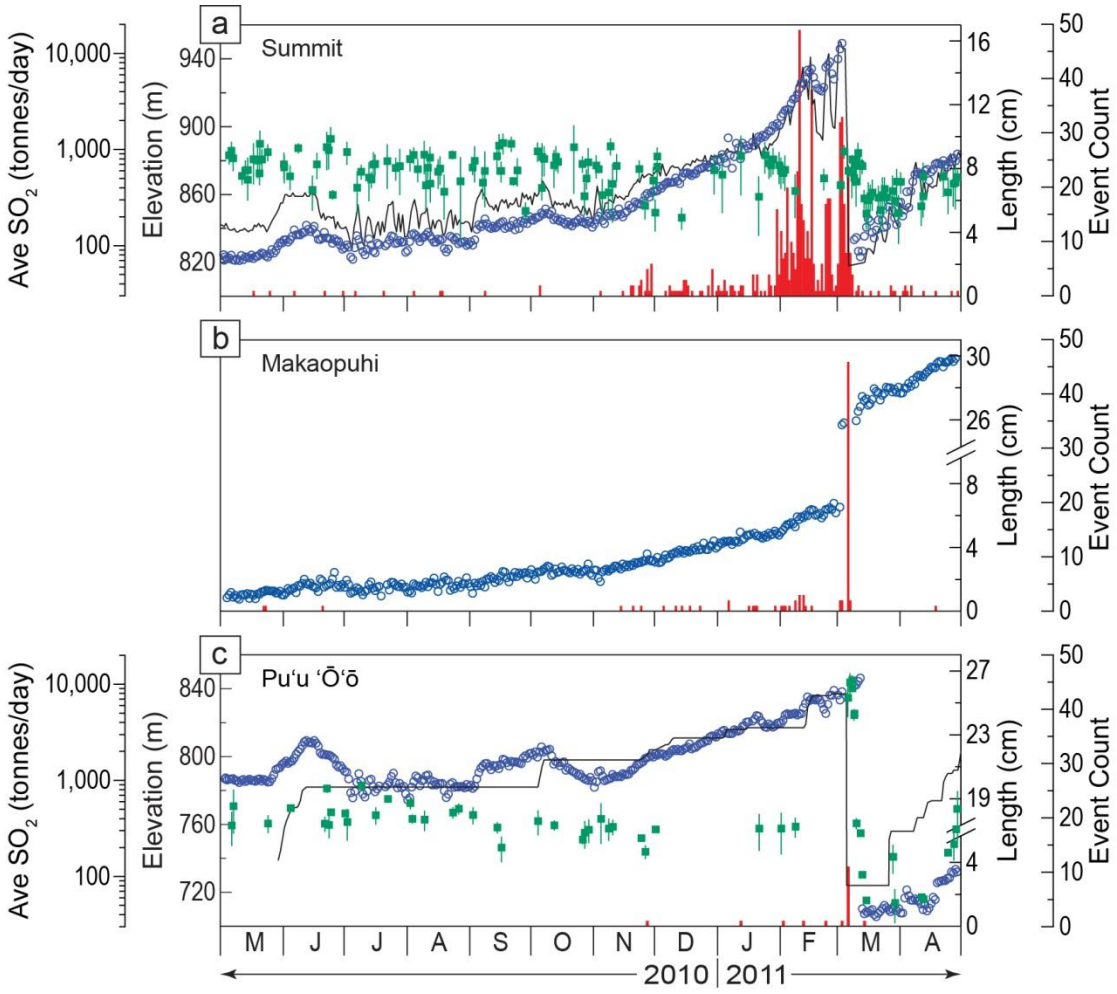

Figure 5.4 Time series of geological, geophysical, and geochemical data for the interval May 1, 2010, to April 30, 2011, from (a) Kīlauea's summit (March 2011 GPS offset ~12 cm contraction); (b) the region around Makaopuhi and Nāpau Craters (March 2011 GPS offset ~18 cm extension; GPS scale broken to accommodate data); and (c) Pu'u 'Ō'ō (March 2011 GPS offset ~25 cm contraction; GPS scale broken to accommodate data). Black line, summit lava lake elevation and Pu'u 'Ō'ō crater floor elevation (pronounced lava-level oscillations at summit in response to summit DI events); red bars, earthquake count; blue circles, GPS line length between stations AHUP and UWEV at summit, NUPM and KTPM near Makaopuhi Crater, and PUOC and SPIL at Pu'u 'Ō'ō (positive GPS line length change interpreted as inflation, although a few centimeters per year of line length increase also occurs from seaward south flank motion); green squares, average SO2 emissions (lines show one standard deviation). (SO2 release at Kīlauea sensitive to near-surface eruptive processes. Consequently, observed SO2 emission rate variability incorporates influence of shallow changes in magmatic system, such as convective lava lake circulation and free-surface activity level. Another factor, radiative transfer, affects absolute uncertainty associated with measured emission rates at Kīlauea since 2008 (Elias and Sutton, 2012).)

Kīlauea's summit (Fig. 5.4). DI events and associated fluctuations in tube effusion resumed in late-January, while crater filling and rising lava-lake level continued.

Puʻu ʻŌʻō's 2010–2011 filling was tracked by a number of geological and geophysical signals. At the summit, deformation measurements indicated inflation (Fig. 5.4a) as magma accumulated within a shallow reservoir beneath the east margin of Halemaʻumaʻu Crater. Seismicity also increased beneath Kīlauea's summit and upper East and upper Southwest Rift Zones, especially after late January 2011 (Figs. 5.4 and 5.5a). This pattern in seismicity is well correlated with times of high summit pressurization (Klein et al., 1987). Seismicity consisted mostly of long period events in the summit and volcano-tectonic events in the rift zones. Across the East Rift Zone near Makaopuhi Crater, extension accompanied a modest increase in seismicity (Fig. 5.4b). At Puʻu ʻŌʻō (Fig. 5.4c), there was almost no increase in located seismicity and no obvious change in tremor, although extension across the crater suggested magma accumulation beneath the cone.

Beginning in February 2011, summit DI events became more distinct, with a series of three relatively large (>5 microradian) events immediately preceding the Kamoamoa eruption. The DI events were mirrored by large swings in lava-lake level (Fig. 5.4a). Tilt and seismicity rates in the summit and upper East Rift Zone were also highly correlated, with seismicity rates approaching zero in the upper East Rift Zone during the deflation phases. Most of the seismicity in the upper East Rift Zone consisted of an event family (multiplet), whose occurrence was modulated by the large DI events occurring in the summit.

By the beginning of March 2011, small but widespread surface flows were scattered about the flow field, and Puʻu ʻŌʻō had filled to within ~20 m of the crater's northeast rim (Fig. 5.6a). At the same time, the summit lava lake within the Overlook crater had risen to within ~62 m of the Halemauʻumaʻu crater floor (Fig. 5.6b)—the highest level recorded to that time. Starting on March 1, seismicity intensified between Makaopuhi and Nāpau craters (Fig. 5.5a), a pattern similar to those observed prior to some previous eruptions in the East Rift Zone, such as those of 1974 and 1983 (Klein et al., 1987). Unlike the earthquakes in the upper East Rift Zone, most of the Makaopuhi–Nāpau earthquakes did not belong to any earthquake family recognized at the Hawaiian

Volcano Observatory, and the few families that did occur were only active for a short time.

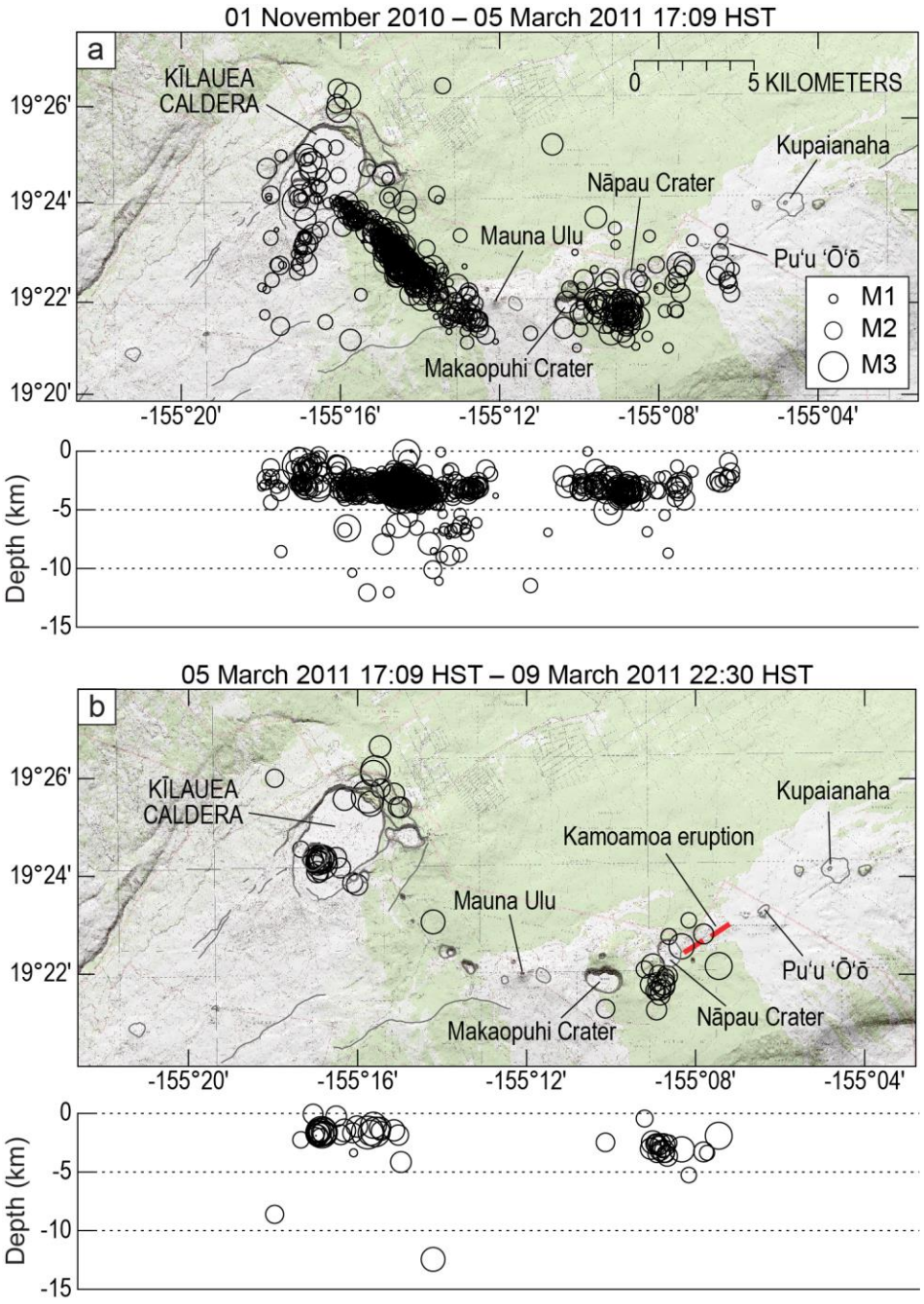

Figure 5.5 Locations of earthquakes at Kīlauea's summit and East Rift Zone (in map view and depth) during (a) November 1, 2010, until Kamoamoa dike reached surface on March 5, 2011, at 1709 HST and (b) effusion of lava from Kamoamoa fissure from March 5 at 1709 HST until March 9 at 2230 HST.

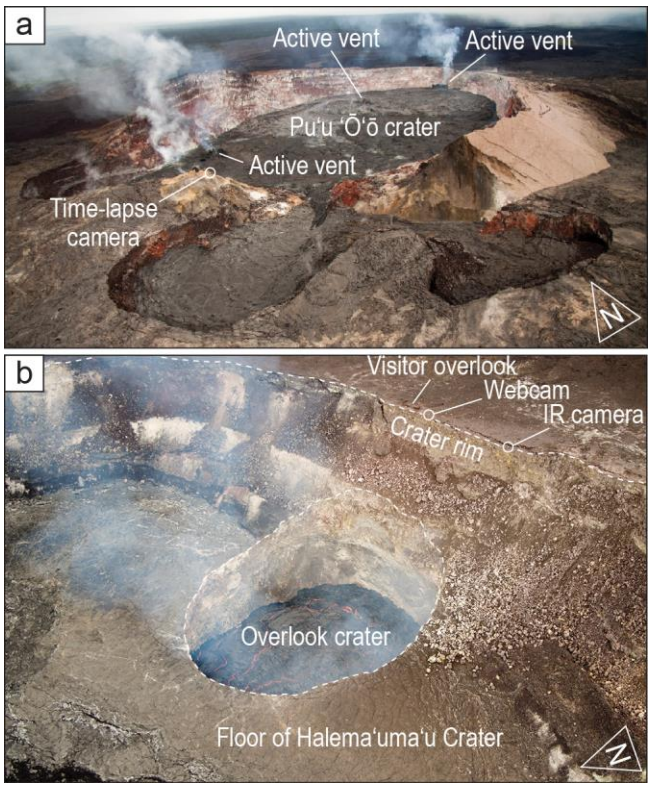

Figure 5.6 Photographs of Pu‘u ‘Ō‘ō and summit lava lake before Kamoamoa eruption. (a) Pu‘u ‘Ō‘ō crater on March 2, 2011. Active vents and time-lapse camera are labeled; light-colored flows in crater are active or very recent. Crater (not including flank pits) ~430 × 270 m, major axis oriented upper right to lower left. (b) Monitoring cameras, visitor overlook, and summit lava lake on March 2, 2011. Dashed white lines, rim of Halema‘uma‘u and Overlook crater. Overlook crater ~190 × 150 m, lava lake ~160 × 140 m. Halema‘uma‘u floor ~85 m below cameras; lava lake ~65 m below Halema‘uma‘u floor.

5.3 The 5–9 March 2011 Kamoamoa fissure eruption

The Kamoamoa fissure eruption of March 5–9, 2011, was the culmination of several months of precursory activity (Figs. 5.4 and 5.5), which included (1) summit and Pu‘u ‘Ō‘ō inflation, (2) accelerated East Rift Zone spreading, (3) increased upper East Rift Zone seismicity, and (4) rising lava levels within the summit eruptive vent and at Pu‘u ‘Ō‘ō. We describe next the characteristics of the Kamoamoa eruption, including

information from geological observations, geophysical data, and geochemical measurements.

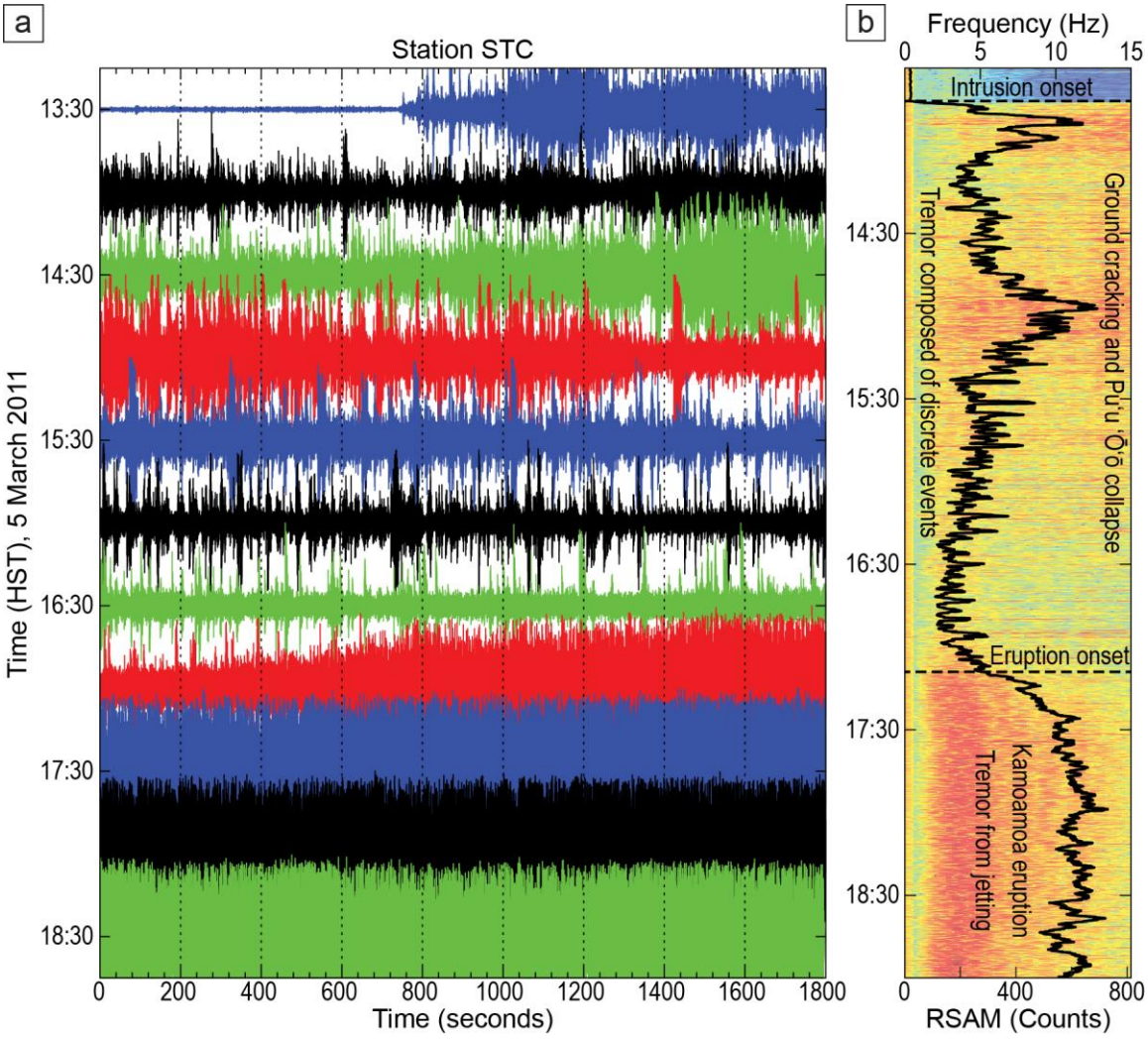

Figure 5.7 Seismicity spanning start of intrusion, subsidence of Pu‘u ‘Ō‘ō, and onset of Kamoamoa eruption. (a) Helicorder view and (b) spectrogram and 1 min averaged seismic amplitude (black line) for period 1330–1900 on March 5, 2011, recorded on STC seismometer.

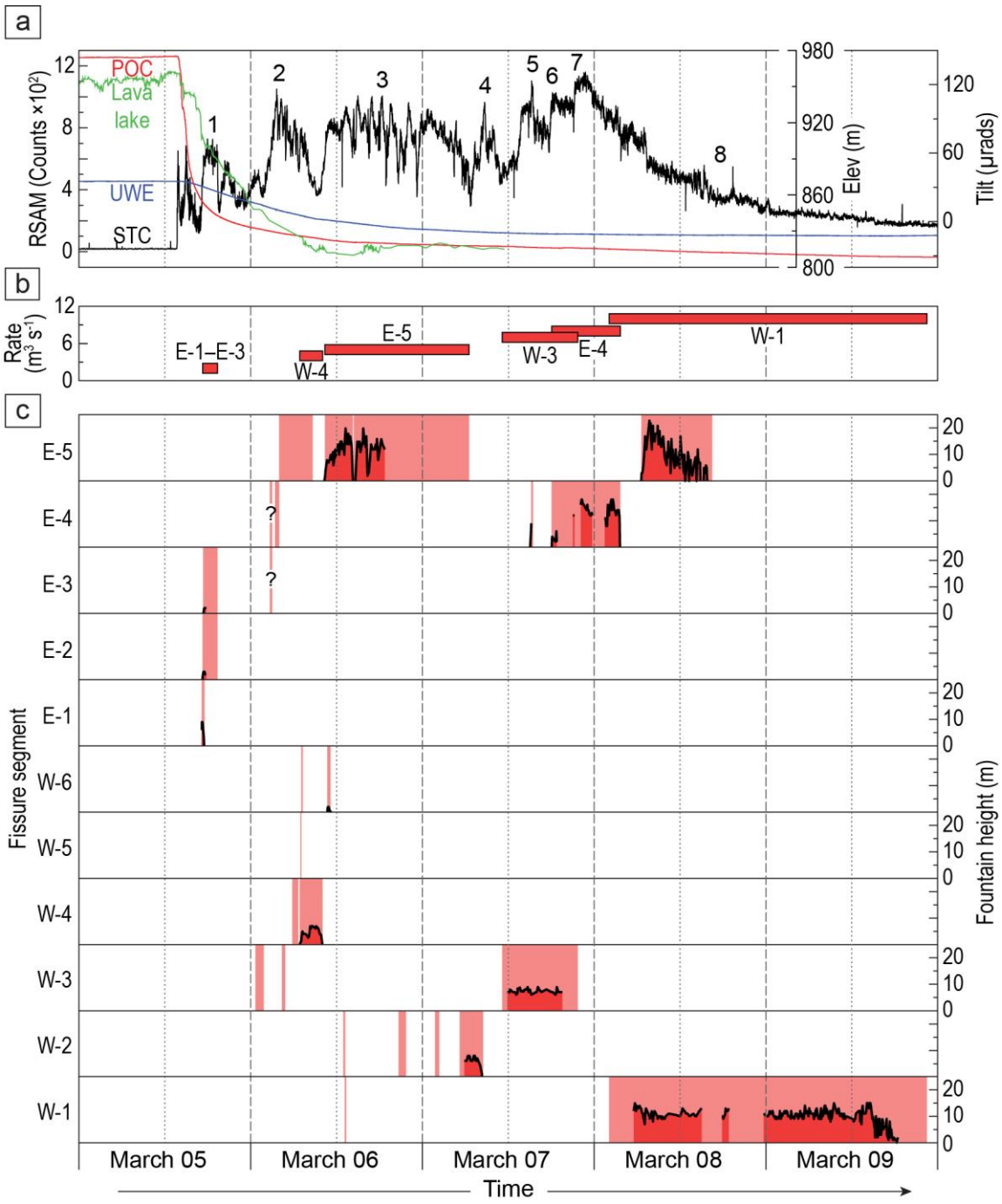

Figure 5.8 Lava level, tilt, and RSAM compared to Kamoamoa eruptive activity. (a) Red line, radial tilt at Puʻu ʻŌʻō (station POC); blue line; radial tilt at summit (station UWE); green line, summit lava lake surface elevation; black line, RSAM near eruption site (station STC). Numbers above RSAM discussed in text (see Section 5.4.7). (b) Time-averaged discharge rate for specific dominant fissures. (c) Pink bars, periods of Kamoamoa eruptive activity showing fountain height (red areas) where quantifiable.

5.3.1 Eruption Onset

The sudden onset of seismic tremor and elevated earthquake activity along Kīlauea's East Rift Zone at 1342 HST (Hawaii-Aleutian Standard Time; UTC -10 hours) on March 5, 2011 (Fig. 5.7), signaled the start of an intrusion a few kilometers up-rift from Puʻu ʻŌʻō. Rapid deflation started at Puʻu ʻŌʻō at almost the same time, and at Kīlauea's summit about 30 minutes later (Fig. 5.8a). Active lava flows on the floor of Puʻu ʻŌʻō crater stagnated, and at ~1420 HST most of the crater floor began to undergo wholesale subsidence (Fig. 5.9).

Puʻu ʻŌʻō subsidence was most rapid during the first 1.5 hours, when the crater floor dropped about 80 m, revealing both solid and molten (or partly molten) layers. As the crater deepened, small rockfalls from the pre-existing crater walls ejected plumes of reddish lithic ash (Fig. 5.10a) that dusted the southwest (downwind) flank of Puʻu ʻŌʻō. Rockfalls continued for the next few hours, even as the pace of subsidence slowed. Subsidence was mostly finished by 1800 HST, with the crater floor having dropped 113 m (Fig. 5.9). For several hours afterward, slices of the pre-existing crater floor occasionally collapsed and sent avalanches of incandescent debris to the bottom of the new depression.

At Kīlauea's summit, the surface of the lava lake within the Overlook crater began to drop shortly after 1400 HST on March 5, reaching a relatively stable level ~205 m below the floor of Halemaʻumaʻu (a drop of ~143 m) by about 0800 the following morning (Fig. 5.11). During this draining, slabs of lava veneer coating the walls of the vent, as well as portions of the vent walls, fell away and plunged into the lava column. Some collapses were large enough to trigger very-long-period (VLP) seismicity recorded on summit seismometers in the fashion described in Chapter 4.

5.3.2 Fissure eruption

The Kamoamoa eruption began at 1709 HST on March 5, when lava broke the surface ~2 km southwest of Puʻu ʻŌʻō and formed an eruptive fissure that propagated northeastward mid-way between Puʻu ʻŌʻō and Nāpau Crater (Figs. 5.2, 5.10 and 5.12). This "eastern" fissure system grew to a total length of 950 m and comprised five distinct

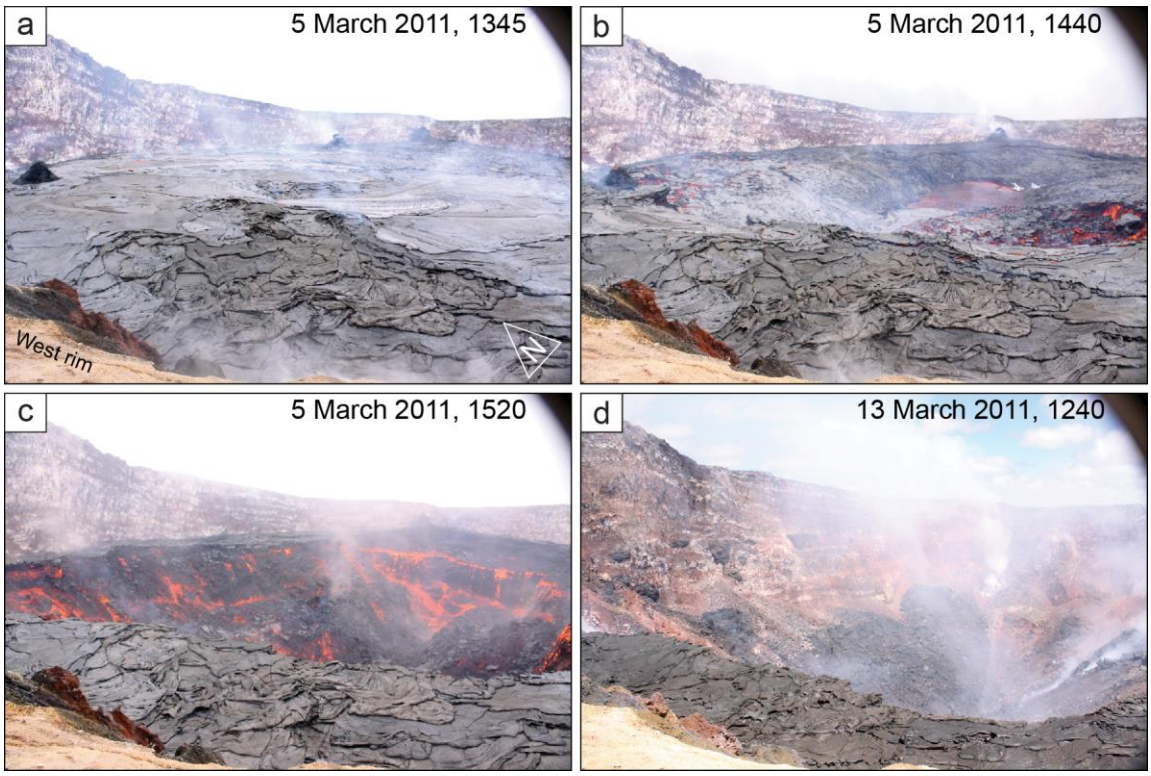

Figure 5.9 Photographs showing subsidence of Pu‘u ‘Ō‘ō crater floor on March 5, 2011, collected by time-lapse camera. Distance from camera to opposite (northeast) rim of crater is ~430 m; camera location shown in Figures 5.2 and 5.6. (a) 1345 HST, immediately after onset of tremor but before onset of subsidence. (b) 1440 HST, ~20 min after subsidence onset. Central part of crater sagging to form elongate trough aligned with East Rift Zone orientation; ring fractures beginning to form. (c) 1520 HST, ~1 h after subsidence onset. Crater floor has dropped along ring fractures, exposing incandescent lava fill accumulated over preceding several months. (d) 1240 HST on March 13, eight days after subsidence. Deepest part of crater ~133 m below northeast rim.

fissures (E-1 to E-5, labeled from southwest to northeast; Fig. 5.2). A “western” fissure system (Figs. 5. 2 and 5.13) opened early on March 6 about 1 km farther southwest and propagated both northeast and southwest. This fissure system reached a final length of 1,050 m and comprised six individual fissures (W-1 to W-6, labeled from southwest to northeast; Fig. 5.2). The eastern and western fissure systems were separated by 360 m of heavily cracked ground. Eruption along both fissure systems was initially sporadic, and activity migrated from one spot to another in semi-random fashion, repeatedly starting and stopping (Fig. 5.8). Early on March 8, the eruption became focused near the opposing ends of the two fissure systems (Figs. 5.13 and 5.14).

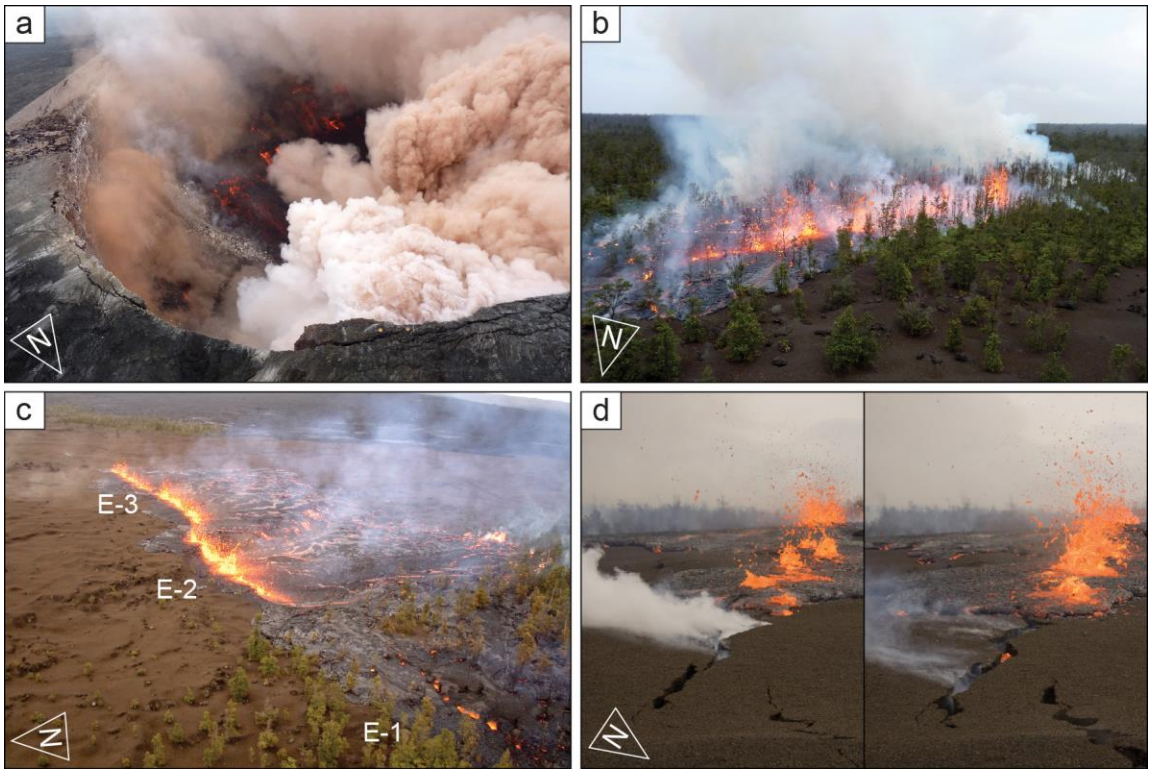

Figure 5.10 Photographs showing Kamoamoa eruption on March 5, 2011. (a) Subsidence of Pu‘u ‘Ō‘ō’s crater floor at 1634 HST. Note incandescent rubble from recent crater-filling lava. Photo by David Okita, Volcano Helicopters. (b) Fissure E-1 at 1719, 10 minutes after eruption onset. Photo by David Okita, Volcano Helicopters. (c) Fissures E1 (inactive), E2, and E3 at 1745 HST. Low topography directing most of flow southward. (d) Southwest view down axis of fissure E-3 during fissure propagation. Left-hand photo taken 1731 HST showing heavy white fume coming from crack. Right-hand photo taken 59 s later shows wispy bluish fume and lava at top of dike just coming into view. Note change in crack width during interval between photos.

To the northeast, low fountaining from a ~75-m-long line of discrete points along the southwest end of fissure E-5 constructed an elongate (120 × 65 m) pyroclastic cone complex that eventually reached a maximum height of ~13 m (Figs. 5.13 and 5.14). The optically dense part of the fountains was up to ~25 m high, and small particles reached at least twice that height during discrete bursts. The instantaneous discharge rate was relatively low, with eruptive output slowly building the pyroclastic cone and feeding a small, slow-moving lava flow exiting from the northeast end of the cone. The gas output, however, was high, as suggested by loud pulsatory outgassing and relatively wide dispersal of tephra. At times, large pulses of incandescent (in daylight) fume would break

through the fountains like a jet and produce a lava "spray" laced with sparse small clots of lava. Eruptive activity at E-5 waxed and waned repeatedly—at times, the fountains would die down to almost nothing, then quickly rebuild to their previous level (Fig. 5.8c).

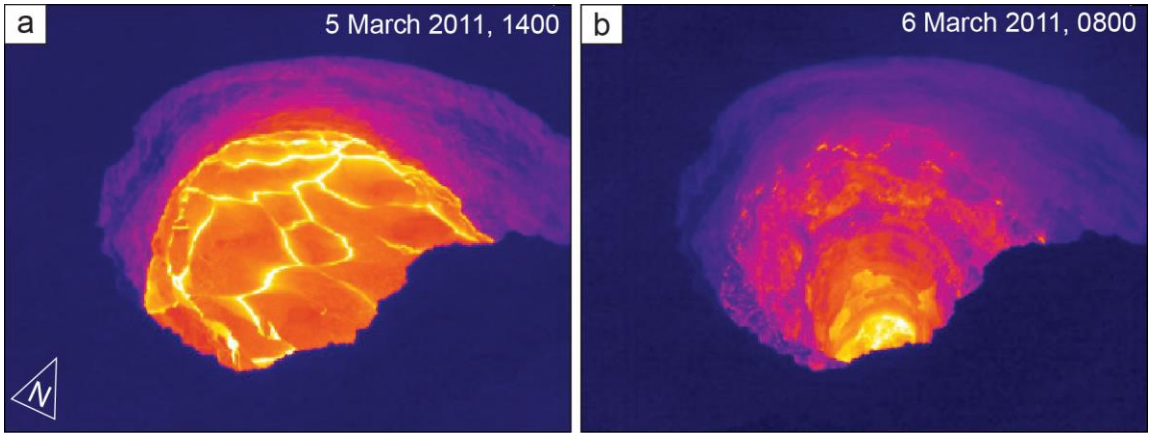

Figure 5.11 Infrared camera images of lava lake in Overlook crater at southeast edge of Halemaʻumaʻu at (a) 1400 HST on March 5, 2011, immediately before onset of draining, and (b) 0800 HST on March 6, 2011, after lava lake level had dropped ~143 m and stabilized.

At the W-1 fissure, a ~200-m-long line of fountains with the optically dense part up to ~15 m high (and small clasts reaching occasionally to ~50 m) constructed an elongate (115 × 55 m) pyroclastic cone complex with a maximum height of ~14 m (Figs. 5.13 and 5.14). The instantaneous discharge rate at W-1 appeared to be far greater than at E-5, and W-1 fed a channelized ʻaʻā flow that advanced southeastward (Fig. 5.14c,d). A perched lava pond grew atop the northeastern half of the W-1 fissure at the head of the lava channel (Fig. 5.14c). No pyroclastic edifice was constructed over the fountains on the northeastern half of W-1, because flowing lava constantly removed spatter from the site of the eruption (e.g., Parcheta et al., 2012). The smaller of the W-1 fountains were episodically drowned by the lava pond (e.g., Wilson and Head, 1981), sometimes disappearing completely for a few seconds before bursting back through the pond surface moments later.

Fissure E-5 shut down on the afternoon of March 8 (Fig. 5.8c), although distant webcam views indicated occasional spatter bursts overnight. W-1, however, remained active through the next day. Late in the afternoon of March 9, W-1 began to wane, and

the lava level in the perched pond over the northeast end of the fissure began to drop. The fissure shut down at about 2230 HST on March 9, marking the end of the Kamoamoa eruption (Fig. 5.8c). The channelized ʻaʻā flow stalled soon afterward, having reached a final length of 3.3 km (Fig. 5.2). Kīlauea's East Rift Zone was quiet for several days following the end of the Kamoamoa eruption. During mid-morning on March 26, lava began erupting on Puʻu ʻŌʻō's crater floor, ending an East Rift Zone eruption hiatus of 16.5 days.

5.4 Results

5.4.1 Puʻu ʻŌʻō crater subsidence on 5 March

Prior to subsidence, Puʻu ʻŌʻō had filled to within about 20 m of the northeast rim of the cone (Fig. 5.6a); the crater floor was then at an elevation of about 840 m (Fig. 5.4c; the northeast rim elevation was 860 m). The crater floor, held up by the magma body beneath Puʻu ʻŌʻō, dropped as the magma drained away. After subsidence, the crater floor was measured by laser rangefinder as 133 m below the northeast rim, or at an elevation of 727 m. The result was a 380 × 245 m concave depression (Fig. 5.9d) with a depth of 113 m (compared to the pre-subsidence crater floor height; Fig. 5.4c). The shape of the Puʻu ʻŌʻō crater floor after subsidence can be approximated by a half ellipsoid. A subsidence volume (V_s) can therefore be calculated from:

$$V_s = \frac{\pi\, l\, w\, h}{6} \tag{5.1}$$

where

l is the crater length,
w is the crater width, and
h is the amount of subsidence.

Using the dimensions above, the volume of the crater subsidence is calculated to be 5.5×10^6 m^3. Assuming the duration of the subsidence to be 3.7 hours (based on camera

observations), this equates to an average volume loss rate of ~400 m^3 s^{-1}. The magma body that drained from beneath Pu‘u ‘Ō‘ō was likely a mix of (1) magma that had not yet circulated to the surface and was too deep to have experienced significant vesiculation, and (2) magma that had mostly outgassed to atmospheric pressure, and in which its remaining vesicles may have collapsed upon being carried back to the depth of the storage chamber; therefore, the calculated volume and volume loss rate could approach dense-rock equivalent (DRE) values.

In comparison with volume-loss approximations for two previous crater subsidences at Pu‘u ‘Ō‘ō, which were also calculated using the formula for a half ellipse (equation 5.1), the volume derived for the 2011 subsidence falls between the 13×10^6 m^3 for the 1997 subsidence associated with episode 54 (Heliker et al., 2003) and the 4.2×10^6 m^3 for the 2007 subsidence associated with episode 56 (see Chapter 2). Though the subsidence of Pu‘u ‘Ō‘ō’s crater floor was not fully brittle, involving both brittle and ductile layers, the subsequent crater fill was probably, in part, a column of brecciated material that occupied a volume greater than that of the same material preceding the collapse (Roche et al., 2001). Thus, the crater subsidence volumes calculated in each of these cases may represent minimum values for the actual volume lost from the magma storage body beneath Pu‘u ‘Ō‘ō, because the crater floor subsidence included some disaggregation.

Montgomery-Brown et al. (2010) calculated an approximate volume loss from Pu‘u ‘Ō‘ō during the episode 56 eruption in 2007 by multiplying the time elapsed from the end of the eruption until lava reappeared in Pu‘u ‘Ō‘ō by the long-term supply rate to Kīlauea (0.12 km^3 yr^{-1}; Heliker and Mattox, 2003). Following this example, the 16.5-day hiatus between the end of the Kamoamoa eruption and the reappearance of lava in Pu‘u ‘Ō‘ō corresponds to a volume of 5.4×10^6 m^3—strikingly similar to the value calculated from the volume of crater subsidence. As noted earlier, however, the discharge rate starting at least by mid-2010 was lower than the long-term discharge rate, perhaps by as much as 25–50% (see Chapter 3), which could reflect a decrease in the rate of supply to Pu‘u ‘Ō‘ō. While the actual supply rate at the time of the Kamoamoa eruption remains uncertain, the similarity between these two methods of approximating volume-loss could be interpreted to indicate that there was actually no significant change in supply rate and

the discharge rate derived in Chapter 3 is incorrect. Alternatively, the similarity between the values derived by the two methods could be coincidental.

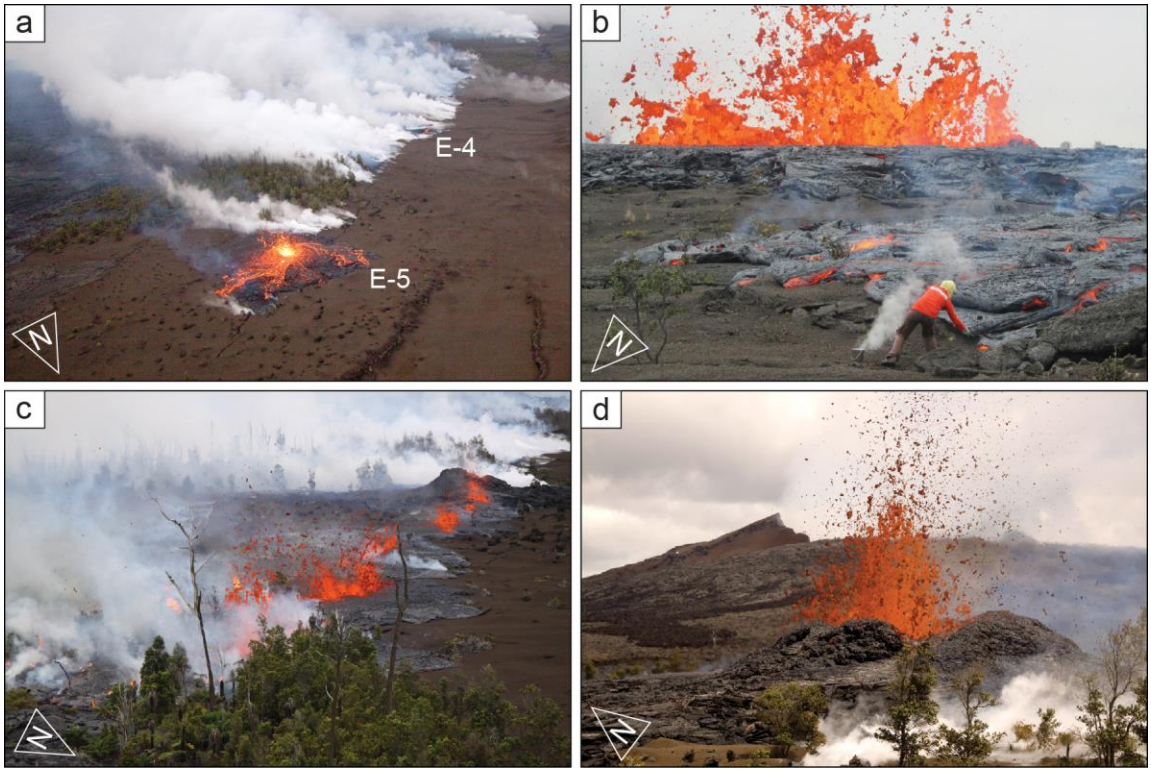

Figure 5.12. Photographs showing Kamoamoa eruption on March 6, 2011. (a) Weak fountaining from fissure E-5 at 0648 HST. Incandescent ground cracks delineate fissure E-4 in middle ground, with fume from fissures E1–E3 just beyond; distant western fissures fuming at upper right. (b) Fountaining (~7 m high) from fissure W-4 at 0830 HST, ~75 m beyond geologist collecting molten lava sample. (c) Fountaining from fissure E-5 at 1032 HST, shortly after fissure opened farther northeast and then propagated southwestward back to the E-5 cone. (d) Main fountaining source on fissure E-5 at 1229 HST. Pu‘u ‘Ō‘ō west flank in background.

5.4.2 Summit lava lake draining

Before the Kamoamoa eruption started, the level of the summit lava lake in the Overlook crater was ~62 m below the floor of Halema‘uma‘u Crater (Fig. 5.6b)—an elevation of ~961 m (Fig. 5.4a). The lava lake had a northwest-southeast-oriented major

Figure 5.13 Photographs of Kamoamoa eruption during March 8–9, 2011. (a) Eastern and western fissure systems at 1226 HST on March 8, 2011, after activity focused at fissures E-5 and W-1. Nāpau Crater at upper right; yellow circle, STC seismometer. (b) Fountaining and pyroclastic cone at fissure E-5 at 0809 HST on March 8, 2011. (c) Fountaining and pyroclastic cone at fissure W-1 at 0953 on March 9, 2011. Lava accumulated in perched pond (left side of photo with small fountain) before feeding channelized flow.

axis of ~160 m and a northeast-southwest-oriented minor axis of ~140 m. By about 0800 HST on March 6 (the morning following the onset of the Kamoamoa eruption), the lake's surface had dropped to ~205 m below the vent rim to an elevation of ~818 m (a drop of 143 m; Fig. 5.8a). The walls of the evacuated crater appeared to be roughly vertical, although they may have been slightly inclined, suggesting that the bottom of the crater was narrower than the top. Because this subtle geometry cannot be resolved, the volume

of lava drained from the lake (V_d) is derived by modeling the summit vent as an elliptical cylinder:

$$V_d = \frac{\pi\, l\, w\, h}{4} \tag{5.2}$$

where

l is the lake length,
w is the lake width, and
h is the amount of lava-lake drop.

Using the vent dimensions stated above and a lava level drop of 143 m, the volume of lava drained from the lake is ~2.5×10^6 m^3. This suggests an average bulk-volume-loss rate of ~39 m^3 s^{-1} during the first 18 hours of drainage, although lava level measurements indicate that the volume-loss rate was not constant, instead slowing during those 18 hours (Fig. 5.8a). Using gravity data recorded on the southeast rim of Halemaʻumaʻu Crater (station HOVL), Carbone et al. (2013) calculated an average lava lake density of ~950 kg m^{-3}, or about a third of the DRE density of ~2800 kg m^{-3}. This corresponds to an average DRE volume loss rate of ~13 m^3 s^{-1} during drainage and a total DRE volume loss of ~0.8×10^6 m^3. This estimate, added to the modeled (from InSAR and GPS data) volume loss of 1.7×10^6 m^3 from the shallow summit magma reservoir (Lundgren et al., 2013), gives a nominal summit volume loss of ~2.5×10^6 m^3.

5.4.3 Kamoamoa fissure eruption rates

The Kamoamoa eruption was active for a total duration of 4.2 days. The detailed observations made during the eruption, coupled with field mapping and estimates of flow thickness, allow calculation of the mean output rate for the entire eruption, as well as for distinct periods during the eruption. Table 5.1 provides a summary of the duration, area covered, volume erupted, and time-averaged discharge rate for individual fissures over the course of the eruption. DRE volumes are based on a void space correction factor of

25%, the value used by Wolfe et al. (1988) for Puʻu ʻŌʻō ʻaʻā flows. Durations are based on observed start and stop times of eruptive activity, which, when not precisely known, are defined as the temporal mid-point between bracketing observations. Inaccuracy in our estimates of flow thickness is the largest source of uncertainty in calculating volume, which could be in error by as much as ±50%.

Table 5.1 Area, DRE volume, duration, time-averaged discharge, and distance to STC seismometer for Kamoamoa eruptive fissures.

Fissure	Area (ha)	DRE Volume (m^3)	Duration (h)	Discharge Rate ($m^3\ s^{-1}$)	Distance to STC (m)
E-1, E-2, and E-3[a]	4.12	0.015×10^6	2.2	~2	580; 510; 475
E-4[b]	23.82	0.27×10^6	9.5	~8	440
E-5[c]	19.0	0.33×10^6	17.7	~5	500
W-1[d]	68.61	1.68×10^6	44.4	~10	1765
W-2[e]	4.0	0.03×10^6	3.3	~3	1580
W-3[f]	22.43	0.26×10^6	10.6	~7	1500
W-4[g]	5.70	0.043×10^6	4.1	~3	
W-4 w/no graben[g]	5.25	0.039×10^6	2.5	~4	
W-4 w/graben[g]	na	0.065×10^6	4.1	~4	1120
W-5 and W-6[h]	0.35	0.0013×10^6	1.0	~0.4	1020; 940
Total	139.06	2.7×10^6	89.5	~8	—

Notes: DRE volume calculated assuming 25% void space. Three different sets of values shown for fissure W-4 (see text for discussion). Total volume uses "W-4 w/graben" value. Total duration is actual time spent in eruption (i.e., not counting inactive periods).

[a]Average flow thickness for fissures E-1, E-2, and E-3 estimated at 0.5 m.

[b]Average flow thickness for fissure E-4 estimated at 1.5 m. Duration of E-4 does not include initial E-4 activity on March 6 or ~20 minutes of E-4 activity during afternoon of March 7. Both were periods of very low discharge.

[c]Flows from fissure E-5 subdivided into areas with average thicknesses of 1–3 m. Small volume of E-5 cone not included. Duration of E-5 considers main effusive period from this fissure.

[d]Flows from fissure W-1 subdivided into areas with average thicknesses of 1–6 m. Duration of W-1 considers only main effusive period from this fissure. Small volume of W-1 cone not included.

[e]W-2 lava buried by W-1 and W-3 flows before mapped. Area and thickness (1.5 m) approximated from oblique aerial and ground photographs.

[f]Flows from fissure W-3 subdivided into areas with average thicknesses of 1–3 m. Duration of W-3 considers main effusive period from this fissure.

[g]Average thickness of W-4 flow outside graben estimated at 1 m (based on thickness of lava exposed in tree molds).

[h]Fissures W-5 and W-6 represent two different eruptive periods on 6 March, but lumped because of small volume erupted. Average flow thickness estimated at 0.5 m.

During the eruption, lava flows covered 1.39 km^2 with a total volume of ~2.7×10^6 m^3 DRE (Table 5.1). This estimate is considerably lower than that calculated from gas emissions (a minimum of 7.6×10^6 m^3 DRE; see Gas geochemistry results, below). The

gas-based lava-discharge estimate, however, reflects the volume of magma that outgassed even though not all of this magma necessarily erupted. In fact, the outgassed volume is no more than a factor of 2 lower than the dike volume modeled from deformation data (15.6×10^6 m^3 DRE (Lundgren et al., 2013); see Deformation results, below). The outgassed volume may therefore be a better reflection of not only the magma that erupted, but also that which intruded shallowly but did not erupt, either freezing in place or convecting to deeper levels.

Using the mapped flow volume and duration, the time-averaged discharge rate of the Kamoamoa eruption was approximately 8 m^3 s^{-1}. More than half of the volume was erupted from the W-1 fissure, with fissures W-3, E-4, and E-5 composing most of the remainder. The other fissures contributed very little to the overall volume of the flow field, although the amount erupted from fissure W-4 is unknown, since a significant portion of its volume poured into a graben north of the fissure between 0736 and 1003 HST on March 6. If the mapped surface area of that part of the flow in the graben is disregarded, a new volume and time-averaged discharge rate for lava from fissure W-4 that was extruded outside the graben prior to 0736 can be calculated; these assumptions yield a time-averaged discharge rate that is 53% higher. Assuming this higher rate for the entire duration of W-4 activity, a revised volume of lava erupted from fissure W-4 can be calculated (Table 5.1). This is probably more representative of W-4 output than the initial value calculated from surface area and average thickness alone, but it does not change the mean output rate calculated for the entire eruption.

For much of the Kamoamoa eruption, discharge occurred simultaneously from multiple fissures, and discharge from a particular fissure was sometimes episodic and interspersed with activity from other fissures (Fig. 5.8c). In general, however, the time-averaged discharge rate increased over the course of the eruption (Fig. 5.8b), and near the end it had reached a level nearly three times higher (~10 m^3 s^{-1}) than the long-term average rate (~4 m^3 s^{-1}) over the course of the Pu‘u ‘Ō‘ō eruption (Sutton et al., 2003).

As with other fissure eruptions and dike intrusions during Kīlauea’s ongoing East Rift Zone activity (e.g., Owen et al., 2000; Rivalta and Segall, 2008; Montgomery-Brown et al., 2010), there is a discrepancy between the volume of magma withdrawal and that

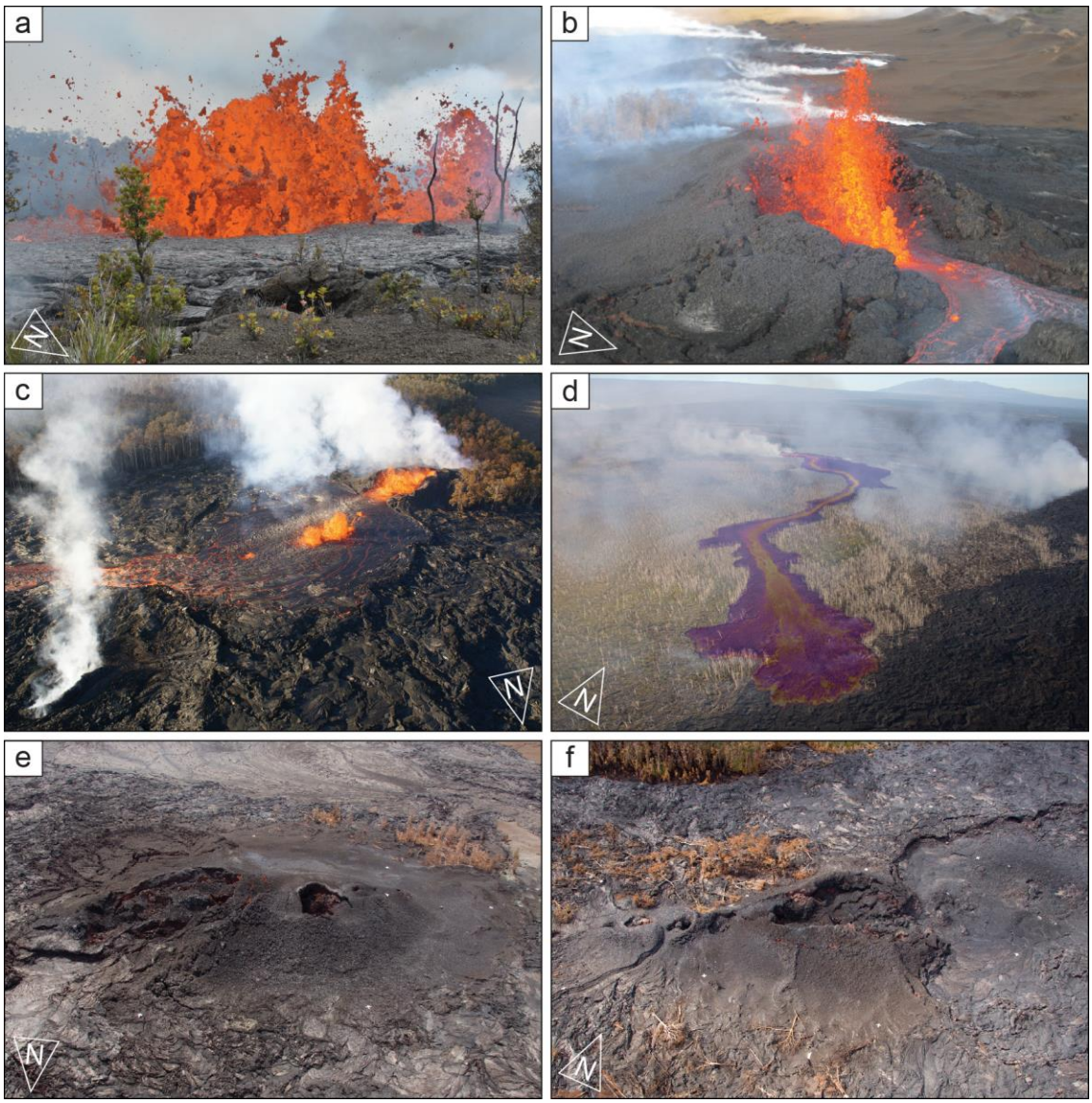

Figure 5.14 Photographs showing Kamoamoa eruption during March 7–9, 2011, and E-5 and W-1 pyroclastic cones on March 17, 2011. (a) 8-m-high fountain on fissure W-3 at 1328 HST on March 7 feeding fast-moving flow extending beyond left side of photo. (b) Fountain 15–20 m high over fissure E-5 at 0810 HST on March 8. (c) Fountains up to 13 m high from fissure W-1 at 0712 HST on March 9. Northeast part of fissure (to left) erupting through perched lava pond, which feeds channelized flow. Inactive fissure W-2 fuming at lower left; edge of Nāpau Crater at upper right. (d) Channelized ʻaʻā flow from fissure W-1 reaching edge of older Puʻu ʻŌʻō flow field at 0727 HST on March 9. Photo overlain with handheld thermal camera (FLIR SC620) image, clipped to match shape of flow, captured at same time. (e) Pyroclastic cone constructed over main vents of fissure E-5 as seen on March 17, after Kamoamoa eruption ended. (f) Pyroclastic cone constructed over main vents of fissure W-1 as seen on March 17.

associated with dike intrusion and eruption. DRE volume loss at the summit and Pu‘u ‘Ō‘ō combine to total 8.0×10^6 m^3, compared to the DRE erupted volume (from field mapping) plus modeled dike volume of 18.3×10^6 m^3. The erupted/intruded volume is therefore more than double that lost from beneath the summit and Pu‘u ‘Ō‘ō (Lundgren et al., 2013)—nearly the same as the ratio between erupted/intruded and lost volumes calculated for the June 2007 intrusion and eruption (Montgomery-Brown et al., 2010). As pointed out by Lundgren et al. (2013), this falls within the range of expected volume ratios for compressible magma (Rivalta and Segall, 2008); therefore, no additional sources of magma are required to explain the volume discrepancy.

5.4.4 Petrology

During 2000–2001, the petrologic character of East Rift Zone lava shifted to that of a hybrid comprising two components: (1) a volatile-rich, high-MgO, high-temperature magma that is fed to Kīlauea from the mantle, and (2) a partially outgassed, lower-MgO, lower-temperature, partially crystallized resident magma that was stored at shallow levels beneath the summit and within the rift zones (e.g., Thornber et al., 2015). Through the early 2000s, lava composition showed a pattern of decreasing magnesia (MgO) and eruption temperatures, but this trend reversed in 2006 in tandem with a surge in magma supply to Kīlauea that caused an influx of hotter recharge magma to the eruption site (Poland et al., 2012). By 2009 (well into episode 58), however, whole-rock concentrations of MgO had begun declining again, reaching values near 7.0 weight percent by early 2011. Corresponding magmatic temperatures, based on MgO glass thermometry (Helz and Thornber, 1987), were about 1140°C. Mineral phenocrysts in erupted lavas were an assemblage of clinopyroxene, plagioclase, and lower-magnesium olivine. These observations suggest a progressive increase in the proportion of cooler resident magma (relative to hotter recharge magma) being erupted from the episode 58 vent after 2009. Thornber et al. (2015) gives a thorough overview of the petrologic trends and petrographic character of erupted products throughout this period, as well as subsequent periods discussed below.

Lavas discharged during the Kamoamoa fissure eruption have significantly lower whole-rock magnesia concentrations than those erupted during episode 58, ranging from

6.1 to 6.7 weight percent and corresponding to cooler magmatic temperatures (1130–1145°C). The mineral assemblage remains a mix of clinopyroxene, plagioclase, and olivine; however, these phenocrysts display an array of disequilibrium textures indicative of a complex heating and cooling history (Thornber et al., 2015). As the eruption progressed, the last products from fissure W-1 had chemical compositions which trended toward values typical of those observed during episode 58. It seems, then, that the dike that fed the Kamoamoa eruption either originated from or encountered (and mingled with) a pod of cooler magma that had been stored within the East Rift Zone (Fig. 5.2). The East Rift Zone probably contains numerous such isolated magma storage zones, and the area beneath Makaopuhi Crater, where the dike originated (see Deformation results, below), has long been thought to be a region of magma storage (Fig. 5.2; e.g., Swanson et al., 1976). The cooler component was gradually flushed over the course of the eruption, and, by March 9, lavas began to resemble the compositions erupted from the East Rift Zone prior to the Kamoamoa activity. In contrast, gases released from fissure W-1 showed an evolved composition even when last measured a few hours before the eruption shut down (USGS unpublished data).

After the Kamoamoa eruption ended, whole-rock magnesia concentrations that erupted within Pu‘u ‘Ō‘ō crater varied erratically between 6.5 and 7.5 weight percent, but the overall trend was a return to values seen during episode 58 (although magmatic temperatures were slightly cooler, with values around 1140°C or less) (Thornber et al., 2015). Mineral assemblages continued to include clinopyroxene, plagioclase, and lower-magnesium olivine, and phenocryst textures still suggested disequilibrium conditions—a testament to the disruption in the East Rift Zone plumbing system wrought by the Kamoamoa eruption.

5.4.5 Gas Geochemistry

The Kamoamoa eruptive episode produced the highest SO_2 emission rates recorded at Kīlauea since Pu‘u ‘Ō‘ō’s high fountaining episodes during 1983–1986. For five sets of measurements spanning March 6–9, emissions averaged 8,500 ± 2,500 t d^{-1}, with a peak daily value of 11,000 ± 1,500 t d^{-1} on March 8 (Fig. 5.4). These reported emission rates represent a minimum constraint because recent studies indicate that dense, SO_2-rich

plumes, like that of the Kamoamoa eruption, result in an underestimation of column SO_2 and, therefore, calculated emission rates (Elias and Sutton, 2012; Kern et al., 2012).

Neither the East Rift Zone SO_2 emissions nor those of the summit showed any clear premonitory changes during the year leading up to the eruption—in fact, both sites displayed subtly declining SO_2 emissions (Fig. 5.4a,c). Furthermore, summit CO_2 emissions, which are closely tied to the magma supply rate to the volcano (Gerlach et al., 2002, Poland et al., 2012), showed relatively steady, or even declining, emissions for the year running up to the eruption, suggesting no significant changes in magma supply prior to the Kamoamoa eruption.

Post-Kamoamoa SO_2 emissions from the East Rift Zone declined rapidly, hovering at or below the lower limit of quantification (approximately 100 t d^{-1}) for six weeks before finally recovering and surpassing the pre-eruption levels (Fig. 5.4c). Summit SO_2 emissions after the Kamoamoa eruption decreased as well, although in a more muted fashion, with values never dropping below 200 t d^{-1} (Fig. 5.4a).

Taken together, the post-eruptive SO_2 extinction from Kīlauea‘s East Rift Zone, and the sharp depression of summit emissions through and beyond the Kamoamoa eruption, supports the idea that the dike feeding the Kamoamoa fissure system tapped magma sources beneath both the summit and Pu‘u ‘Ō‘ō. A rough gas-based estimate of lava output for the Kamoamoa eruption, using the method of Sutton et al. (2001), indicates that 7.6×10^6 m^3 of dense rock equivalent (DRE) magma was outgassed to atmospheric pressure during March 6–9, although only a fraction of this may have actually erupted. The gas data suggest that this value is a minimum magma-outgassed constraint, as it is based on minimum-constraint SO_2 emission rates. Actual values could be up to a factor of three higher.

5.4.6 Deformation

The Kamoamoa eruption was accompanied by deflation at the summit and Pu‘u ‘Ō‘ō, as well as by widening of the East Rift Zone (Figs. 5.8a and 5.15). Subsidence at the summit occurred at a steadily decreasing rate over the course of the eruption and switched to inflation at about 1700 HST on March 9 (shortly before the end of activity at fissure W-1). GPS results indicate a maximum subsidence during March 5–9 of 15 cm

along the east margin of Halemaʻumaʻu Crater. Summit deformation modeled from Interferometric Synthetic Aperture Radar (InSAR) and Global Positioning System (GPS) data suggest a volume loss of 1.7×10^6 m^3 from a magma reservoir at 1.7 km depth (Lundgren et al., 2013), which is a known area of magma storage that has deflated during previous East Rift Zone dike intrusions and eruptions (e.g., Owen et al., 2000; Montgomery-Brown et al., 2010). At Puʻu ʻŌʻō, deflation also waned over time but continued beyond the end of the eruption until the afternoon of March13. Deformation at Puʻu ʻŌʻō was highly localized, suggesting a source perhaps only a few hundred meters deep, which is consistent with previous estimates of Puʻu ʻŌʻō magma storage (Heliker et al., 2003).

Deformation modeling based on InSAR and GPS data from the East Rift Zone indicate that the magma initially feeding the Kamoamoa eruption originated at ~3 km depth near the eastern edge of Makaopuhi Crater (Lundgren et al., 2013) and ascended along an inclined (~45º) trajectory. The eruption began when the magma arrived at the surface ~3.5 hours later, after traveling an ascent-path distance of ~4.25 km. This suggests that the dike tip advanced at an average velocity of ~1.2 km hr^{-1} (0.3 m s^{-1}), similar to average dike propagation rates for past Kīlauea intrusions (~1 km hr^{-1}; Klein et al., 1987; Okamura et al., 1988; Mangan et al., 1995; Owen et al., 2000; Cervelli et al., 2002). The horizontal component of this vector equates to ~0.8 km hr^{-1} (0.2 m s^{-1}). Field observations of the opening of fissures E-1 to E-3 show that the fissures ruptured over a distance of 330 meters in about 25 minutes, or 0.8 km hr^{-1}—the same as the horizontal propagation rate of the dike as it ascended toward the surface.

The East Rift Zone spread apart by several meters at the site of the Kamoamoa eruption, with progressive opening over time as indicated by both fracture measurements and InSAR data (Lundgren et al., 2013). The ground between the eastern and western fissure systems is covered by tephra from the 1983–1986 high fountains of the Puʻu ʻŌʻō eruption. As a result, cracks that formed due to emplacement of the Kamoamoa dike were very well exposed (Fig. 5.16a). A transect perpendicular to the rift zone on March 6 measured the opening amounts of cracks in the area, finding a total of 1.5 m of cumulative crack opening over a distance of 200 m (Fig. 5.16b). The total opening was 2.75 m when the transect was repeated on March 9 (Fig. 5.16b). These amounts are

minima, since the northern end of the transect terminated against a pre-existing graben that experienced an unknown amount of opening. InSAR data from different days of the eruption corroborate these results, showing increasing displacement across the dike over time. The total dike volume at the end of the eruption, based on models of InSAR and GPS displacements, was 15.6×10^6 m^3 (Lundgren et al., 2013).

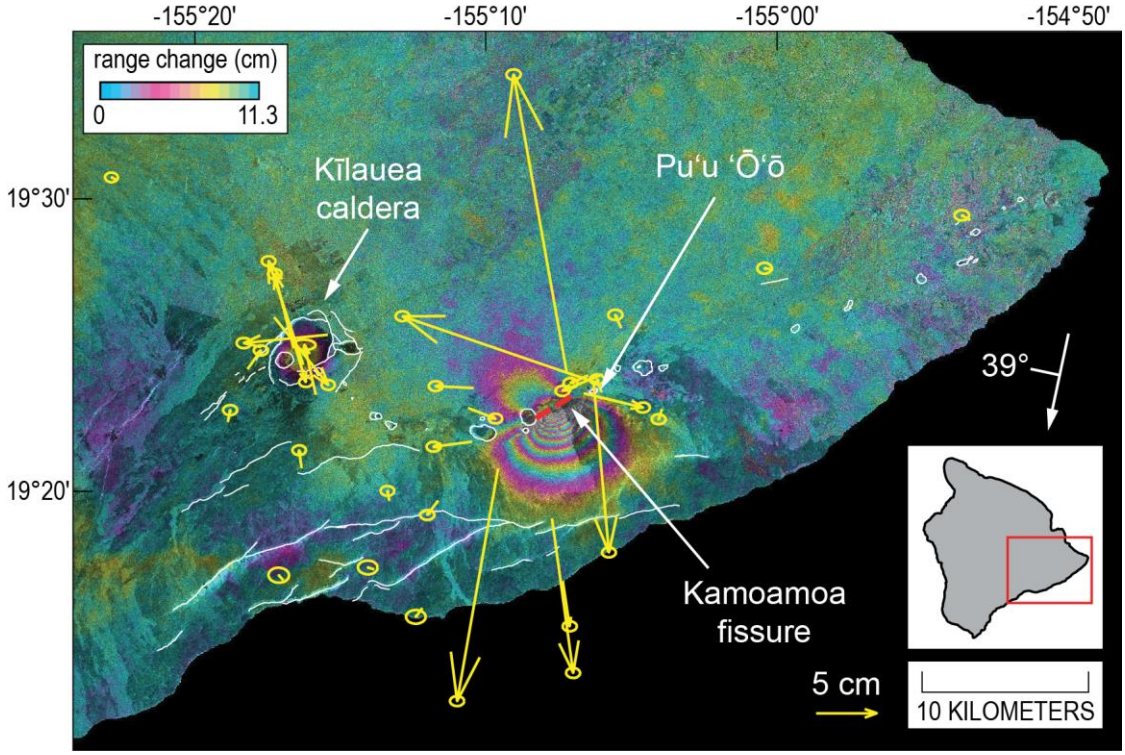

Figure 5.15 Interferogram from PALSAR instrument on ALOS satellite spanning January 24–March 11, 2011 (orbital path 601). White arrow and degree value at right, flight direction and look angle (in degrees from vertical). Yellow arrows, horizontal displacements from GPS with estimated error ellipses; length of yellow arrow scale in lower right shows 5 cm displacement. Red lines in area of greatest deformation, western and eastern Kamoamoa eruptive fissures. (Inset) Island of Hawai'i, showing map area.

5.4.7 Seismicity

At approximately the same time as the onset of subsidence at Pu'u 'Ō'ō, seismic amplitudes (expressed in terms of Real-time Seismic Amplitude Measurement (RSAM); Endo and Murray, 1991) increased dramatically (Figs. 5.7 and 5.8) on stations located

along the East Rift Zone (PAU, STC and KNH). The seismic signal was initially composed of discrete events that were often so close together temporally that they combined to create a tremor-like signal (Fig. 5.7a). Most of these events did not record on enough stations to be located; however, it is clear that the seismicity was associated both with dike propagation between Makaopuhi Crater and Nāpau Crater and the failure of Pu‘u ‘Ō‘ō’s crater floor. Long-period and volcano-tectonic events were simultaneously present. Once fountaining along the Kamoamoa fissure started, the character of tremor changed at the station closest to the fissure site (STC), becoming more energetic and also having a broader and higher-frequency spectral signature than previous activity (Fig. 5.7b).

For the remainder of the eruption, tremor recorded at station STC (using RSAM as a proxy) had frequencies between 1.5 and 7 Hz, and tremor amplitudes generally matched changes in fountaining (Fig. 5.8). The amplitude of tremor (and RSAM value) recorded on STC depended on two factors: (1) the intensity of the source, and (2) the distance from the source to the seismometer. The distance between STC and the fountaining source centroid on each fissure ranged from 440 m (E-4) to 1765 m (W-1) (Table 5.1). Clearly, when two fountaining sources occurred simultaneously, the closer source was the dominant signal, assuming both sources had similar intensities.

Over the course of the eruption, large changes in RSAM corresponded to variations in fountain behavior. A significant bump in RSAM during ~1700–1930 HST on March 5 corresponded to the initiation of fountaining from fissures E-1, E-2 and E-3 (see 1, Fig. 5.8a). Even though the fountain heights and rate of extrusion were low, STC was only ~500 m away, and thus the response in RSAM was significant. Activity resumed shortly after midnight on March 6 with fountaining at fissure W-3 (1500 m distance from STC) occurring during a small, temporary bump in RSAM. Another small rise in RSAM started at ~0140 HST on March 6 but began to climb more rapidly at ~0240, when sporadic activity started at fissures E-3 and (or) E-4 and propagated to E-5 (~500 m from STC; see 2, Fig. 5.8a). Fissure W-4 activated during the decline of this RSAM anomaly, but W-4’s distance from STC resulted in no significant contribution to the RSAM compared to the decline in activity at the eastern fissures. Another increase in RSAM started at ~0945 HST on March 6. As the RSAM ramped up, eruptive activity resumed at fissure E-5

(~500 m from STC). Modulations in RSAM for the subsequent 12 hours may be explained by changes in observed fountain height at E-5 (see 3, Fig. 5.8a).

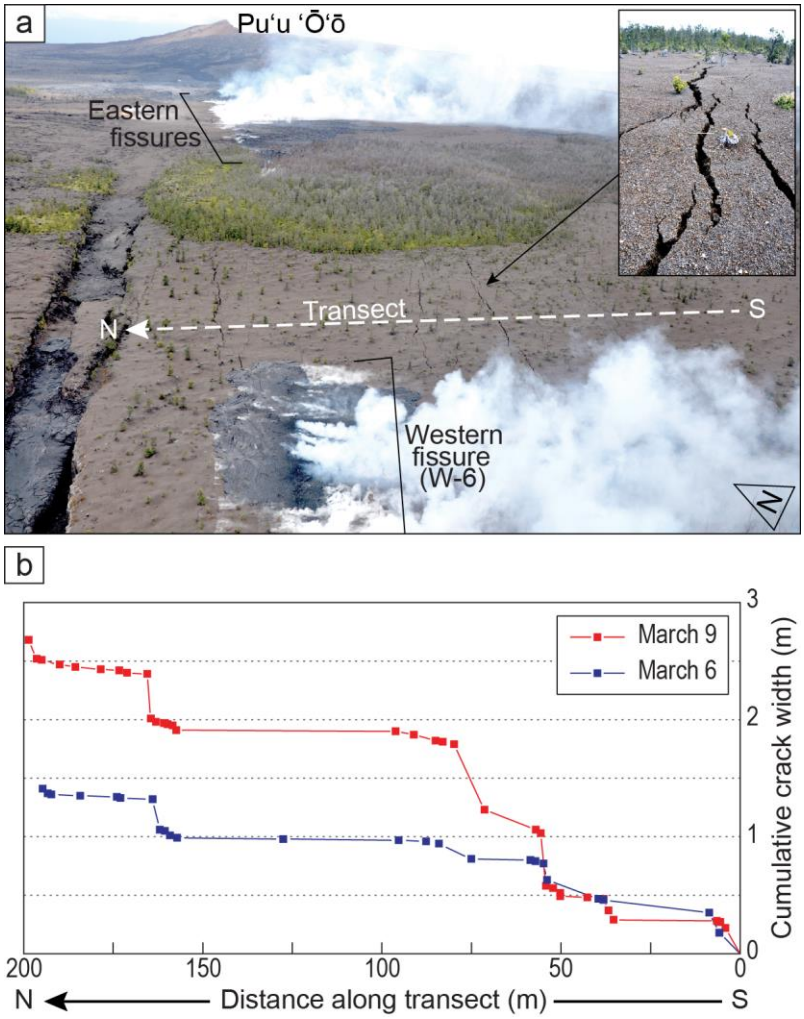

Figure 5.16 Photographs showing fractured, tephra-covered ground between eastern and western fissure systems on (a) March 7, 2011. Fissure W-6 at bottom. Dashed white line, transect along which crack opening was measured. (Inset) March 6, 2011, photograph of ground cracks. (b) Graph showing cumulative crack width along south-to-north transect shown in (a). Blue line, March 6, 2011 (~1130 HST); red line, March 9 (~1430 HST). Strike of western fissure intersects transect between 100 and 160 m.

On March 7 at ~0700 HST, RSAM values started to increase at the same time as the cessation of eruptive activity from fissure E-5 and shortly after the onset of eruptive activity from fissure W-2 (see 4, Fig. 5.8a). The RSAM increase peaks at about the same time as the cessation of W-2 activity. Since RSAM did not correlate with earlier changes

in fountaining from western fissures, and in this case ramped up and peaked as fissure W-2 was shutting down, it seems unlikely that this RSAM increase was related to W-2 activity. On the other hand, no eruptive activity from any eastern fissure matches the RSAM increase either. While the RSAM increase could correlate with loud outgassing from eastern fissures without eruption, no ground observations can verify if that was, indeed, the case.

A slight increase in RSAM began at ~1110 HST on March 7, at about the same time as the onset of fountaining at fissure W-3. At ~1315 HST, RSAM began to increase rapidly. This increase does not correlate with obvious eruptive activity from any eastern fissure, but it does spike during a brief fountaining episode from fissure E-4 (440 m from STC) at ~1520 HST (see 5, Fig. 5.8a). A step in RSAM at ~1800 HST can be attributed to another episode of fountaining from E-4 (see 6, Fig. 5.8a), and a second step at ~2115 occurs in tandem with an increase in E-4 fountain height (see 7, Fig. 5.8a). The subsequent long decline in RSAM that extended to the end of the eruption (see 8, Fig. 5.8a) reflects a shift in activity from the eastern fissures to W-1, the fissure farthest from STC (~1765 m). In the analysis above, the link between amplitudes and eruption activity is very strong. This suggests that the source of the tremor with this spectral character can be attributed in most instances to near-surface processes associated with fountaining, which includes not only outgassing and the movement of magma, but possibly also the impact of spatter on the ground surface.

Tremor with peak frequencies between 0.1 Hz and 0.5 Hz was also recorded on near-summit stations during the Kamoamoa eruption. The tremor was recorded at distances >12 km but was strongest in the summit area. Previous studies of Very Long Period (VLP) seismic sources with nearly identical frequency content have been attributed to magma movement though the shallow conduit system at the summit of Kīlauea (Dawson et al., 2010). A source invoking magma flow out of the shallow summit conduit system is consistent with seismic observations, deflation, and falling lava lake level.

5.5 Discussion

The exceptional suite of geological, geophysical, and geochemical observations collected before and during the Kamoamoa eruption provides an excellent window into the mechanism for eruptive activity that can be applied to future episodes of eruptive change at Kīlauea (and elsewhere). Based on these data, it can be concluded that the Kamoamoa eruption was caused by an imbalance between the rates of magma supply and eruption. Similar imbalances, regardless of whether they are controlled by an increase in supply or a decrease in output, have caused other changes in activity during the Pu‘u ‘Ō‘ō eruption, such as at the June 2007 eruption at Kāne Nui o Hamo. This is in contrast to eruptive changes that occur in response to the "passive" opening of the rift (e.g. January 1997 and September 1999 intrusions (Owen et al., 2000; Cervelli et al., 2002)), which is related to seaward motion of Kīlauea's south flank.

The time-averaged discharge rate of the episode 58 vent in 2007 was approximately 6 m^3 s^{-1} (0.18 km^3 yr^{-1}; Poland et al., 2012). By mid-2010, however, the time-averaged discharge rate from that vent had dropped precipitously by several times (to ~1–2 m^3 s^{-1}; see Chapter 3). The decline in discharge rate was reflected in a waning of lava flow activity on the flow field between the East Rift Zone and the ocean, as well as by a decrease in the SO_2 emission rate from the East Rift Zone. Unfortunately, the SO_2 emission rates cannot be used to precisely quantify the discharge rate as was possible prior to 2008 (Sutton et al., 2001, 2003) because lava erupting from the East Rift Zone after 2008 is thought to have already partly outgassed as it circulated through the summit lava lake (Elias and Sutton, 2012). Nevertheless, the decrease in SO_2 emission rates from the East Rift Zone during 2009–2010 (which, at the end of 2010, were the lowest recorded to that time since vehicle-based measurements began in 1992 (Elias and Sutton, 2012)) supports direct geological observations of a decline in discharge rate.

The influence of a decrease in magma throughput on the shallow, subhorizontal conduit connecting Pu‘u ‘Ō‘ō to the episode 58 vent, its top at a depth of no more than a few hundred meters (Fig. 5.2; Poland et al., 2008a), probably induced cooling and shrinking of the conduit. This would have the effect of reducing the conduit's cross-sectional area and, hence, its carrying capacity. The reduction in carrying capacity was probably exacerbated by interruptions in magma transport from the summit to the East

Rift Zone caused by repeated DI events. When the DI events stopped occurring for several months starting in November 2010, the conduit was not able to accommodate the supply of magma being fed constantly from the summit, and pressure built quickly within Kīlauea's shallow magma plumbing system (beneath the summit and within the East Rift Zone). The increase in pressure was manifested as uplift at the summit and Puʻu ʻŌʻō and as extension across the East Rift Zone (Fig. 5.4), and also as an increase in the number of earthquakes beneath the summit and upper East Rift Zone (Figs. 5.4 and 5.5). Eventually, the system reached its breaking point, and the weakest link—in this case, the East Rift Zone near Nāpau Crater—failed. This is not surprising, given the history of the area, which has been the site of frequent eruptions over the past several decades, including in 1961, 1963, 1965, 1968, 1983 (episode 1 of the Puʻu ʻŌʻō eruption), and 1997 (episode 54 of the Puʻu ʻŌʻō eruption). These and previous eruptions might have left residual pods of melt in the subsurface that could be incorporated into subsequent eruptions, as indicated by petrologic evidence from early Puʻu ʻŌʻō lavas (Garcia et al., 1992) and the 1997 Nāpau Crater eruption (Thornber et al., 2003), as well as the Kamoamoa eruption.

The pressurization of Kīlauea's magma plumbing system, as well as periods of filling of the Puʻu ʻŌʻō crater during 2010 (in particular, the sustained filling that began in November of that year), is interpreted as being caused by an imbalance between the amount of magma arriving at Puʻu ʻŌʻō and the amount being erupted from the episode 58 vent. A small increase in the rate of magma supply to Kīlauea also cannot be ruled out, especially since supply has been shown to fluctuate on time scales of years (Poland et al., 2012). Such an increase in supply could not have been large, given the lack of any substantive change in the rate of CO_2 emission from the summit, and may be part of a natural waxing and waning of magma supply that is generally too small to be recognized. Regardless, the volume of magma reaching Puʻu ʻŌʻō exceeded that which could be erupted from the episode 58 vent, resulting in a backup that caused the volcano's summit and East Rift Zone magma systems to pressurize and eventually rupture, leading to the Kamoamoa fissure eruption.

Although fed initially by magma from both Puʻu ʻŌʻō and the summit, the summit probably contributed the bulk of the magma being erupted after the first few hours. Deflation at Kīlauea's summit decayed rapidly and smoothly following eruption onset

(Fig. 5.8a), and there were no geophysical changes that matched the intermittency of the Kamoamoa eruption as it jumped between fissures during the initial three days of the eruption. If the transport of magma from the summit to the Kamoamoa eruption site occurred in a steady-state fashion, as suggested by the smoothness of the tilt record, then variations in eruptive location and output must have been caused by more localized factors, such as changes in magma viscosity, the near-surface stress field, or the shape of the erupting fissures over time. As with many basaltic fissure eruptions, activity eventually focused on a single fissure (W-1), which was the dominant source of lava discharge over the last two days of the eruption (Fig. 5.8c; Table 5.1).

Once the excess pressure that had accumulated during 2010 and early 2011 had dissipated, the pressure gradient between the summit and the Kamoamoa fissure was not sufficient to sustain the eruption. This allowed activity to cease, and the Kamoamoa dike presumably cooled thereafter due to the large thermal gradient between the dike and the surrounding country rock (Wilson and Head, 1981). After the eruption ended, pressure began to climb within Kīlauea's magma storage areas and transport pathways in response to the continuous supply of magma to the volcano. This pressure led to the reappearance of the summit lava lake in the Overlook crater and was eventually directed toward restarting eruptive activity at Puʻu ʻŌʻō, probably because that well-worn conduit remained hot and provided an easy way for magma to reach the surface along the East Rift Zone.

The 2010–2011 gradual abandonment of the episode 58 vent and onset of the episode 59 Kamoamoa fissure eruption bears striking resemblance to the 1991–1992 slowdown of the episode 48 Kupaianaha vent and onset of the episode 49 fissure. In the latter case, output from Kupaianaha waned over several months, while the summit inflated and eruptive activity increased at Puʻu ʻŌʻō (Kauahikaua et al., 1996). Also during 1990–1991, a series of seismic swarms in the upper East Rift Zone, interpreted as intrusions, interrupted magma flow to the eruption site (Kauahikaua et al., 1996; Heliker and Mattox, 2003). Kauahikaua et al. (1996) interpreted these events as an indication that cooling and crystallization had caused the magma reservoir beneath Kupaianaha to become increasingly isolated from the rest of the magmatic system, which led to a decline in the magma pressure driving the eruption. The up-rift buildup in pressure in

response to the Kupaianaha slowdown probably led to the episode 49 fissure eruption between Puʻu ʻŌʻō and Kupaianaha in November 1991 (Mangan et al., 1995), although Kupaianaha continued to be weakly active until February 1992 (Kauahikaua et al., 1996).

Based on the examples from the Kupaianaha decline and episode 49 fissure eruption and from the episode 58 decline and Kamoamoa fissure eruption, it should be possible to project the likelihood of future changes in eruptive activity several months in advance, provided the activity follows a similar pattern. Such changes are most likely to occur when eruption is occurring at a vent away from Puʻu ʻŌʻō but still connected to Puʻu ʻŌʻō via a shallow conduit. Our model is not, however, suitable for forecasting fissure eruptions like that which occurred in 1997 from Nāpau Crater (Owen et al., 2000; Thornber et al., 2003). As discussed above, that eruption, as well as a dike intrusion in 1999 (Cervelli et al., 2002), were inferred to have resulted from passive opening of the East Rift Zone due to seaward motion of the south flank, and neither event was preceded by summit inflation or increased East Rift Zone spreading. The transitions of eruptive activity away from both the episode 48 (in 1991–1992) and episode 58 (2011) vents, and the ensuing fissure eruptions, were, in contrast, associated with waning lava effusion and pressurization of the magmatic system.

The magma transport pathway between the summit and Puʻu ʻŌʻō is robust after decades of activity and continues to be used, even when lava effusion is focused away from Puʻu ʻŌʻō. In contrast, conduits associated with vents that are satellitic to Puʻu ʻŌʻō tend to be shallow and more susceptible to choking by minor changes in magma supplied to the vent. Repeated interruptions in magma flow from the summit to the East Rift Zone, either due to up-rift intrusions, DI events, or other processes, could therefore cause the satellite vent system to cool and become isolated. The discharge rate would wane as a result, causing pressurization of Kīlauea's magma plumbing system manifested as inflation of the summit (along with inflation at the eruption site and spreading of the East Rift Zone), increases in seismicity along the upper East Rift Zone, and rising lava level within the summit eruptive vent. Eruptive activity at the satellite vent would decline, while lava effusion at Puʻu ʻŌʻō would increase. Once a critical threshold is reached, the conduit system will rupture in response to the building pressure.

5.6 Summary and Conclusions

The March 5–9, 2011, Kamoamoa fissure eruption (episode 59) occurred as part of a shift in vent location of the long-lived Puʻu ʻŌʻō eruption at Kīlauea, which has been ongoing since 1983. On the afternoon of March 5, a dike began propagating from the East Rift Zone conduit between Makaopuhi and Nāpau craters (a site of repeated fissure eruptions since the 1960s), originating from and (or) intersecting and incorporating older, cooler, more evolved magma. Magma from Puʻu ʻŌʻō was also diverted into the growing dike, causing the cone's crater floor to drop. The lava lake in the Overlook crater began to drain as magma likewise withdrew from beneath Kīlauea's summit. The dike reached the surface about 3.5 hours after its initiation and fed an eruption that extended over more than 2 km along two fissure systems (each of which was composed of 5–6 fissures). Eruptive activity jumped between the fissures during the first three days before finally settling on the westernmost fissure for the final day of the eruption. The total volume erupted was approximately 2.7×10^6 m^3, and the peak eruption rate was about 3 times higher than the long-term average eruption rate from Puʻu ʻŌʻō.

The Kamoamoa eruption was probably a result of the gradual shutdown of the episode 58 vent, which was located about 2 km down-rift of Puʻu ʻŌʻō. The vent had been active since 2007 but experienced a slow decline in eruption rate that became evident in 2010. Repeated interruptions in magma flow from the summit to the East Rift Zone due to cycles of summit deflation and inflation may have led to the gradual cooling and isolation of the episode 58 conduit, which in turn caused pressurization within Kīlauea's magma system. The pressurization was manifested by inflation of the summit and Puʻu ʻŌʻō, spreading of the East Rift Zone, increased seismicity along the upper East Rift Zone, and rising lava levels within both the summit eruptive vent and Puʻu ʻŌʻō's crater. The activity culminated in the Kamoamoa fissure eruption, after which the locus of long-term lava effusion moved back to Puʻu ʻŌʻō, and the episode 58 vent ceased erupting altogether. The 2010–2011 pattern of activity strongly resembled that of 1990–1992, when waning of the Kupaianaha eruptive vent culminated in an East Rift Zone fissure eruption and subsequent shift in eruptive activity to Puʻu ʻŌʻō. Based on these patterns and the excellent geological, geophysical, and geochemical monitoring of

Kīlauea, it should be possible to recognize similar progressions months in advance of any shifts in eruption style and/or location.

Chapter 6

Conclusions

6.1 Overview: Role of imaging technology in geological observations

Kīlauea Volcano offers a unique opportunity for the study of basaltic volcanism because it hosts frequent and relatively benign activity (at least for the last two centuries) that is generally accessible year-round. It is for this reason, and the desire to enhance global knowledge, that Thomas Jaggar established the Hawaiian Volcano Observatory at Kīlauea in 1912. Subsequent geological observations at Kīlauea have formed the foundation of many landmark studies. However, while eruptions at Kīlauea tend to be approachable, direct observations are often impractical. It may be days, weeks, or even years between significant events. Many events are short-lived, and access, when those events do occur, is not instantaneous. Thus, many important eruptive changes, especially at their onset, have been missed. In addition, while the eye is a fantastic tool, many characteristics of eruptive activity occur at time- or length-scales not easily discernable, either being too fast or too slow.

To overcome these limitations, and to explore new avenues of research, modern digital cameras and imaging technologies have been applied increasingly to volcanological studies. High-frame-rate, telemetered webcam networks and high-resolution time-lapse camera systems now monitor volcanoes across the globe, and the images they collect, often through integration with geophysical and geochemical data, have given scientists new insights into an array of volcanic processes. High-speed camera systems are now able to acquire images at rates comparable to those achievable by geophysical monitoring systems, such as seismometers. Conversely, the ability to review long sequences of images, representing durations of hours, days, or weeks, in time-lapse movies that last seconds, gives us a means of studying change that occurs over long periods. Such geological observations can be combined with geophysical observations that operate over similar time spans, such as tiltmeters and GPS receivers.

The research described in Chapters 2 through 5, which form the body of this dissertation, all relied on time-lapse and (or) webcam imaging technologies, without which these studies would have been far less robust or even impossible. Because of their reliance on observations acquired via cameras, these chapters are examples of one way in which volcanology is evolving. Other new research avenues will undoubtedly arise as camera systems continue to improve, for example by the development of affordable, high-resolution long-wave infrared cameras. Even new improvements in battery and solar recharging technologies will be important, by permitting the development of more compact and portable camera systems.

6.2 Research limitations

6.2.1 Chapter 2

The research presented in Chapter 2 would have benefited from additional camera systems providing more thorough visual coverage of the crater in Puʻu ʻŌʻō. This was impossible, however, given the lack of additional resources, both in terms of equipment and time. Achieving the right balance of equipment coverage versus the time investment required to deploy and maintain that equipment will always be a challenge.

Better topography of Puʻu ʻŌʻō crater would have also aided this study. The work done was the best that could be achieved at the time. Now, newly developed structure-from-motion software packages permit the construction of digital elevation models from oblique aerial photographs captured with handheld digital cameras. Puʻu ʻŌʻō crater was largely fume-free during its refilling, which would have been the ideal situation for capturing photographs that could be processed via structure-from-motion software.

6.2.2 Chapter 3

The uniqueness of the sinuous tumulus that developed on the coastal plain near the Kalapana Gardens subdivision was not recognized until after it had begun to form. Once it formed, however, it would have been useful to immediately record repeat transects over the tumulus with kinematic GPS. This would have given a detailed growth history of the tumulus. Moreover, the width and depth of the axial crack could have been measured at

each of those transects at the same time. Producing this dataset, however, would have been challenging. With the lava flow threatening houses in Kalapana Gardens, mapping the flow margins, assessing potential flow paths, and producing maps for Hawai‘i County Civil Defense and the public were the priority. Time for additional work was not always available.

Photographing the sinuous tumulus was challenging, because of its length and the bland gray color of young basaltic lava. The paucity of photographs, especially aerial views, is unfortunate. I have learned from this shortsightedness and have since made a conscious effort to capture an abundance of field photographs. Camera memory cards are inexpensive and can now hold hundreds of high-resolution photographs, so that poses no barrier to capturing more pictures than may seem necessary. One downside, however, is the additional time spent cataloging a multitude of photographs.

As noted in Chapter 3, several time-lapse camera systems were deployed on and adjacent to the sinuous tumulus. Most of these deployments relied on inexpensive time-lapse cameras used for watching birds and other wildlife. These systems were used because of the perceived likelihood of their destruction by lava flows. The cameras proved to be unreliable. They produced low quality images, and the resulting image sequences were so strongly affected by wind shake that quantification of tumulus motion was impossible. In hindsight, placement of cameras atop the sinuous tumulus was perhaps the safest place for close-up views. The low quality cameras were finally replaced by high-quality, custom-made time-lapse systems, but the tube beneath the sinuous tumulus was abandoned shortly afterward, and so the improved camera systems captured data for only a short time.

6.2.3 Chapter 4

Relatively fast (4 frames per second) webcam acquisition was crucial to visualizing the small explosive eruptions that occurred at Kīlauea’s summit in early 2011, on which this study is based. While a slower webcam was deployed on the rim of Halema‘uma‘u since September 2008, the high-quality webcam used in this study was not installed until September 2009, and higher-rate data were collected from May 2010. The changes in the

systems used at the summit were driven in large part by evolution of camera and telemetry technologies. The 2010 system was not available in 2008–2009.

Though better observations are always valuable, understanding the contributions of the various processes involved in driving the summit explosions is the more important goal. This will always be challenging, but an integrative modeling approach, which melds the ideas presented here, including the Worthington jet model, with the shock vesiculation model of Carey et al. (2012), may help untangle the processes involved. There is clearly a lack of analog studies of splashes comparable to the scenario we describe. Most of those studies focus on small, spherical objects impacting water, whereas the research presented in Chapter 4 would have benefited from studies which looked at large irregular masses impacting water, at impacts by disaggregated groups of objects of varying size, and by objects impacting fluids of different viscosities.

6.2.4 Chapter 5

The Kamoamoa eruption may be the best documented eruption in Hawai‘i, but more thorough observations of fissure propagation and fountaining, along with the collection of tephra at regular intervals from a fountain at the same time that the fountain was documented by video, would have added significant value to the research. This was prevented, mostly, by a lack of manpower, which always presents a challenge during eruptive crises at Kīlauea. Better management of people and other resources, as well as a better prioritization of duties, will play an important role in managing future eruption responses, though having these resources available and in place at the onset of new eruptive activity remains elusive and unlikely.

6.3 Research ideas for the future

These studies have spawned an array of questions that fall outside the scope of this dissertation. In addition, the camera imagery used in these studies is but a small subset of a record from time-lapse cameras and webcams collected as part of an ongoing eruption response. This image record includes many other camera observations that reveal a variety of other new processes, or have shed new light on old processes, that could be the

basis of future studies. Several such studies are addressed below to give a flavor of the types of research projects that could be produced.

6.3.1 Endogenous crater floor uplift

Endogenous uplift of Puʻu ʻŌʻō crater in 2007, as described in Chapter 2, occurred with even more profound consequences in 2011, in the aftermath of the Kamoamoa eruption (Chapter 5). In fact, recognition of the 2011 uplift, based on the sequence of events in 2007, prepared scientists in advance for the subsequent August 2011 flank eruption at Puʻu ʻŌʻō. These two recent instances of uplift may also be direct analogs for the endogenous uplift described from Kīlauea's caldera during the mid-19th century (see section 1.3) and at Halemaʻumaʻu during the early 20th century (Jaggar, 1947, p. 113–114), suggesting a fundamental process that distributes stress and pressure during shallow accumulation of magma at Kīlauea. The crater floor subsidence at Puʻu ʻŌʻō in August 2011 also revealed a juvenile rind coating the crater wall. This rind was inferred to be the remnant of a dike that fed lava onto the crater floor from the circumferential fault accommodating the uplift, and it probably acted as a lubricant that aided the uplift. Descriptions of subsidence at Halemaʻumaʻu during the early 20th century remark on a very similar coating on the crater wall (Jaggar, 1947, p. 135).

6.3.2 Eruption along cone sheets at Puʻu ʻŌʻō

Most flank eruptions at Puʻu ʻŌʻō can be classified into two categories—eruptions from vertical fissures (up-rift or down-rift) aligned with the East Rift Zone, and eruptions from inwardly inclined fissures circumferential to Puʻu ʻŌʻō cone (cone sheets), which have not been described there before. The two most obvious examples of the second group are the August 2011 breakout and the June 2014 breakout. Other major breakouts at Puʻu ʻŌʻō probably also fall into this category, but their characterization is less clear. The 2011 and 2014 events both occurred during periods of high pressure (inferred from geological and geophysical observations) and their respective dikes probably rose from the shallow magma body beneath Puʻu ʻŌʻō, following the stress field caused by the weight of the Puʻu ʻŌʻō cone. As these intrusions started, the overlying flank of Puʻu ʻŌʻō was uplifted abruptly, as documented by time-lapse cameras and webcams. The

dikes also splayed vertically as they intruded, resulting in offset dike segments, much like those formed by vertical dikes elsewhere in the rift zone. A detailed study of cone sheet emplacement would be, to my knowledge, unique, integrating geological observations with geophysical modeling of tilt and GPS data.

6.3.3 Characterization of low-intensity Hawaiian fountains

As mentioned in section 6.2.4, Kīlauea offers the opportunity of improved characterization of low-intensity Hawaiian fountains, because many of its fissure eruptions can be closely accessed. Under the right conditions, another eruption like the 2011 Kamoamoa eruption would offer an outstanding opportunity to collect tephra from a fountain being simultaneously documented with video. These, along with a detailed study of pyroclast parameters, such as density and vesicularity, and deposit measurements like isomass, would provide yet another one-of-a-kind dataset.

6.3.4 Cross-section through a sinuous tumulus

During 2014–2015, lava flows encroached on and threatened the town of Pāhoa in the Puna district. In several areas along the length of the flow, the feeder tube developed a raised, ridge-like sinuous tumulus, similar to that which formed near Kalapana Gardens subdivision during 2010. In one location, a sinuous tumulus grew over the tube where it crossed a street on the outskirts of Pāhoa. In September 2015, several months after the flow was abandoned, the County of Hawai‘i Department of Public Works opened bids for reestablishment of this roadway at its original grade. This work will expose a complete cross-section through the flow and the sinuous tumulus, allowing a unique opportunity to characterize its internal stratigraphy and the underlying lava tube.

6.4 Some wider applications of studies at Kīlauea

The rapid advances in digital imaging technologies, which continue to change and improve at a rapid pace, have breathed new life into the study of physical volcanology. The studies presented here, and the volcanological community in general, have all benefited from these technologies.

Geological observations often take a back seat to numerical models. Observations, however, play a vital role in constraining those models. One clear example from this research is the determination that rockfalls were the trigger for the small explosive eruptions at Halemaʻumaʻu after the vent opened in 2008. One of the first publications about the summit eruption inferred that the explosive events were the result of large gas slugs bursting through the top of the lava column; the interpretation was based on seismic data and overlooked the clear association between rockfalls and explosions. The geological observations my colleagues and I collected established this link undeniably, defined a new class of small explosive eruption, and highlighted a new hazard at Kīlauea's summit. It remains to be seen if this class of eruption is unique to the current Halemaʻumaʻu eruption, or if eruptions triggered by rockfalls will be identified elsewhere.

The detailed geological observations during the 2011 Kamoamoa eruption, in particular several videos that show Hawaiian fountaining along the fissure system, engendered new insights into this eruptive style and the dynamics of fissure opening and propagation. These have helped guide ideas about the early stages of fissure eruption (Parcheta, 2013; Parcheta et al., 2013). The eruption observations also show a behavior that occupies a middle ground between Hawaiian and Strombolian activity (Orr et al., 2013), highlighting inconsistencies in how these terms are used by volcanologists, based on the style with which they are most familiar. Scientists who work primarily in Hawaiʻi would likely identify this style of activity as Hawaiian fountaining, while scientists who work primarily in Italy might call it Strombolian. These two styles of activity describe end-member conditions but are inadequate for activity with characteristics of both styles. This has led to new considerations for how to classify Strombolian and Hawaiian eruption based on measureable parameters.

The identification of raised ridges as sinuous tumuli over lava tubes within volcanic provinces on Mars will likely play a role in the ongoing discussion of the relative importance of water in shaping the Martian landscape. Research continues in this area, along with identifying other lava flow features in Hawaiʻi as analogs to features observed in Mars imagery. Research on the sinuous tumulus that formed in 2010 accompanied study of the ongoing Puʻu ʻŌʻō eruption. A key observation was the association between

cycles in summit deformation and the occurrence of breakouts from the sinuous tumulus, several of which threatened nearby houses. Recognition of this association improved hazard assessments and provided a means of forecasting activity that proved useful for Hawai‘i County Civil Defense. The relation between summit deformation and flow-field activity is now well established and regularly used by the Hawaiian Volcano Observatory to forecast and track activity as part of the ongoing eruption monitoring of Kīlauea.

Finally, watching for crater floor uplift at Pu‘u ‘Ō‘ō is one of many key observations carried out during monitoring of Kīlauea’s East Rift Zone eruption, and it stems from my work at Pu‘u ‘Ō‘ō in 2007. Its recognition has already proved useful and allowed early preparation for the August 2011 breakout at Pu‘u ‘Ō‘ō. Though not described previously elsewhere, identifying crater floor uplift may prove important at other basaltic volcanoes as well. Moreover, further modeling of the crater floor uplift may help constrain the size and depth of the magma storage beneath Pu‘u ‘Ō‘ō, which would broaden our understanding of the emplacement and evolution of the shallowest magma bodies within the crust.

References

Anderson, K.R., Poland, M. P., Johnson, J. H., and Miklius, A., 2015, Episodic deflation-inflation events at Kīlauea Volcano and implications for the shallow magma system: *in*: Carey, R., Cayol, V., Poland, M., Weis, D., (eds.), Hawaiian Volcanoes, from Source to Surface. American Geophysical Union Monograph 208, 229–250.

Anderson, S.W., Stofan, E.R., Smrekar, S.E., Guest, J.E., and Wood, B., 1999, Pulsed inflation of pahoehoe lava flows: implications for flood basalt emplacement. Earth and Planetary Science Letters 168(1–2), 7–18.

Anderson, S.W., McColley, S.M., Fink, J.H., and Hudson, R.K., 2005, The development of fluid instabilities and preferred pathways in lava flow interiors: Insights from analog experiments and fractal analysis. Geological Society of America Special Papers 396, 147–161.

Anderson, S.W., Smrekar, S.E., and Stofan, E.R., 2012, Tumulus development on lava flows: insights from observations of active tumuli and analysis of formation models. Bulletin of Volcanology 74(4), 931–946.

Atkinson, A., Griffin, T.J., and Stephenson, P.J., 1975, A major lava tube system from Undara Volcano, North Queensland. Bulletin of Volcanology 39, 266–293.

Atkinson, A., and Atkinson, V.G., 1995, Undara Volcano and its tubes. Anne and Vernon Atkinson, Brisbane, Queensland.

Baker, S., and Amelung, F., 2012, Top-down inflation and deflation at the summit of Kīlauea Volcano, Hawaii observed with InSAR. Journal of Geophysical Research 117(B12406).

Baker, V.R., 2001, Water and the martian landscape. Nature 412(6843), 228–236.

Banks, M.E., Lang, N.P., Kargel, J.S., McEwen, A.S., Baker, V.R., Grant, J.A., Pelletier, J.D., and Strom, R.G., 2009, An analysis of sinuous ridges in the southern Argyre Planitia, Mars using HiRISE and CTX images and MOLA data. Journal of Geophysical Research 114(E9), E09003.

Bleacher, J.E., Sakimoto, S.E.H., Garvin, J.B., and Wong, M., 2003, Deflation/erosion rates for the Parva Member, Dorsa Argentea Formation and implications for the south polar region of Mars. Journal of Geophysical Research 108(E7), 5075.

Bleacher, J.E., Greeley, R., Williams, D.A., Werner, S.C., Hauber, E., and Neukum, G., 2007a, Olympus Mons, Mars: Inferred changes in late Amazonian aged effusive activity from lava flow mapping of Mars Express High Resolution Stereo Camera data. Journal of Geophysical Research 112, E04003.

Bleacher, J.E., Greeley, R., Williams, D.A., Cave, S.R., and Neukum, G., 2007b, Trends in effusive style at the Tharsis Montes, Mars, and implications for the development of the Tharsis province. Journal of Geophysical Research 112, E09005.

Bergmann, R., van der Meer, D., Stijnman, M., Sandtke, M., Prosperetti, A., and Lohse, D., 2006, Giant bubble pinch-off. Physical Review Letters 96(15), 154505.

Burr, D.M., Bruno, B.C., Lanagan, P.D., Glaze, L.S., Jaeger, W.L., Soare, R.J., Wan Bun Tseung, J.-M., Skinner Jr., J.A., and Baloga, S.M., 2009, Mesoscale raised rim depressions (MRRDs) on Earth: A review of the characteristics, processes, and spatial distributions of analogs for Mars. Planetary and Space Science 57, 579–596.

Burr, D.M., Williams, R.M.E., Wendell, K.D., Chojnacki, M., and Emery, J.P., 2010, Inverted fluvial features in the Aeolis/Zephyria Plana region, Mars: Formation mechanism and initial paleodischarge estimates. Journal of Geophysical Research 115(E7), E07011.

Carbone, D., Poland, M.P., Patrick, M.R., and Orr, T.R., 2013, Continuous gravity measurements reveal a low-density lava lake at Kīlauea Volcano, Hawai‘i. Earth and Planetary Science Letters 376(0): 178–185.

Carey, R.J., Manga, M., Degruyter, W., Swanson, D., Houghton, B., Orr, T., and Patrick, M., 2012, Externally triggered renewed bubble nucleation in basaltic magma: The 12 October 2008 eruption at Halema‘uma‘u Overlook vent, Kīlauea, Hawai‘i, USA. Journal of Geophysical Research: Solid Earth 117(B11).

Cashman, K.J., and Kauahikaua, J.P., 1997, Reevaluation of vesicle distributions in basaltic lava flows. Geology 25(5), 419–422.

Cervelli, P., Segall, P., Amelung, F., Garbeil, H., Meertens, C., Owen, S., Miklius, A., and Lisowski, M., 2002, The 12 September 1999 Upper East Rift Zone dike intrusion at Kilauea Volcano, Hawaii. Journal of Geophysical Research 107(B7), 13.

Cervelli, P.F., and Miklius, A., 2003, The shallow magmatic system of Kilauea volcano. 149–163.

Chitwood, L.A., 1994, Inflated basaltic lava—Examples of processes and landforms from central and southeast Oregon. Oregon Geology 56, 11–21.

Chouet, B.A., Dawson, P.B., James, M.R., and Lane, S.J., 2010, Seismic source mechanism of degassing bursts at Kilauea Volcano, Hawaii: Results from waveform inversion in the 10–50 s band. Journal of Geophysical Research 115, B09311.

Clague, D.A., and Dalrymple, G.B., 1987, The Hawaiian-Emperor volcanic chain; part 1. Geologic evolution. *in*: Decker, R.W., Wright, T.L., Stauffer, P.H., (eds.), Volcanism in Hawaii: U.S. Geological Survey Professional Paper 1350 (1), 5–54.

Clague, D.A., and Heliker, C., 1993, The ten-year eruption of Kilauea Volcano. U.S. Geological Survey Earthquakes and Volcanoes 23(6), 244–254.

Crumpler, L.S., Aubele, J.C., and Zimbelman, J.R., 2007, Volcanic features of New Mexico analogous to volcanic features on Mars. *in*: Chapman, M.G., (ed.), The Geology of Mars: Evidence from Earth-Based Analog. Cambridge University Press, Cambridge, UK.

Dana, J.D., 1887, History of the changes in the Mt. Loa craters. American Journal of Science, Third Series 34(200), 81–97.

Dawson, P., Benítez, M., Chouet, B., and Wilson, D., 2010, Monitoring very-long-period seismicity at Kilauea Volcano, Hawaii. Geophysical Research Letters 37(L18306), 1–5.

DePaolo, D.J., and Stolper, E.M., 1996, Models of Hawaiian volcano growth and plume structure: Implications of results from the Hawaii Scientific Drilling Project. Journal of Geophysical Research 101(B5), 11643–11654.

Duncan, A.M., Guest, J.E., Stofan, E.R., Anderson, S.W., Pinkerton, H., and Calvari, S., 2004, Development of tumuli in the medial portion of the 1983 aa flow-field,

Mount Etna, Sicily. Journal of Volcanology and Geothermal Research 132(2–3), 173–187.

Duraiswami, R.A., Bondre, N.R., Dole, G., Phadnis, V.M., and Kale, V.S., 2001, Tumuli and associated features from the western Deccan Volcanic Province, India. Bulletin of Volcanology 63(7), 435–442.

Easton, R.M., 1987, Stratigraphy of Kīlauea Volcano, *in*: Decker, R.W., Wright, T.L., Stauffer, P.H., (eds.), Volcanism in Hawaii: U.S. Geological Survey Professional Paper 1350 (1), 243–260.

Eaton, J.P., and Murata, K.J., 1960, How volcanoes grow. Science 132(3432), 925–938.

Elias, T., and Sutton, A.J., 2012, Sulfur dioxide emission rates from Kīlauea Volcano, Hawai‘i, 2007–2010. U.S. Geological Survey Open-File Report 2012–1107, 25 p.

Ellis, W., 1963, Narrative of a tour of Hawaii, or Owhyhee; with remarks on the history, traditions, manners, customs and language of the inhabitants of the sandwich Islands. Reprint of the London 1827 Edition and the Hawaii 1917 Edition. Advertiser Publishing Company, LTD., Honolulu, Hawaii. 342 p.

Endo, E.T., and Murray, T., 1991, Real-time seismic amplitude measurement (RSAM): a volcano monitoring and prediction tool. Bulletin of Volcanology 53(7), 533–545.

Fee, D., Garces, M., Orr, T., and Poland, M., 2011, Infrasound from the 2007 fissure eruptions of Kīlauea Volcano, Hawai‘i. Geophysical Research Letters 38 (L06309), 5.

Fiske, R.S., and Kinoshita, W.T., 1969, Inflation of Kilauea Volcano prior to its 1967–1968 eruption. Science 165(3891), 341–349.

Fiske, R.S., Rose, T.R., Swanson, D.A., Champion, D.E., and McGeehin, J.P., 2009, Kulanaokuaiki Tephra (ca. A.D. 400–1000): Newly recognized evidence for highly explosive eruptions at Kilauea Volcano, Hawai‘i. Geological Society of America Bulletin 121(5-6), 712–728.

Garcia, M.O., Rhodes, J.M., Wolfe, E.W., Ulrich, G.E., and Ho, R.A., 1992, Petrology of lavas from episodes 2–47 of the Puu Oo eruption of Kilauea Volcano, Hawaii: Evaluation of magmatic processes. Bulletin of Volcanology 55(1-2), 1–16.

Gekle, S., and Gordillo, J.M., 2010, Generation and breakup of Worthington jets after cavity collapse. Part 1. Jet formation: Journal of Fluid Mechanics 663, 293–330.

Gerlach, T.M., McGee, K.A., Elias, T., Sutton, A.J., and Doukas, M.P., 2002, Carbon dioxide emission rate of Kilauea Volcano: Implications for primary magma and the summit reservoir. Journal of Geophysical Research 107(2189).

Glaze, L.S., Anderson, S.W., Stofan, E.R., Baloga, S., and Smrekar, S.E., 2005, Statistical distribution of tumuli on pahoehoe flow surfaces: Analysis of examples in Hawaii and Iceland and potential applications to lava flows on Mars. Journal of Geophysical Research, Solid Earth 110(B8), B08202.

Ghatan, G.J., and Head, J.W., III, 2004, Regional drainage of meltwater beneath a Hesperian-aged south circumpolar ice sheet on Mars. Journal of Geophysical Research 109(E7), E07006.

Greeley, R., 1987, The role of lava tubes in Hawaiian volcanoes. *in*: Decker, R.W., Wright, T.L., and Stauffer, P.H., (eds.), Volcanism in Hawaii: U.S. Geological Survey Professional Paper 1350 (2), 1589–1602.

Hamilton, C.W., Fagents, S.A., and Wilson, L., 2010, Explosive lava–water interactions in Elysium Planitia, Mars: constraints on the formation of the Tartarus Colles cone groups. Journal of Geophysical Research 115, E09006.

Hamilton, C.W., Fagents, S.A., and Thordarson, T., 2011, Lava–ground ice interactions in Elysium Planitia, Mars: geomorphological and geospatial analysis of the Tartarus Colles cone groups. Journal of Geophysical Research 116, E03004.

Hamilton, C., Glaze, L., James, M., and Baloga, S., 2013, Topographic and stochastic influences on pāhoehoe lava lobe emplacement. Bulletin of Volcanology 75(11), 1–16.

Haney, M.M., Power, J., West, M., and Michaels, P., 2012, Causal instrument corrections for short-period and broadband seismometers. Seismological Research Letters 83(5), 834–845.

Harlow, F.W., and Shannon, J.P., 1967, The splash of a liquid drop: Journal of Applied Physics 38(10), 3855–3866.

Harris, A., Pirie, D., Horton, K., Garbeil, H., Pilger, E., Ramm, H., Hoblitt, R., Thornber, C., Ripepe, M., Marchetti, E., and Poggi, P., 2005, DUCKS: Low cost thermal monitoring units for near-vent deployment. Journal of Volcanology and Geothermal Research 143(4), 335–360.

Head, J.W., and Pratt, S., 2001, Extensive Hesperian-aged south polar ice sheet on Mars: Evidence for massive melting and retreat, and lateral flow and ponding of meltwater. Journal of Geophysical Research 106(E6), 12275–12299.

Head, J.W., Wilson, L., Dickson, J., and Neukum, G., 2006, The Huygens-Hellas giant dike system on Mars: Implications for Late Noachian–Early Hesperian volcanic resurfacing and climatic evolution. Geology 34(4), 285–288.

Heliker, C., and Wright, T.L., 1991, Lava-flow hazards from Kilauea's current eruption. Geotimes, 36(5), 16–18.

Heliker, C.C., Mangan, M.T., Mattox, T.N., Kauahikaua, J.P., and Helz, R.T., 1998, The character of long-term eruptions: inferences from episodes 50–53 of the Puʻu ʻŌʻō - Kūpaianaha eruption of Kīlauea Volcano. Bulletin of Volcanology 59(6), 381–393.

Heliker, C., and Mattox, T.N., 2003, The first two decades of the Puʻu ʻŌʻō–Kupaianaha eruption; chronology and selected bibliography. *in*: Heliker, C., Swanson, D.A., Takahashi T.J., (eds.). The Puʻu ʻŌʻō-Kupaianaha Eruption of Kīlauea Volcano, Hawaii: The First 20 Years. U.S. Geological Survey Professional Paper 1676, 1–27.

Heliker, C., Kauahikaua, J., Sherrod, D.R., Lisowski, M., and Cervelli, P., 2003, The rise and fall of Puʻu ʻŌʻō cone, 1983–2002. *in*: Heliker, C., Swanson, D.A., Takahashi T.J., (eds.). The Puʻu ʻŌʻō-Kupaianaha Eruption of Kīlauea Volcano, Hawaii: The First 20 Years. U.S. Geological Survey Professional Paper 1676, 29–51.

Helz, R.T., and Thornber, C.R., 1987, Geothermometry of Kilauea Iki lava lake, Hawaii. Bulletin of Volcanology 49(5), 651–668.

Hoblitt, R.P., Orr, T.R., Castella, F., and Cervelli, P.F., 2008, Remote-controlled pan, tilt, zoom cameras at Kīlauea and Mauna Loa volcanoes, Hawaiʻi: U.S. Geological Survey Scientific Investigations Report 2008–5129, 14 p.

Hoblitt, R.P., Orr, T.R., Heliker, C., Denlinger, R.P., Hon, K., and Cervelli, P.F., 2012, Inflation rates, rifts, and bands in a pāhoehoe sheet flow. Geosphere 8(1), 179–195.

Holcomb, R.T., 1987, Eruptive history and long-term behavior of Kilauea volcano. *in*: Decker, R.W., Wright, T.L., Stauffer, P.H., (eds.), Volcanism in Hawaii: U.S. Geological Survey Professional Paper 1350 (1), 261–350.

Hon, K., Kauahikaua, J., Denlinger, R., and Mackay, K., 1994, Emplacement and inflation of pahoehoe sheet flows: observations and measurements of active lava flows on Kilauea Volcano, Hawaii. Geological Society of America Bulletin 106(3), 351–370.

Hon, K., and Orr, T., 2011, Hydrothermal hexahydrite spherules erupted during the 2008–2010 summit eruption of Kīlauea Volcano, Hawai‘i. Bulletin of Volcanology 73(9), 1369–1375.

Houghton, B.F., Swanson, D.A., Carey, R.J., Rausch, J., and Sutton, A.J., 2011, Pigeonholing pyroclasts: Insights from the 19 March 2008 explosive eruption of Kilauea volcano. Geology, 39(3), 263–266.

Hsiao, M., Lichter, S., and Quintero, L.G., 1988, The critical Weber number for vortex and jet formation for drops impinging on a liquid pool. Physics of Fluids 31(12), 3560–3562.

Jaggar, T.A., 1947, Origin and development of craters. Baltimore, Waverly Press, Inc., 508 p.

Johnson, D.M., Hooper P.R., and Conrey, R.M., 1999, XRF analysis of rocks and minerals for major and trace elements on a single low dilution Li-tetraborate fused bead. Advances in X-ray Analysis 41, 843–867.

Kauahikaua, J., Mangan, M., Heliker, C., and Mattox, T., 1996, A quantitative look at the demise of a basaltic vent: the death of Kupaianaha, Kilauea Volcano, Hawai‘i. Bulletin of Volcanology 57(8), 641–648.

Kauahikaua, J., Cashman, K.V., Mattox, T.N., Heliker, C.C., Hon, K.A., Mangan, M.T., and Thornber, C.R., 1998, Observations on basaltic lava streams in tubes from Kilauea Volcano, Island of Hawaii. Journal of Geophysical Research 103(B11), 27303–27323.

Kauahikaua, J., 2007, Lava flow hazard assessment, as of August 2007, for Kīlauea East Rift Zone eruptions, Hawai‘i Island. U.S. Geological Survey Open-File Report 2007-1264, 9 p.

Keller, G.V., Grose, L.T., Murray, J.C., and Skokan, C.K., 1979, Results of an experimental drill hole at the summit of Kilauea Volcano, Hawaii. Journal of Volcanology and Geothermal Research 5(3-4), 345–385.

Kern, C., Deutschmann, T., Werner, C., Sutton, A.J., Elias, T., and Kelly, P.J., 2012, Improving the accuracy of SO_2 column densities and emission rates obtained from upward-looking UV-spectroscopic measurements of volcanic plumes by taking realistic radiative transfer into account. Journal of Geophysical Research: Atmospheres 117(D20), D20302.

Keszthelyi, L.P., and Pieri, D.C., 1993, Emplacement of the 75-km-long Carrizozo lava flow field, south-central New Mexico. Journal of Volcanology and Geothermal Research 59(1-2), 59–75.

Keszthelyi, L., Jaeger, W., McEwe, A., Tornabene, L., Beyer, R.A., Dundas, C., and Milazzo, M., 2008, High Resolution Imaging Science Experiment (HiRISE) images of volcanic terrains from the first 6 months of the Mars Reconnaissance Orbiter Primary Science Phase. Journal of Geophysical Research 113, E04005.

Keszthelyi, L., 2012, Rate of solidification of silicate melts on the Earth, Moon, Mars, and beyond. Proceedings of the 43rd Lunar and Planetary Science Conference, Contribution 1659, Woodlands, Texas, 19–23 Mar.

Klein, F.W., Koyanagi, R.Y., Nakata, J.S., and Tanigawa, W.R., 1987, The seismicity of Kilauea's magma system. *in*: Decker, R.W., Wright, T.L., Stauffer, P.H., (eds.), Volcanism in Hawaii: U.S. Geological Survey Professional Paper 1350 (2), 1019–1185.

Lefort, A., Burr, D.M., Beyer, R.A., and Howard, A.D., 2012, Inverted fluvial features in the Aeolis-Zephyria Plana, western Medusae Fossae Formation, Mars: Evidence for post-formation modification. Journal of Geophysical Research 117(E3), E03007.

Lohse, D., Bergmann, R., Mikkelsen, R., Zeilstra, C., van der Meer, D., Versluis, M., van der Weele, K., van der Hoef, M., and Kuipers, H., 2004, Impact on soft sand: Void collapse and jet formation. Physical Review Letters 93(19), 1–4.

Lundgren, P., Poland, M., Miklius, A., Orr, T., Yun, S.-H., Fielding, E., Liu, Z., Tanaka, A., Szeliga, W., Hensley, S., and Owen, S., 2013, Evolution of dike opening

during the March 2011 Kamoamoa fissure eruption, Kīlauea Volcano, Hawai`i. Journal of Geophysical Research: Solid Earth 118.

Macdonald, G.A., 1955, Hawaiian volcanoes during 1952, U.S. Geological Survey Bulletin 1021B, 15–108.

Mangan, M.T., Heliker, C.C., Mattox, T.N., Kauahikaua, J.P., and Helz, R.T., 1995, Episode 49 of the Pu‘u ‘O‘o–Kupaianaha eruption of Kilauea volcano – breakdown of a steady-state eruptive era. Bulletin of Volcanology 57(2), 127–135.

Mastin, L.G., 1997, Evidence for water influx from a caldera lake during the explosive hydromagmatic eruption of 1790, Kilauea volcano, Hawaii. Journal of Geophysical Research: Solid Earth 102(B9), 20093–20109.

Mattox, T.N., Heliker, C., Kauahikaua, J., and Hon, K., 1993, Development of the 1990 Kalapana flow field, Kilauea Volcano, Hawaii. Bulletin of Volcanology 55(6), 407–413.

McPhie, J., Walker, G., and Christiansen, R., 1990, Phreatomagmatic and phreatic fall and surge deposits from explosions at Kilauea volcano, Hawaii, 1790 a.d.: Keanakakoi Ash Member. Bulletin of Volcanology 52(5), 334–354.

Miklius, A., and Cervelli, P., 2003, Interaction between Kilauea and Mauna Loa. Nature 421(6920), 229.

Montgomery-Brown, E.K., Sinnett, D.K., Poland, M., Segall, P., Orr, T., Zebker, H., and Miklius, A., 2010, Geodetic evidence for en echelon dike emplacement and concurrent slow slip during the June 2007 intrusion and eruption at Kīlauea volcano, Hawaii. Journal of Geophysical Research 115(B7).

Mouginis-Mark, P.J., and Rowland, S.K., 2008, Lava flows at Arsia Mons, Mars: Insights from a graben imaged by HiRISE. Icarus 198.

Nichols, R.L., 1939, Surficial banding and shark's-tooth projections in the cracks of basaltic lava. American Journal of Science 237, 188–194.

Okamura, A.T., Dvorak, J.J., Koyanagi, R.Y., and Tanigawa, W.R., 1988, Surface deformation during dike propagation, *in*: Wolfe, E.W., (ed.), The Puu Oo eruption of Kilauea Volcano, Hawaii; episodes 1 through 20, January 3, 1983, through June 8, 1984. U.S. Geological Survey Professional Paper 1463, 165–182.

Okubo, P., Nakata, J., Chouet, B., and Dawson, P., 1996, The February 1, 1996, Kilauea summit earthquake swarm [abs.]. Eos (Transactions, American Geophysical Union) 77(46), F798.

Orr, T.R., and Hoblitt, R.P., 2008, A versatile time-lapse camera system developed by the Hawaiian Volcano Observatory for use at Kīlauea Volcano, Hawai‘i. U.S. Geological Survey Scientific Investigations Report 2008-5117, 8 p.

Orr, T.R., 2011, Selected time-lapse movies of the East Rift Zone eruption of Kīlauea Volcano, 2004–2008. U.S. Geological Survey Data Series 621, 15 p., 26 time-lapse movies.

Orr, T., Houghton, B., Poland, M., Patrick, M., Thelen, W., Sutton, A., Parcheta, C., and Thornber, C., 2013, Low intensity Hawaiian fountaining as exemplified by the March 2011, Kamoamoa eruption at Kilauea Volcano, Hawaii. Abstract V33F-01 presented at 2013 Fall Meeting, AGU, San Francisco, California, 9–13 December.

Owen, S., Segall, P., Lisowski, M., Miklius, A., Murray, M., Bevis, M., and Foster, J., 2000, January 30, 1997 eruptive event on Kilauea Volcano, Hawaii, as monitored by continuous GPS. Geophysical Research Letters 27(17), 2757–2760.

Parcheta, C.E., Houghton, B.F., and Swanson, D.A., 2012, Hawaiian fissure fountains 1: decoding deposits—episode 1 of the 1969–1974 Mauna Ulu eruption. Bulletin of Volcanology 74(7), 1729–1743.

Parcheta, C., 2013, Weak-intensity, basaltic, explosive volcanism: Dynamics of Hawaiian fountains [Ph.D. dissertation]. University of Hawai‘i at Mānoa, 200 p.

Parcheta, C., Orr, T., and Houghton, B., 2013, Chronology-based Physical Volcanology of the 2011 Kamoamoa Eruption of Kīlauea. Abstract V33F-02 presented at 2013 Fall Meeting, AGU, San Francisco, California, 9–13 December.

Patrick, M.R., Orr, T., Wilson, D., Dow, D., and Freeman R., 2011a, Cyclic spattering, seismic tremor, and surface fluctuation within a perched lava channel, Kīlauea Volcano. Bulletin of Volcanology 73(6), 639–653.

Patrick, M., Wilson, D., Fee, D., Orr, T., and Swanson, D., 2011b, Shallow degassing events as a trigger for very-long-period seismicity at Kīlauea Volcano. Hawai‘i: Bulletin of Volcanology 73(9), 1179–1186.

Patrick, M.R., and Orr, T., 2012, Rootless shield and perched lava pond collapses at Kīlauea Volcano, Hawai'i. Bulletin of Volcanology 74(1), 67–78.

Patrick, M., Orr, T., Sutton, A.J., Elias T., and Swanson, D., 2013, The first five years of Kīlauea's summit eruption in Halemaʻumaʻu, 2008–2013. U.S. Geological Survey Fact Sheet 2013–3116, 4 p.

Paskievitch, J., Read, C., and Parker, T., 2010, Remote telemetered and time-lapse cameras at Augustine Volcano. *in*: Power, J.A., Coombs, M.L., Freymueller, J.T., (eds.), The 2006 eruption of Augustine Volcano, Alaska. U.S. Geological Survey Professional Paper 1769, 285–293.

Peck, D.L., and Minakami, T., 1968, The formation of columnar joints in the upper part of Kilauean lava lakes, Hawaii. Geological Society of America Bulletin 79(9), 1151–1166.

Peterson, D.W., Holcomb, R.T., Tilling, R.I., and Christiansen, R.L., 1994, Development of lava tubes in the light of observations at Mauna Ulu, Kilauea Volcano, Hawaii. Bulletin of Volcanology 56(5), 343–360.

Poland, M., Miklius, A., Orr, T., Sutton, J., Thornber, C., and Wilson, D., 2008a, New episodes of volcanism at Kilauea Volcano, Hawaii. Eos (Transactions, American Geophysical Union) 89(5), 37–38.

Poland, M.P., Dzurisin, D., LaHusen, R.G., Major, J.J., Lapcewich, D., Endo, E.T., Gooding, D.J., Schilling, S.P., and Janda, C.G., 2008b, Remote camera observations of lava dome growth at Mount St. Helens, Washington, October 2004 to February 2006. *in*: Sherrod, D.R., Scott, W.E., Stauffer, P.H., (eds.), A Volcano Rekindled: The Renewed Eruption of Mount St. Helens, 2004–2006. Geological Survey Professional Paper 1750, 225–236.

Poland, M.P., Miklius, A., Lundgren, P., and Sutton, A.J., 2011, Repeated deflation-inflation events at Kilauea Volcano, Hawai'i: What's up (and down) with that? American Geophysical Union Fall Meeting, San Francisco, Calif., 5–9 Dec., V51G-01

Poland, M.P., Miklius, A., Sutton, A.J., and Thornber, C.R., 2012, A mantle-driven surge in magma supply to Kilauea Volcano during 2003–2007. Nature Geoscience 5(4), 295–300.

Poland, M.P., Miklius, A., Montgomery-Brown, E.K., 2014, Magma supply, storage, and transport at shield-stage Hawaiian volcanoes. *in*: Poland, M.P., Takahashi, T.J., Landowski, C.M., (eds), Characteristics of Hawaiian volcanoes. U.S. Geological Survey Professional Paper 1801, 179–234.

Rivalta, E., and Segall, P., 2008, Magma compressibility and the missing source for some dike intrusions. Geophysical Research Letters 34(L04306).

Roche, O., van Wyk de Vries, B., and Druitt, T.H., 2001, Sub-surface structures and collapse mechanisms of summit pit craters. Journal of Volcanology Geothermal Research 105(1-2), 1–18.

Rossi, M.J., and Gudmundsson, A., 1996, The morphology and formation of flow-lobe tumuli on Icelandic shield volcanoes. Journal of Volcanology Geothermal Research 72(3–4), 291–308.

Ryan, M.P., 1987, Neutral buoyancy and the mechanical evolution of magmatic systems. *in*: Mysen, B.O., (ed.), Magmatic Processes: Physiochemical Principles. The Geochemical Society, 259–287.

Schaefer, C.J., and Kattenhorn, S.A., 2004, Characterization and evolution of fractures in low-volume pahoehoe lava flows, eastern Snake River Plain, Idaho. Geological Society of America Bulletin 116(3-4), 322–336.

Scherbaum, F., and Bouin, M.P., 1997, FIR filter effects and nucleation phases. Geophysical Journal International 130(3), 661–668.

Self, S., Keszthelyi, L., and Thordarson, T., 1998, The importance of pāhoehoe. Annual Review of Earth and Planetary Science 26(1), 81–110.

Sen, G., and Jones, R.E., 1990, Cumulate Xenolith in Oahu, Hawaii: Implications for Deep Magma Chambers and Hawaiian Volcanism. Science 249(4973), 1154–1157.

Stearns, H.T., 1926, The Keaiwa or 1823 Lava Flow from Kilauea Volcano, Hawaii. The Journal of Geology 34(4), 336–351.

Stephenson, P.J., Burch-Johnston, A.T., Stanton, D., and Whitehead, P.W., 1998, Three long lava flows in north Queensland. Journal of Geophysical Research 103(B11), 27359–27370.

Sutton, A.J., Elias, T., Gerlach, T.M. and Stokes, J.B., 2001, Implications for eruptive processes as indicated by sulfur dioxide emissions from Kilauea Volcano, Hawai`i, 1979–1997. Journal of Volcanology Geothermal Research 108(1–4), 283–302.

Sutton, A.J., Elias, T., and Kauahikaua, J., 2003, Lava-effusion rates for the Pu‘u ‘Ō‘ō - Kupaianaha eruption derived from SO_2 emissions and very low frequency (VLF) measurements. *in*: Heliker, C., Swanson, D.A., Takahashi T.J., (eds.). The Pu‘u ‘Ō‘ō-Kupaianaha Eruption of Kīlauea Volcano, Hawaii: The First 20 Years. U.S. Geological Survey Professional Paper 1676, 137–148.

Swanson, D.A., Jackson, D.B., Koyanagi, R.Y., and Wright, T.L., 1976, The February 1969 east rift eruption of Kilauea Volcano, Hawaii. U.S. Geological Survey Professional Paper 891, 33p.

Swanson, D., Wooten, K., and Orr, T., 2009, Buckets of ash track tephra flux from Halema‘uma‘u Crater, Hawai‘i. Eos (Transactions, American Geophysical Union) 90(46), 427.

Swanson, D.A., Rose, T.R., Fiske, R.S., and McGeehin, J.P., 2012, Keanakāko‘i Tephra produced by 300 years of explosive eruptions following collapse of Kīlauea's caldera in about 1500 CE. Journal of Volcanology and Geothermal Research 215-216(0), 8–25.

Swanson, D.A., Rose T.R., Mucek, A.E., Garcia, M.O., Fiske, R.S., and Mastin, L.G., 2014, Cycles of explosive and effusive eruptions at Kīlauea Volcano, Hawai‘i. Geology 42(7), 631–634.

Swanson, D.A., Weaver, S.J., Houghton, B.F., 2015, Reconstructing the deadly eruptive events of 1790 CE at Kīlauea Volcano, Hawai‘i. Geological Society of America Bulletin 127(3-4), 503–515.

Thornber, C.R., 1997, HVO/RVTS-1; a prototype remote video telemetry system for monitoring the Kilauea East Rift Zone eruption. U.S. Geological Survey Open-File Report 97-537, 18 p.

Thornber, C.R., Sherrod, D.R., Siems, D.F., Heliker, C.C., Meeker, G.P., Oscarson, R.L., and Kauahikaua, J.P., 2002, Whole-rock and glass major-element geochemistry of

Kilauea Volcano, Hawaii, near-vent eruptive products—September 1994 through September 2001. U.S. Geological Survey Open-File Report 2002-17, 9 p.

Thornber, C.R., Heliker, C., Sherrod, D.R., Kauahikaua, J.P., Miklius, A., Okubo, P.G., Trusdell, F.A., Budahn, J.R., Ridley, W.I., and Meeker, G.P., 2003, Kilauea east rift zone magmatism; an episode 54 perspective. Journal of Petrology 44(9), 1525–1559.

Thornber, C.R., Orr, T.R., Heliker, C., and Hoblitt, R.P., 2015, Petrologic testament to changes in shallow magma storage and transport during 30+ years of recharge and eruption at Kīlauea Volcano, Hawai‘i. *in*: Carey, R., Cayol, V., Poland, M., Weis, D., (eds.), Hawaiian Volcanoes, from Source to Surface. American Geophysical Union Monograph 208, 147–188.

Thoroddsen, S.T., Etoh, T.G., Takehara, K., and Takano, Y., 2004, Impact jetting by a solid sphere. Journal of Fluid Mechanics 499, 139–148.

Trusdell, F., 2011, Dueling volcanoes: How activity levels at Kilauea influence eruptions at Mauna Loa. American Geophysical Union Fall Meeting, San Francisco, Calif., 5–9 Dec., V33E-08.

Walker, G.P.L., 1991, Structure, and origin by injection of lava under surface crust, of tumuli, “lava rises”, “lava-rise pits”, and “lava-inflation clefts” in Hawaii. Bulletin of Volcanology 53(7), 546–558.

Walker, G.P.L., 2009, The endogenous growth of pahoehoe lava lobes and morphology of lava-rise edges. *in*: Thordarson, T., Self, S., Larsen, G., Rowland, S.K., Hoskuldsson, A., (eds.), Studies in volcanology—the legacy of George Walker (Special Publications of IAVCEI No. 2). The Geological Society, 17–32.

Waltham, T., Bell, F., and Culshaw, M., 2005, Sinkholes and subsidence—karst and cavernous rocks in engineering and construction. Springer, Berlin, 382 p.

Wentworth, C.K., and Macdonald, G.A., 1953, Structures and forms of basaltic rocks in Hawaii. U.S. Geological Survey Bulletin 994, 98 p.

Whitehead, P.W., and Stephenson, P.J., 1998, Lava rise ridges of the Toomba basalt flow, north Queensland, Australia. Journal of Geophysical Research: Solid Earth 103(B11), 27371–27382.

Williams, K.E., Toon, O.B., Heldmann, J.L., and Mellon, M.T., 2009, Ancient melting of mid-latitude snowpacks on Mars as a water source for gullies. Icarus 200(2), 418–425.

Wilson, D., Elias, T., Orr, T., Patrick, M., Sutton, A.J., and Swanson, D., 2008, Small explosion from new vent at Kilauea's summit. EOS, Transactions, American Geophysical Union 89(22), 203.

Wilson, L., and Head, J.W., 1981, Ascent and eruption of basaltic magma on the Earth and Moon. Journal of Geophysical Research 86(B4), 2971–3001.

Wolfe, E.W., Garcia, M.O., Jackson, D.B., Koyanagi, R.Y., Neal, C.A., and Okamura, A.T., 1987, The Puu Oo eruption of Kilauea Volcano, episodes 1–20, January 3, 1983, to June 8, 1984. *in*: Decker, R.W., Wright, T.L., Stauffer, P.H., (eds.), Volcanism in Hawaii. Geological Survey Professional Paper 1350(1), 471–508.

Wolfe, E.W., Neal, C.A., Banks, N.G., and Duggan, T.J., 1988, Geologic observations and chronology of eruptive events. *in*: Wolfe, E.W., (ed.), The Puu Oo eruption of Kilauea Volcano, Hawaii; episodes 1 through 20, January 3, 1983, through June 8, 1984. U.S. Geological Survey Professional Paper 1463, 1–97.

Wooten, K.M., Thornber, C.R., Orr, T.R., Ellis, J.F., and Trusdell, F.A., 2009, Catalog of tephra samples from Kilauea's summit eruption, March-December 2008. U.S. Geological Survey Open-File Report 2009-1134, 26 p.

Worthington, A.M., 1908, A study of splashes. London, Longmans, Green & Co., 129 p.

Wright, T.L., 1984, Origin of Hawaiian tholeiite: A metasomatic model. Journal of Geophysical Research 89(B5), 3233–3252.

Wright, T.L., and Klein, F.W., 2014, Two hundred years of magma transport and storage at Kīlauea Volcano, Hawai'i, 1790–2008. U.S. Geological Survey Professional Paper 1806, 258 p.

Wyllie, P.J., 1988, Solidus curves, mantle plumes, and magma generation beneath Hawaii. Journal of Geophysical Research 93(B5), 4171–4181.

Zimbelman, J.R., and Johnston, A.K., 2001, Improved topography of the Carrizozo lava flow: Implications for emplacement conditions. *in*: Crumpler, L.S., Lucas, S.G., (eds.), Volcanology in New Mexico. New Mexico Museum of Natural History and Science, Bulletin 18, 31–136.

Zimbelman, J.R., and Johnston, A.K., 2002, New precision topographic measurements of Carrizozo and McCartys basalt flows, New Mexico. *in*: Lueth, V.W., Giles, K.A., Lucas, S.G., Kues, B.S., Myers, R.G., Ulmer-Scholle, D.S., (eds.), Geology of White Sands. New Mexico Geological Society Guidebook, 53rd Field Conference, 121–127.

Zimbelman, J.R., and Griffin, L.J., 2010, HiRISE images of yardangs and sinuous ridges in the lower member of the Medusae Fossae Formation, Mars. Icarus 205(1), 198–210.